

Integrative studies of chromosome structural proteins by
improving targeted protein degradation system and
developing biochemical reconstitution system

Yesbolatova, Aisha

Doctor of Philosophy

Department of Genetics
School of Life Science

The Graduate University for Advanced Studies,

SOKENDAI

Table of Contents

Abstract	1
Chapter 1. The Improvement of Auxin-Inducible Degron System	4
Introduction	4
Targeted Protein Degradation for Functional Studies	4
Overview of Auxin-Inducible Degron (AID)	10
Results	16
Inhibition of OsTIR1 by Auxinole as a Strategy to Suppress Basal Degradation in AID	16
TOL2 Transposon-based One-Step Construction of AID Mutants	21
Development of Auxin-Inducible Degron 2	25
Discussion	36
Materials and Methods	39
Chapter 2. Biochemical Characterization of The Fission Yeast Cohesin Complexes	44
Introduction	44
Results	51
Discussion	57
Materials and Methods	59
Supplementary Materials	64
Chapter 1	64
Chapter 2	70
References	74
Acknowledgments	91

Abstract

Genomic DNA, the blueprint of life, is packed, duplicated, and expressed with the aid of thousands of chromosomal proteins, many of which are derived from essential genes. Gene disruption is one of the powerful approaches for dissecting a protein function of interest but remains difficult to apply it to proteins essential for cell viability. Hence, novel approaches that enable intended protein degradation by combining genetic manipulation and chemical biology are getting more attention in a wide range of recent biology. The auxin-inducible degron (AID) technology is a plant-derived degron-based protein degradation application that allows rapid and specific depletion of a protein of interest (POI) in non-plant cells by utilizing the ubiquitin-proteasome system of the host organisms, with an option of re-expression after target depletion. This can be applied to a wide range of organisms including human cells by introducing the two factors via genetic modifications: ectopic expression of the auxin-perceptive plant protein, transcription inhibition response 1 (TIR1), and introduction of the AID tag (TIR1 recognition peptide) to POI. The addition of auxin mediates the recognition of the AID tag by the auxin receptor TIR1, which recruits an endogenous ubiquitin ligase complex for ubiquitylation and proteasomal degradation of the POI. Typically, a POI is degraded within an hour upon the addition of auxin, bearing the AID system as one of the fastest protein depletion technologies. This acute and efficient degradation allows us the direct functional analysis of many proteins, in particular those required for cell viability, before secondary effects of protein depletion are accumulated.

In principle, no protein degradation should take place in the absence of auxin. However, due to the nature of the TIR1 (ubiquitin ligase) – AID tag-fused POI recognition and the presence of auxin-like chemicals in the cell culture medium, even in the absence of auxin, basal degradation is observed, which occasionally hampers functional analyses. An

additional drawback of the system is the use of relatively high concentrations of auxin. Even though the concentrations used for human culture cells do not affect their growth, this is a potential problem for the application to mice and other multicellular organisms. *Therefore, the main goal of Chapter 1 is to resolve the issues of basal degradation and high auxin concentration to make AID a robust technology that can be used as a standard tool for genetic perturbation to study protein function and ultimately be applied to mice.*

First, I addressed the problems of basal degradation in the absence of auxin. The first described result is the use of the inhibitor auxinole for timely control of degradation and re-expression of the AID tag-fused proteins. Second, I took another approach to improve the AID system from the genetic perspective by developing an all-in-one plasmid encoding the TOL2 transposon sites and all required components for stable integration and controlling the expression of transgenes. Genetic manipulations for generating AID mutants can be performed using the clustered regularly interspaced short palindromic repeats (CRISPR)–CRISPR-associated protein 9 (Cas9)-mediated genome editing. By combining it with TOL2 transposase encoding plasmid and CRISPR–Cas9 knockout plasmid for simultaneous transfection, I created a new protocol for generating AID mutants in polyploid human cells.

The final and major result is creating the updated version of the AID technology, AID2, by increasing the specificity of the TIR1 – AID tag interaction to suppress basal degradation and decrease the ligand concentration. This was done by introducing a mutation to the TIR1 receptor and using an auxin analog that binds specifically to the mutant receptor. Due to the high specificity of the new receptor – inducer pair, the problem of basal degradation was mostly eliminated. Importantly, I found that several hundred times lower inducer concentration is required for efficient protein degradation. Moreover, the improved system allows for the construction of AID mutants previously proved to be complicated or impossible. This improvement significantly enhances the utility of the AID technology and

reveals new perspectives for its use, such as the application to stem cells, mice, and other multicellular organisms.

In Chapter 2, I took a different approach to characterize one of the essential chromosomal proteins, cohesin, by establishing biochemical reconstitution assays using purified protein components. Cohesin is a ring-shaped protein complex that mediates sister chromatid cohesion, one of the chromosomal structures essential for faithful chromosome segregation during cell division. I have reconstituted the meiosis-specific cohesin complex to analyze its ATP-dependent DNA loading, which is vital for creating sister chromatid cohesion. I found that meiotic cohesin topologically entraps DNA in a similar way to the somatic version of cohesin whereas its dissociation appears to be differently regulated. The established *in vitro* assay will provide a novel opportunity for molecular studies of meiotic chromosome organization driven by meiotic cohesin complexes.

Chapter 1

The Improvement of Auxin-Inducible Degron System

Introduction

Targeted Protein Degradation for Functional Studies

The most direct approach to defining the biological role of a protein is gene inactivation. By targeting a gene of interest through the disruption of its open reading frame and blocking its expression in cells and whole organisms, it is possible to achieve various gene modifications, including gene inactivation. This reductionist approach remains one of the most efficacious ways to deduce gene function from the perturbations of a normal phenotype since the first gene targeting experiments in yeast and cultured mammalian cells in the 1980s¹⁻⁸. It was later explained by the precise enzymatic activity inside cells laying behind the mechanism of homologous recombination⁹⁻¹¹. Although a significant development, gene targeting through homologous recombination is much less efficient in higher organisms compared to bacteria and yeast, leaving almost half of the mouse genome left untargeted¹².

With the advent of methods to introduce targeted genetic modifications such as zinc-finger nucleases (ZFNs), transcription activator-like effector nucleases (TALENs), and CRISPR-associated nucleases, the gene targeting became very efficient¹³. However, still for many proteins, especially in higher organisms and derived cultured cells, studying the protein function by depletion is difficult or impossible to achieve through knockout because these proteins are essential for cell viability. In addition, gene knockout generates permanent protein loss limiting the scope of its usage for functional protein studies. Therefore, the search for a method to recapitulate knockout for essential proteins is as relevant as ever.

To address this problem, the concept of genetic interference for loss-of-function experiments was developed. Knockdown approaches include RNA-based RNA interference

(e.g., small interfering RNA (siRNA) and short hairpin RNA (shRNA)), DNA-based RNA interference (e.g., antisense oligonucleotides (ASO)), and CRISPR-mediated gene knockdown (e.g. CRISPR interference (CRISPRi) using dCas9 and Cas13 family enzymes)¹⁴⁻²³. Nonetheless, these approaches are not robust enough to give a precise idea of a protein function. Protein may not be depleted completely and the degradation time is slow, thus, secondary phenotypes may give obscure results before the immediate effect of the depletion is seen.

Knockout and knockdown methods mentioned above are difficult to be used for targeting essential proteins. As a result, many new techniques are being developed now to account for the difficulties with protein degradation for basic research and applications in drug discovery. Among them are novel ligand-induced protein degradation approaches such as degradation tag (dTAG), Halotag-hydrophobic tag (HyT), Halo-Proteolysis-targeting chimera (HaloPROTAC), destabilizing domain (DD), auxin-inducible degron (AID), and many others²⁴⁻²⁸. In the next part, a brief description of some of these technologies will be given (**Table 1** and **Fig. 1**), followed by a more detailed discussion of AID, which is the main subject of Chapter 1²⁹⁻³¹.

Many of the protein depletion methods mentioned above rely on the cell's ubiquitin proteasome degradation pathway. The protein ubiquitination proceeds through the function of the series of enzymes which include E1 (ubiquitin-activating enzyme), E2 (ubiquitin-conjugating enzyme), and E3 (ubiquitin ligase)³²⁻³⁶. E1 activates ubiquitin and brings it to E2, creating an E2-ubiquitin conjugate. E3 ligase directly binds the substrate and ubiquitin-bound E2, thereby bringing them close to each other to facilitate the ubiquitin transfer from E2 to the substrate. Substrate specificity for ubiquitination depends on the E3 ligase. One type of E3 ligases is cullin–RING ligase (CRL) protein complexes containing a cullin (CUL) family protein which serves a scaffold to which RING finger protein binds at the amino-

terminal (N-terminal) and substrate-specific receptor binds at the carboxy-terminal (C-terminal). The RING finger protein recruits E2 and the receptor binds to a substrate. The examples of the RING finger protein include RBX1, and RBX2. The examples of the cullin family protein include CUL1, CUL2, CUL3, CUL4A/4B, CUL5, and CUL7^{37, 38}. The examples of the substrate-specific receptor are estimated to comprise 300 different proteins in humans³⁹.

Degradation tag (dTAG)

Degradation tag (dTAG) technology needs three major components: an FKBP12^{F36V}-fused POI, the endogenous CUL4–RING E3 ligase complex, and a small synthetic molecule that can bind both (summarized in **Table 1** and **Fig. 1A**)²⁴. The target protein is tagged with the designed 12-kDa tag (FKBP12^{F36V}) through transgene expression or CRISPR–Cas9-mediated locus-specific knock-in^{40, 41}. After a heterobifunctional degrader ligand (e.g., dTAG-13) is added to cultured cells, FKBP^{12F36V}-fused POI interacts with cereblon (CRBN), which is a component of CUL4–CRBN E3 ubiquitin ligase complex, resulting in targeted POI degradation by the proteasome. Besides cultured cells, dTAG has been applied to mouse xenografts, because the main advantage of this efficient system is low ligand concentration.

HaloTag-hydrophobic tag (HyT)

HaloTag-hydrophobic tag (HyT) technology needs three major components: a 33 kDa-protein HaloTag (e.g., HaloTag2, HaloTag7), and a hydrophobic tag (e.g., HyT13, HyT36), which has a hydrophobic group characteristic in protein misfolding or denaturation (summarized in **Table 1** and **Fig. 1B**)^{25, 42, 43}. When POI-HaloTag fusion protein binds HyT13, it is subjected to the proteasomal degradation through a protein quality control system. At the concentration of at 500 nM–10 mM, HyT13 successfully induces degradation of HaloTag-fused proteins in cultured cells and organisms, such as zebrafish and mice⁴⁴. Due to its high versatility, the

bacterial dehalogenase derived HaloTag serves is used not only for protein degradation, but also for protein purification and microscopy^{25, 45}. It covalently binds to compounds with an alkyl chloride moiety, which is the basis for its many applications.

Halo-Proteolysis-Targeting Chimera (HaloPROTAC)

Halo-Proteolysis-targeting chimera (HaloPROTAC) takes the advantage of the HaloTag technology. It requires three major components: HaloTag7-fused POI, the endogenous CUL2–RING E3 ligase complex (CRL2–VHL), and a HaloPROTAC heterobifunctional ligand that can bind both (summarized in **Table 1** and **Fig. 1C**)²⁶. After a heterobifunctional degrader ligand (e.g., HaloPROTAC3) is added to cultured cells, HaloTag7-fused POI interacts with cereblon (VHL), which is a component of CRL2–CRBN E3 ubiquitin ligase complex (CRL2–VHL), resulting in targeted POI degradation by the proteasome. At the concentration of 625 nM, HaloPROTAC3 induces the degradation of the 90% of the GFP–HaloTag7 reporter, and it is possible for the POI to be re-expressed after the ligand is removed. In comparison to other technologies presented here, the disadvantage of HaloPROTACs is slow degradation with the half-time ranging from 4 to 8 h). Application in animals is awaited.

Destabilizing Domain (DD)

Destabilizing domain (DD) works in an opposite principle than other systems described here. It needs two major components: a DD_{FKBP}-fused POI and a ligand that stabilizes it (e.g., Shield-1) (summarized in **Table 1** and **Fig. 1E**)²⁷. A DD_{FKBP}-fused POI is degraded within hours in the absence of its ligand via the proteasomal pathway through a protein quality control system. In this system, it is possible to re-express the POI in a dose-dependent manner (100 nM–1 mM). The DD technology has large utility in cultured cells and mice^{46- 48}. As a derivative of DD, ligand-induced degradation (LID) reverses the degradation principle.

In LID, a tag consists of a synthetic 19-aa degron fused to the C-terminus of an FKBP12 variant and buried in the binding pocket, disallowing the degradation of POI⁴⁹. When Shield-1 is added, it accesses the binding pocket, exposing the degron tag and inducing POI–LID degradation. The LID tag technology allows tagging a POI at the C-terminus only, whereas there is no such limitation in other technologies.

System	Degron (MW)	CRL E3 ligase	Inducer	Ligand concentration	Number of protein components	Half-life	Tested organisms
dTAG	FKBP12 ^{F36V} (12 kDa)	CUL4–RBX1–CRBN	dTAG13	50 nM – 1 μ M	1	< 1 h	mouse
HaloTag-HyT	HaloTag (3 kDa)	– (chaperone-based protein quality control)	HyT13, 36	500 nM – 10 μ M	1	> 1.5 h	mouse, zebrafish
Halo PROTAC	HaloTag (33 kDa)	CUL2–RBX1–VHL	HaloPROTAC3	500 nM – 1 μ M	1	> 4 h	–
AID	mAID (7 kDa)	CUL1–RBX1–OsTIR1	Auxin (IAA, NAA)	100 μ M – 500 μ M	2	< 30 min	zebrafish, <i>C. elegans</i> , fruit fly, yeast
DD _{FKBP}	DD _{FKBP} (12 kDa)	– (chaperone-based protein quality control)	Shield-1	100 nM – 1 μ M	1	> 45 min	mouse, rat, <i>C. elegans</i>
LID	FKBP12-degron (13 kDa)	– (chaperone-based protein quality control)	Shield-1	100 nM – 2 μ M	1	~ 1 h	–

Table 1. Comparison of targeted protein degradation approaches.

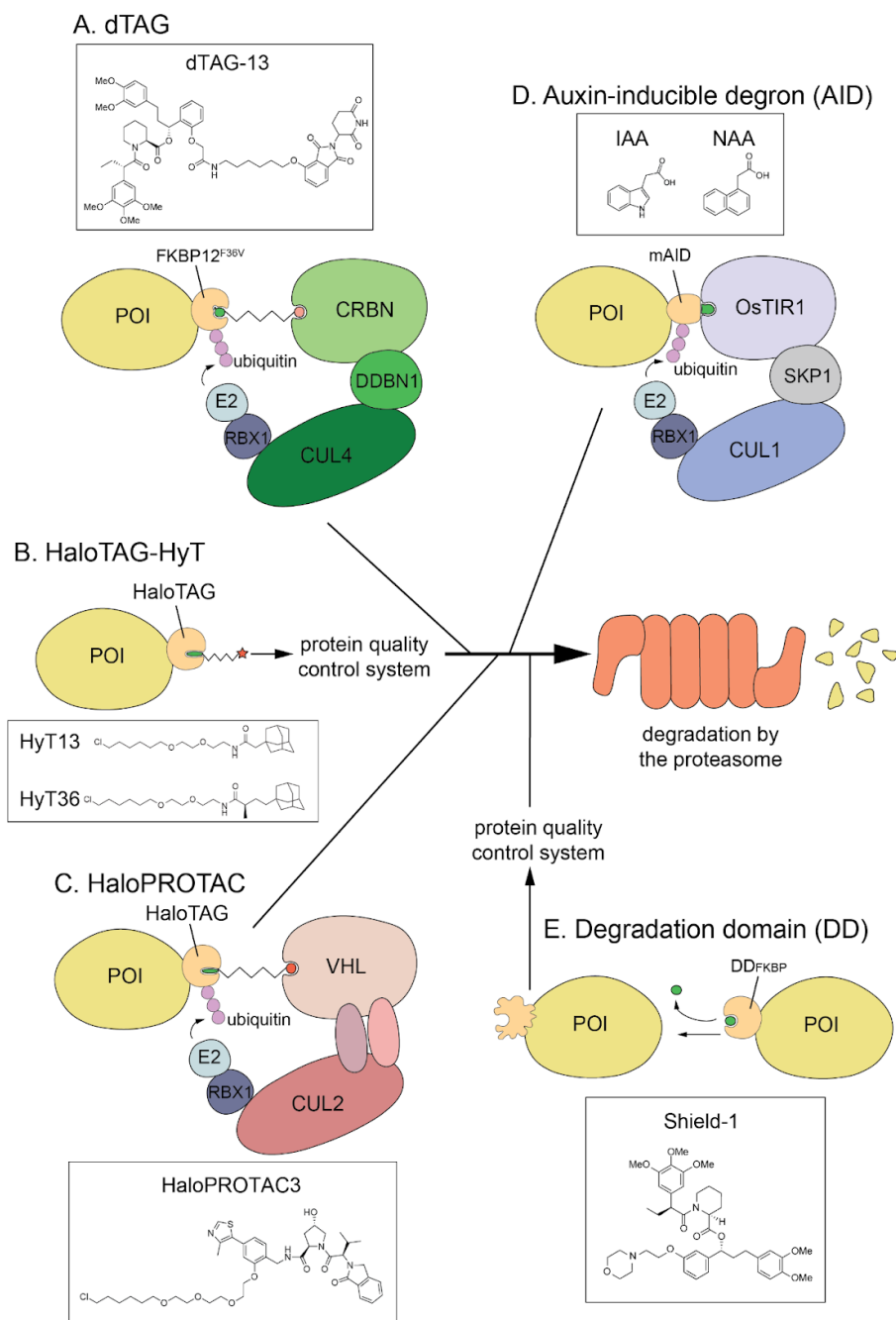


Figure 1. Overview of the systems involved in targeted protein degradation approaches. The chemical structures of ligands are shown in insets related to each panel. (A) In the dTAG system, a heterobifunctional ligand (e.g., dTAG-13) links the genetically introduced FKBP12^{F36V} degron to an endogenous CRL4–CRBN E3 ubiquitin ligase. (B) In the HaloTag-HyT system, an HyT ligand (e.g., Hyt13 and Hy36) contains a hydrophobic moiety that recruits the HaloTag-fused POI to the endogenous protein quality control system. (C) In the HaloPROTAC system, a designed ligand links the HaloTag-fused POI to an endogenous CRL2–VHL E3 ubiquitin ligase. (D) In the AID system, two genetic modifications are performed to generate a mAID degron-fused POI and introduce OsTIR1. Auxin ligand (e.g., IAA and NAA) links the mAID-tagged POI to OsTIR1 which incorporates into the endogenous CRL1–TIR1 E3 ubiquitin ligase. (E) In the DD system, the removal of a specific ligand (e.g., Shield-1) destabilizes the otherwise stably expressed DD tag-fused POI and recruits it to the endogenous protein quality control.

Heterobifunctional and small-molecule degradation inducers both act to increase the proximity between the target protein and a E3 ubiquitin ligase and a POI. However, there are multiple differences when it comes to the design, structure, and properties. First, PROTACs require rational design, especially when it comes to the linker length, but various automated discovery and synthesis platforms and pipelines are being developed rapidly. On the other hand, small-molecule ligands come from nature and are mostly characterized intensively. However, when it comes to designing a small-molecule degrader from scratch, it may prove to be as difficult as for PROTACs. Second, in contrast to PROTACs, molecular glue ligands do not have a linker which results in lower molecular weight and such desirable qualities as enhanced cell permeability and oral bioavailability. Finally, due to their dual nature, heterobifunctional degraders need to bind with the E3 ligase and the target protein simultaneously to induce target degradation. Molecular glue degrader ligands, however, can bind either the E3 ligase complex (more often) or the target protein, and subsequently facilitate their interaction between them. Probabilistically, this increases the efficiency of bringing E3 ligase complex and POI to close proximity.

Overview of Auxin-Inducible Degron (AID)

Auxin-inducible degron (AID) is a protein-degradation technology that utilizes the phytohormone auxin and endogenous ubiquitin proteasome pathway for heterologous targeted protein degradation. The mechanism of auxin-induced protein degradation is based on one of the plant auxin signaling pathways important for growth and development.

In plants, auxin coordinates gene transcription from promoters that contain auxin response elements (AREs) through auxin response factors (ARF) and Aux/IAA (auxin/indole acetic acid) repressors^{50, 51}. ARFs bind specifically to TGTCTC in AREs in promoters of auxin-regulated genes and work with Aux/IAA repressor proteins via hetero- and homo-

dimerization, which depends on auxin^{51, 52}. When the concentration of auxin is low, Aux/IAA repressors dimerize with ARFs on the AREs, blocking ARF function and transcription of auxin-responsive genes. In contrast, when the concentration of auxin increases, the Aux/IAAs are destabilized and degraded, and instead of forming heterodimers with Aux/IAA repressors, ARFs form homodimers AREs, thereby allowing the transcription of auxin-responsive genes.

Most ARFs consist of an N-terminal DNA-binding domain, activation/repression domain, and a C-terminal dimerization domain^{51, 53}. Unlike ARFs, which exert an effect on transcription via auxin-dependent dimerization, transcription inhibition response (TIR1)/auxin signaling F-box (AFB) proteins directly interact with auxin and Aux/IAA protein to mark it for degradation via ubiquitin proteasome pathway. Found through genetic and biochemical studies in *Arabidopsis thaliana*, TIR1 was identified as an auxin receptor and F-box protein involved in the assembly of the SKP1–CUL1–F-box (SCF) E3 ubiquitin ligase^{54- 56}. Next, *Arabidopsis* has 29 members of the Aux/IAA protein family - IAA1–20 and IAA26–34. Common sequence composition among the members contains 4 domains. While domains I, III, and IV are responsible for homo- and hetero-dimerization, domain II is required and sufficient for auxin-dependent degradation in plants via interaction with TIR1⁵⁷. Although Aux/IAA proteins can bind to TIR1 in the absence of auxin, their interaction is enhanced by auxin, which acts as a molecular glue⁵⁸.

Auxin is a collective name for several molecules with a common indole moiety include indole-3-acetic acid (IAA), 4-chloroindole-3-acetic acid, phenylacetic acid, indole-3-butyric acid, and indole-3-propionic acid. IAA is the most prominent representative of auxins, and is primarily used in the AID. Some synthetic analogs of auxin are 1-naphthaleneacetic acid (NAA), 2,4-dichlorophenoxyacetic acid, and 2,4,5-trichlorophenoxyacetic acid. Among synthetic auxins, NAA is used in the AID. The structures of IAA and NAA are shown in **Fig.**

2. In this thesis, IAA was used as a degradation inducer in all experiments with the AID system.

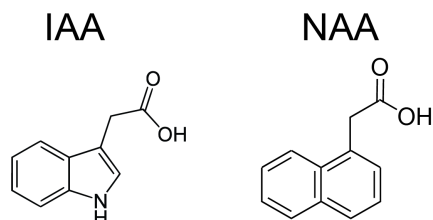


Figure 2. The structure of IAA and NAA. Both molecules are carboxylic acids differing in their aromatic moiety.

Employing this plant pathway, AID was created^{28, 59, 60}. For the AID technology, TIR1 from *Oryza sativa* was selected due to better thermal stability which is necessary for yeast and human cultured cells. Second, the mini-AID (mAID) tag, a short amino acid degron sequence, was derived from the IAA17 protein of *Arabidopsis thaliana*. Molecular modeling and structural analysis revealed that IAA mediates the interaction between the OsTIR1 receptor and mAID tag, as shown in **Fig. 3**^{61, 62}. Similarly, when added to the cell culture medium, IAA brings the OsTIR1 receptor and mAID tag together. OsTIR1 recruits the endogenous SKP1–CUL1–RING E3 ubiquitin ligase, as depicted in **Fig. 4**^{61 - 65}. This leads to the POI–mAID fusion being ubiquitylated and degraded by the proteasome.

In order to establish a human AID mutant cell line for a POI, two genetic modifications are required²⁸. Initially, a parental cell is generated by introducing the OsTIR1 gene at the safe-harbor AAVS1 locus. The second step is tagging an endogenous gene encoding the POI (gene of interest, GOI) with the mAID tag (**Sup. Fig. 1 - 3**)⁶⁶. Both steps are performed using CRISPR–Cas9-based genome editing technique.

Generally, a parental cell line constitutively expressing OsTIR1, such as under a CMV promoter, is preferred since the OsTIR1 expression is uniform. However, sometimes there is

a problem of generating such a cell line due to partial degradation of a POI even in the absence of auxin²⁸. In that case, a parental cell line conditionally expressing OsTIR1, such as under a tetracycline-inducible (Tet) promoter, has to be used. For the latter cell line, the OsTIR1 needs to be expressed by the addition of doxycycline (Dox) which activates the Tet promoter prior to the POI depletion by auxin. This conditional expression system is imperfect in two ways. First, the Dox-induced expression of OsTIR1 is slow, therefore, the subsequent POI degradation efficiency varies among the cells in the same population. Second, during this period some undesirable partial depletion of the POI still takes place before the auxin degradation is initiated. The two drawbacks downgrade the efficiency and speed of protein degradation by the AID system.

Molecular structural analyses revealed that IAA occupies a hydrophobic pocket within the binding pocket of TIR1⁶¹. IAA binding stabilizes the binding pocket and favors the binding of TIR1 to Aux/IAA proteins. Molecular docking experiments provide evidence of the possibility of designing potent auxin agonists and antagonists that can modulate the TIR1 – Aux/IAA interaction⁶⁷⁻⁷¹. Harnessing this idea, it is conceivable that this chemical biology approach can be used to address the problems of AID.

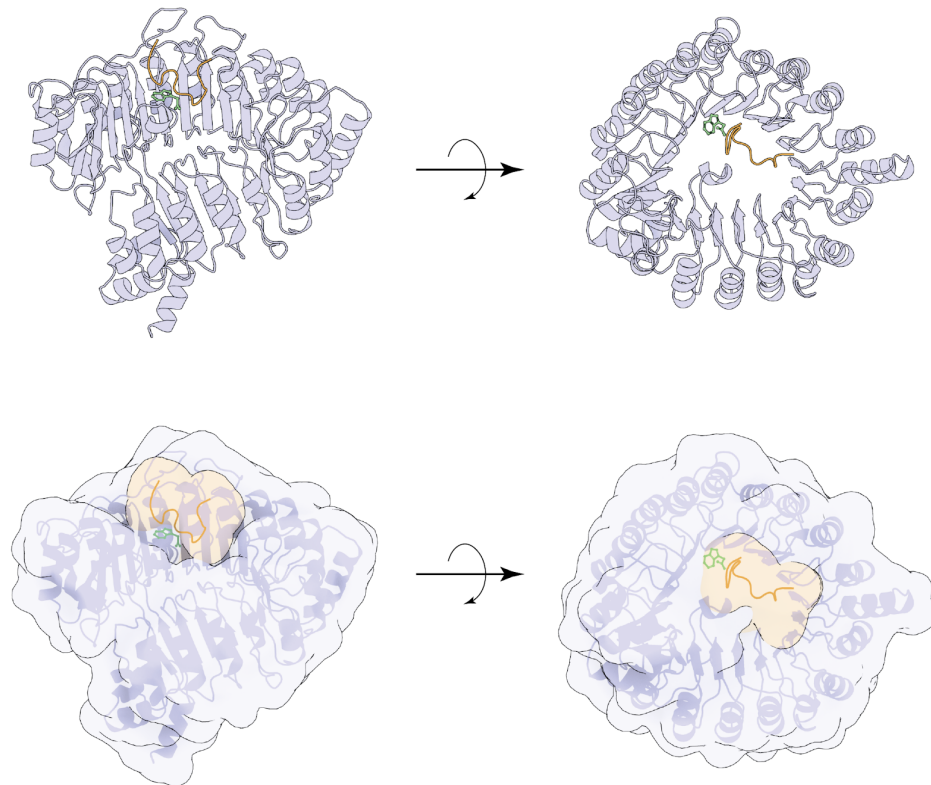


Figure 3. Schematic representation of the tripartite complex formation between OsTIR1, IAA, and mAID. The OsTIR1 is colored purple, IAA – green, and mAID tag – yellow (here IAA7 is used for the illustration)^{61, 62}. IAA occupies a lower part of the binding pocket within OsTIR1, stabilizing the subsequent binding of mAID to OsTIR1. The top row shows the ribbon model, the bottom row shows the space filling model for proteins. The left side shows the side view, the right side shows the top view.

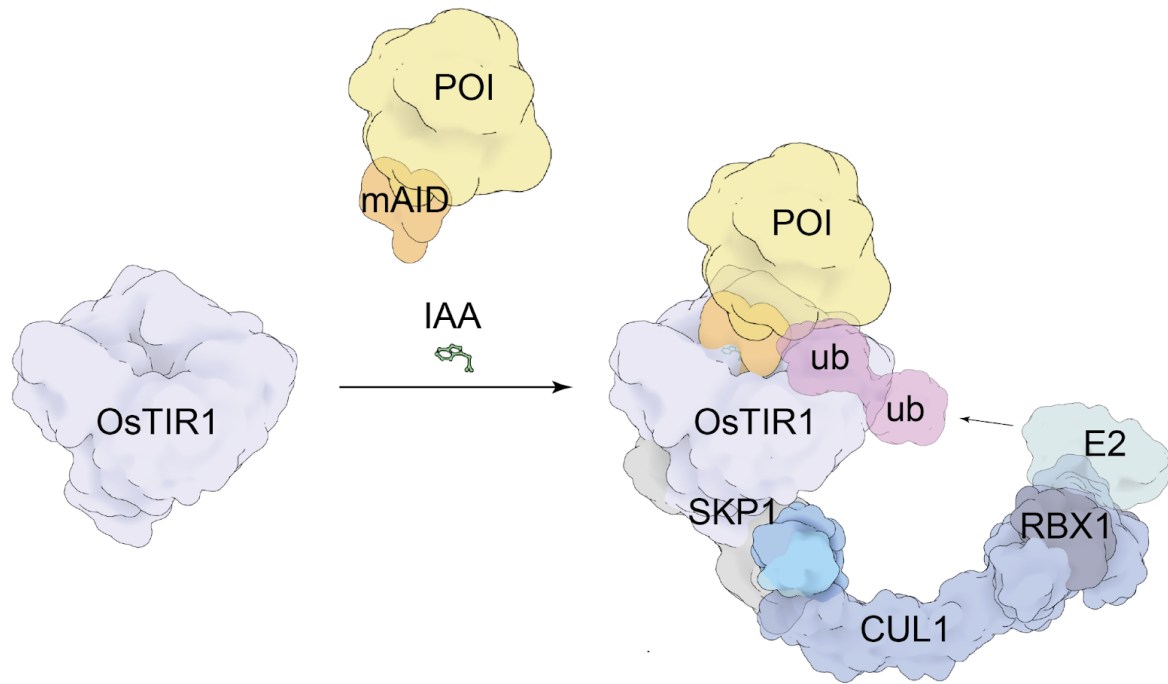


Figure 4. Schematic representation of the ubiquitination of the mAID–fused POI upon the addition of IAA in AID. IAA binds inside the hydrophobic binding site within OsTIR1 and facilitates the interaction of mAID–POI with OsTIR1⁶¹⁻⁶⁵. OsTIR1 acts as F-box subunit of SCF E3 ubiquitin ligase complex, recruiting endogenous SKP1, CUL1, RBX1 and other accessory subunits. Assembled E3 complex recruits E2 which in turn polyubiquitinates mAID–POI, thereby marking it for proteasomal degradation.

Results

Inhibition of OsTIR1 by Auxinole as a Strategy to Suppress Basal Degradation in AID

Molecular modeling suggests that structural IAA analogs with additional moieties that cause steric hindrance can act as potent competitive inhibitors of auxin-inducible degradation. The indole ring of such inhibitors binds the pocket within TIR1 and an additional moiety hinders the binding of the Aux/IAA proteins. Auxinole has been reported to act as such an effective inhibitor for plants including *Arabidopsis thaliana* and *Physcomitrella patens*⁶⁸. Due to the presence of the additional dimethylphenylethyl-2-oxo moiety, auxinole exhibits steric hindrance, thus appears to inhibit the association of OsTIR1 and mAID tag (Fig. 5)⁶⁸. This prompted me to test if auxinole is also applicable to the AID system to suppress basal degradation. Adding auxinole would curb basal degradation, and removing it from the culture medium allow cells to re-express the protein of interest. I initially tested toxicity of auxinole to human colorectal carcinoma cells (HCT116) and confirmed that addition of auxinole to a final concentration of 200 μ M did not affect cell growth at least for 3 days.

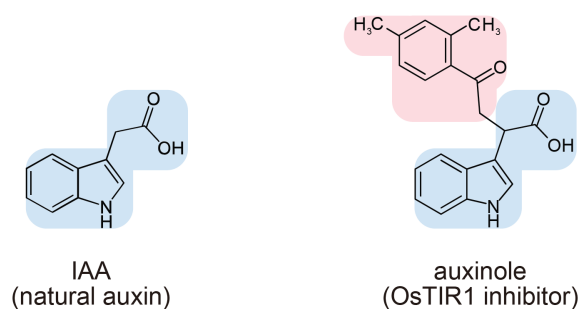


Figure 5. The structure of IAA and auxinole. Auxinole has an additional dimethylphenylethyl-2-oxo moiety (red) which contributes to the steric hindrance to inhibit the interaction of OsTIR1 with auxin and similar compounds.

Next, I tested the functionality of auxinole in the suppression of basal degradation using a subunit of dynein complex, dynein heavy chain 1 (DHC1) as a target. The cytoplasmic dynein complex in mitosis is important for chromosome movements and spindle organization and positioning⁷²⁻⁷⁴. Addition of doxycycline induced OsTIR1 expression, which caused partial depletion of DHC1–mAC and mitotic arrest in many cells in the HCT116 Tet-OsTIR1 background, as reported previously (**Fig. 6A**)²⁸. This showed that OsTIR1 expression, even in the absence of auxin, induced a mitotic phenotype that was analogous to knockdown or inhibition of dynein^{75,76}. The addition of auxinole together with doxycycline clearly suppressed the downregulation of DHC1–mAC and the mitotic arrest (**Fig. 6A**). To test whether DHC1–mAC could be rapidly depleted, I added doxycycline with or without auxinole for 24 h. I monitored the expression levels of DHC1–mAC by flow cytometry, and found that basal degradation was mostly suppressed in the cells treated with doxycycline and auxinole (**Fig. 6B**, boxes in red highlight the difference). Subsequently, the culture media was replaced with fresh one containing doxycycline and IAA, but not auxinole. These results show that DHC1–mAC was rapidly degraded after medium replacement and was mostly depleted within 4 h.

An advantage of AID technology is that the expression level of mAID-fused proteins can be reversibly controlled^{28, 59, 60}. In this respect, auxinole should be useful for re-expression after depletion, because IAA-bound OsTIR1 can remain active for a while, even after the removal of IAA from the culture medium. To test this idea, I used HCT116 CMV-OsTIR1 cells in which the cohesin subunit RAD21 was fused to mAID–mClover (RAD21–mAC)²⁸. Cohesin is one of major chromosome components that controls global chromosome organization in interphase, as well as mediates sister chromatid cohesion, a physical connection formed between newly replicated sisters to ensure their accurate separation during cell division. Initially, I depleted RAD21–mAC by adding IAA for 24 h (**Fig. 7A**).

Subsequently, I replaced the medium with fresh media with or without auxinole, and collected time-course samples to monitor the expression levels of RAD21–mAC by flow cytometry (**Fig. 7B**). I found that recovery of RAD21–mAC was significantly more rapid and sharper when auxinole was added, compared with cells without auxinole. These results suggest that the OsTIR1 inhibitor auxinole is useful for the tight control of the expression of mAID-fused proteins in human cells.

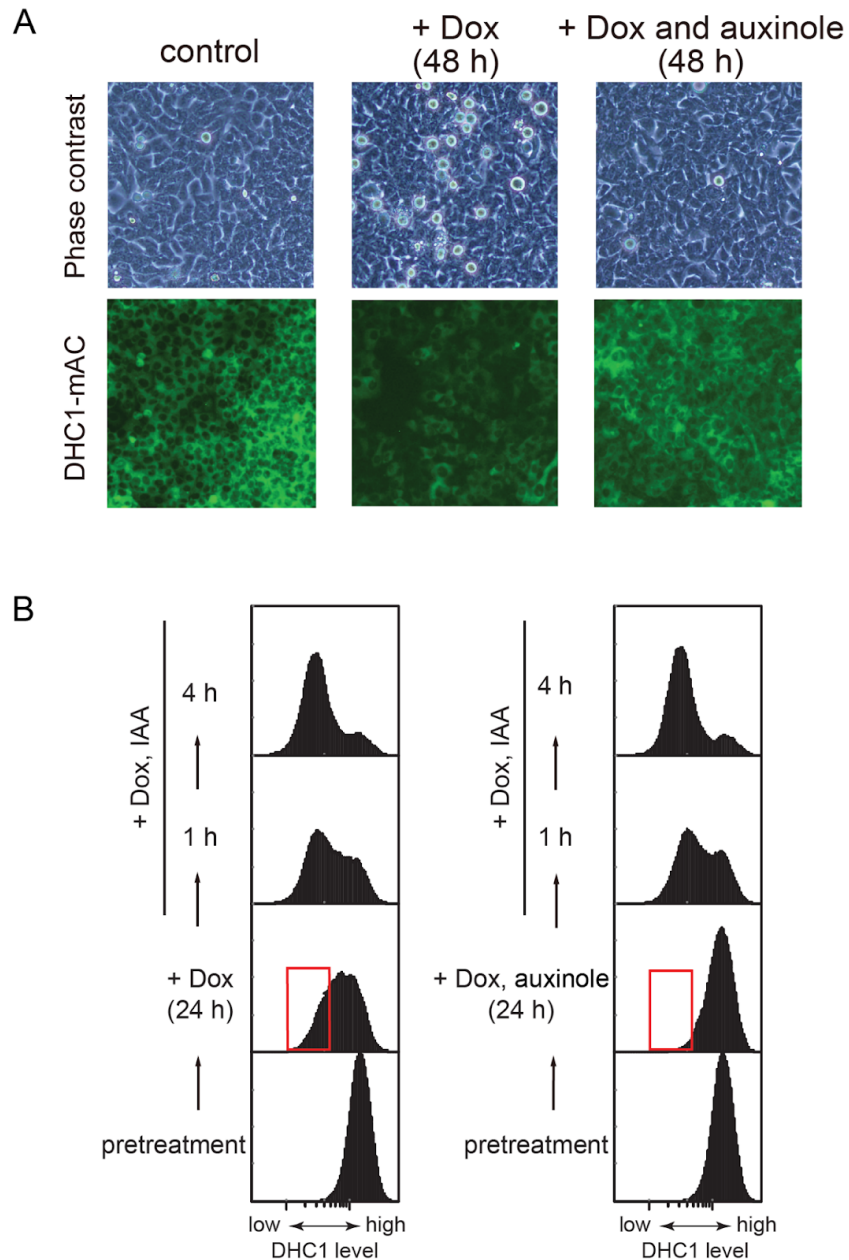


Figure 6. Auxinole inhibits basal degradation in DHC1-mAID-mClover (DHC1-mAC) Tet-OsTIR1 cells. (A) Microscopic images of DHC1-mAC Tet-OsTIR1 cells. The cells were treated with 0.2 $\mu\text{g}/\text{mL}$ of doxycycline (Dox) or Dox with 200 μM auxinole for 48 h before microscopy. (B) Flow cytometry experiment of DHC1-mAC Tet-OsTIR1 cells. The cells were treated with 0.2 $\mu\text{g}/\text{mL}$ of Dox or Dox with 200 μM auxinole for 24 h before replacing the culture medium with Dox and 500 μM IAA.

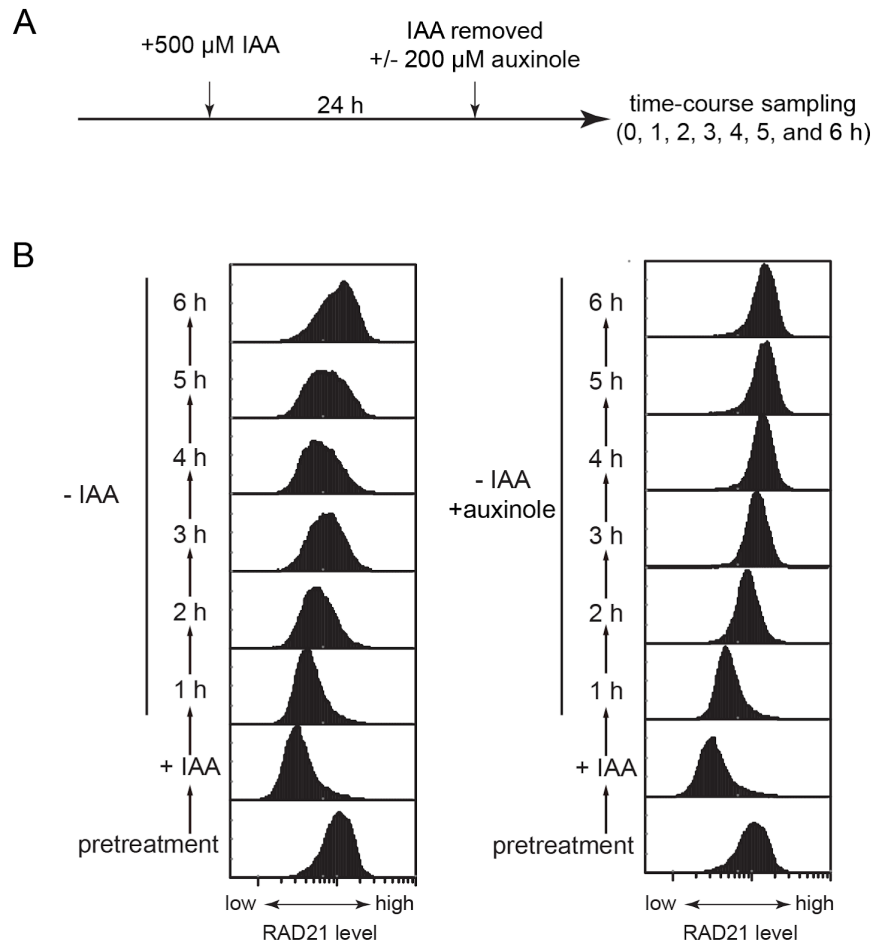


Figure 7. Auxinole facilitates the re-expression of RAD21–mAID–mClover (RAD21–mAC). (A) Scheme of the experimental procedure. The RAD21–mAC CMV-OsTIR1 cells were treated with 500 μM IAA for 24 h before replacing the medium with fresh one containing 200 μM auxinole or without it. (B) Flow cytometry experiment of RAD21–mAC cells.

TOL2 Transposon-based One-Step Construction of AID Mutants

The construction of a new AID mutant cell line for a protein of interest requires two steps as discussed in the overview of AID. This takes more time and labor compared to other ligand-induced protein degradation techniques, such as dTAG or HaloPROTAC. To simplify this procedure, CRISPR–Cas9-mediated gene knockout is combined with the transposon-based supplementation of the mAID-tagged protein of interest together with the OsTIR1 receptor. Specifically, I developed a TOL2 transposon-based bicistronic plasmid expressing the OsTIR1 receptor separated by a P2A self-cleavage sequence from the protein of interest fused with the mAID tag. Transfection with CRISPR-KO plasmid, TOL2-transposon-expressing plasmid, and TOL2 transposase-expressing plasmid can be done simultaneously with stepwise antibiotic resistance selection to harness AID mutants in a one-step procedure⁷⁷.

To control transgene expression, I constructed several bicistronic all-in-one plasmids (**Sup. Fig. 4**). The expression of the first transgene coding for OsTIR1 is controlled by a CAG promoter. The second transgene represents an expression unit with a multiple cloning site (MCS) to insert a cDNA coding the POI and express it fused with a mAID or mAID–EGFP. The first transgene is located upstream the second one, and they are connected via the P2A self-cleaving sequence⁷⁸. Thus, the transcription of the two transgenes happens uninterrupted producing a single product. Afterwards, during translation, OsTIR1 and a mAID-fused protein are cleaved, resulting in the independent expression of OsTIR1 and tagged POI. The transgene expression unit is flanked by TOL2 inverted terminal repeats (ITRs) for the recognition and stable integration to the genome by TOL2 transposase⁷⁹. In addition, these plasmids comprise a puromycin- or hygromycin-resistant marker for selection of clones. I found that these plasmids are fully functional in human HT116 cells, using a nuclear localization signal (NLS) to pAID5.2-N to express OsTIR1 and mAID–EGFP–NLS.

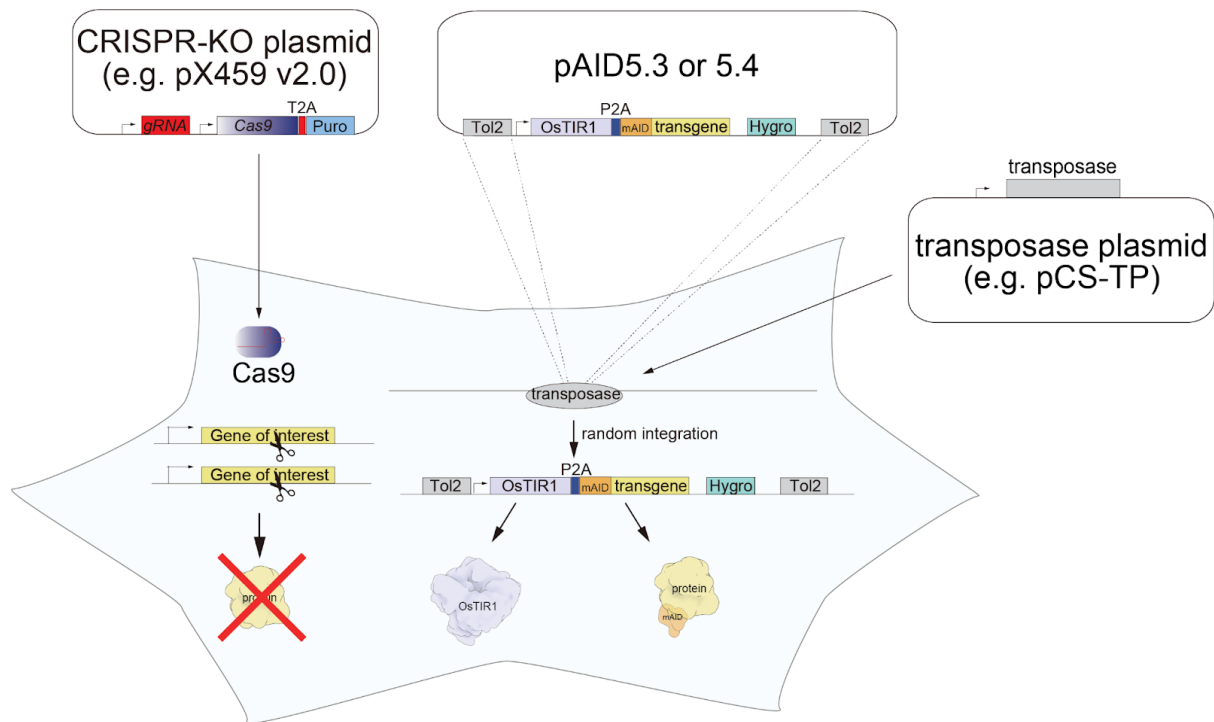


Figure 8. Schematic representation of the construction strategy to generate an AID mutant using CRISPR-KO and bicistronic pAID5 plasmids. The CRISPR-KO plasmid expresses a Cas9–gRNA complex for gene knockout. The bicistronic rescue plasmid is integrated into the genome by the action of TOL2 transposase and expresses both OsTIR1 and mAID-fused protein.

The strategy for generating stable cell lines with this method is shown in **Fig. 8**. To knock out the endogenous gene expressing POI, a CRISPR-KO plasmid is designed so that it cleaves at a specific locus. This plasmid encodes a guide RNA (gRNA), Cas9, and a puromycin resistance gene⁸⁰. Therefore, it is possible to efficiently kill untransfected cells by transiently treating cells with puromycin after transfection. To restore the loss of endogenous POI, I constructed a bicistronic rescue plasmid by cloning POI cDNA in one of the designed plasmids with hygromycin selection marker (**Sup. Fig. 4**). It should be noted that the POI cDNA in the rescue plasmid should contain silent mutations so that it is not recognized by the Cas9–gRNA complex expressed from the CRISPR-KO plasmid. Then, three plasmids, the CRISPR-KO plasmid, the pAID5.3-N-based rescue plasmid, and transposase encoding pCS-TP, are transfected simultaneously into cells. After the transfection, the cells are transiently treated with puromycin and colonies are formed in the presence of hygromycin. Isolated clones are grown and treated with or without 500 μ M IAA for 2 h to degrade POI.

Next, I wished to generate a conditional HeLa mutant for a gene essential for cell viability. As a target, I selected a replication factor, MCM10, which is an essential initiation factor for DNA replication in eukaryotes^{81 - 84}. Using the procedure described above, to knock out the endogenous gene expressing MCM10, I designed a CRISPR-KO plasmid that cleaves the 3' splicing junction at exon 5 (ENSE00000999778). Human MCM10 cDNA was cloned into a pAID5.3-N rescue plasmid. It should be noted that the human MCM10 cDNA in this plasmid was not recognized and cleaved by the Cas9–gRNA complex expressed from the CRISPR-KO plasmid. I transfected the three plasmids, the CRISPR-KO plasmid, the pAID5.3-N-based rescue plasmid, and transposase encoding pCS-TP, into HeLa cells. After the transfection, the cells were transiently treated with puromycin and colonies were formed in the presence of hygromycin. I obtained five positive clones, in which the transgene-derived mAID–MCM10 protein was expressed and the endogenous MCM10 protein was lost. It

should be noted that MCM10 was essential for DNA replication, so that the mAID–MCM10 protein was functional for supporting DNA replication in these clones. Importantly, mAID–MCM10 was depleted by the IAA treatment (**Fig. 9**). Thus, these MCM10 mutant lines generated by one transfection may be used for functional studies of MCM10.

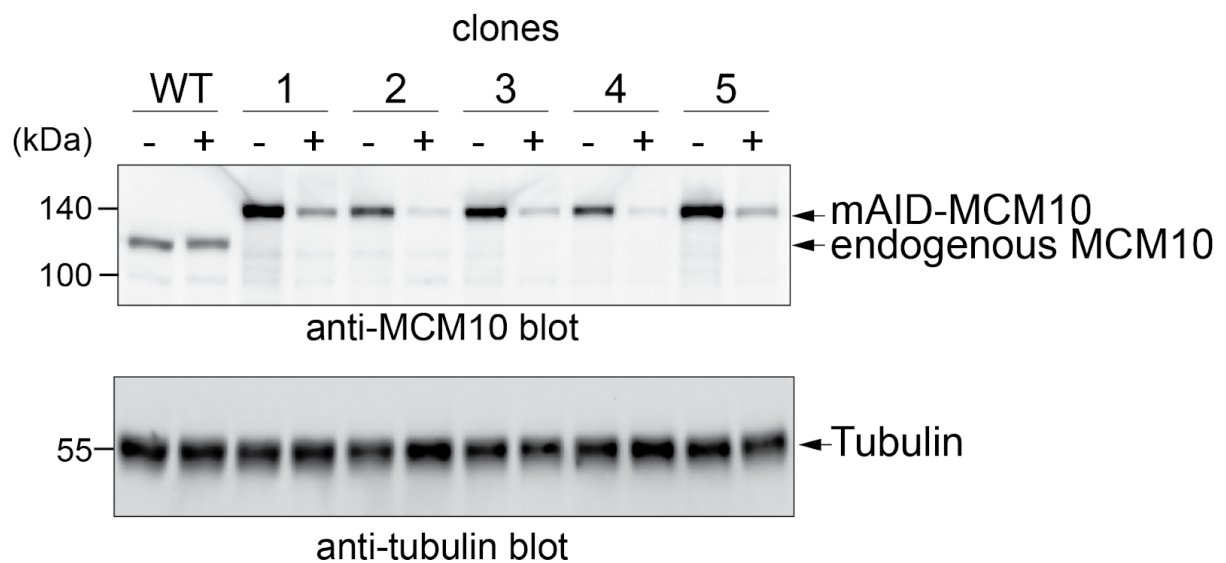


Figure 9. Bicistronic plasmids can be used to generate mAID mutants for functional proteins in one step. Immunoblot to detect endogenous MCM10 and mAID–MCM10. HeLa clones were treated with 500 μ M IAA for 2 h and protein extracts were separated by SDS-PAGE. Tubulin serves as a loading control.

Development of Auxin-Inducible Degron 2

The comparison of the application of various protein degradation strategies demonstrated that AID was not applied to mice. This is because high auxin concentrations are toxic to mice. Moreover, previous efforts to generate the OsTIR1 founder mouse in which target proteins could be tagged failed due to severe basal degradation. For the AID technology to become a useful tool for therapeutic target validation in preclinical research, it was essential to overcome these two major challenges. Several groups attempted to solve these issues, but none succeeded to report the OsTIR1 expressing mouse. One approach to both challenges is increasing the specificity of the receptor-ligand interaction, so that, first, OsTIR1 cannot be activated in the absence of the ligand, and, second, the required ligand concentration is low enough not to exert negative effects on mice.

As introduced in the overview of AID, IAA analogs can be synthesized so that the hydrophobic floor of the TIR1 binding pocket is stabilized even better than in the case of IAA. Similar to this approach, rational design to introduce a mutation in TIR1 binding pocket creating a "hole" and the use of the IAA analog with an additional moiety – "bump" – that can fill up the "hole" can be used to increase the specificity of the AID system to combat both basal degradation and high inducer concentration. This improved version of the system is referred to as Auxin-Inducible Degron 2 (AID2) hereafter⁸⁵.

Following the recent report of the various engineered OsTIR1 mutants and modified auxin compounds in *Arabidopsis thaliana* TIR1 (AtTIR1) – IAA pair to hijack the auxin pathway in plants⁸⁶, I have established an improved AID by using a point-mutation receptor OsTIR1(F74G) (**Fig. 11A**) and an auxin with an additional phenyl group, 5-phenyl-indole-3-acetic acid (5-Ph-IAA) (**Fig. 10**). Other "bumped" IAA analogs tested are listed in **Sup. Fig. 5** and the screening results are shown in **Sup. Fig. 6**.

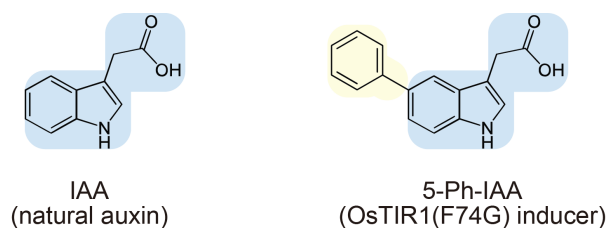


Figure 10. The structure of IAA and 5-Ph-IAA. 5-phenyl-indole-3-acetic acid (5-Ph-IAA) has an additional phenyl moiety (yellow) on the indole ring which occupies the cavity within OsTIR1 created by the F74G mutation.

First, I compared the new system to the original one by monitoring degradation of EGFP reporter protein which is fused with nuclear localization signal (NLS) and mAID (mAID–EGFP–NLS). The strategy for the construction of the reporter cell lines is shown in **Fig. 11B**. First, the mAID–EGFP–NLS construct was transfected to human colon cancer cell line HCT116 cells using piggyBac transposon-mediated random integration. Then, I selected a clone which was highly expressing the EGFP reporter protein by flow cytometry. This was used for the control and parental clone. Subsequently, I introduced the OsTIR1-expressing construct of either WT (used for the original system) or F74G or F74A (two best mutations used in⁸⁶) into the AAVS1 safe-harbor locus using CRISPR–Cas9 system. I confirmed genome integration of the OsTIR1 constructs by PCR amplification and selected clones that contain the constructs in both alleles (**Fig. 11C**). Then, expression of OsTIR1 was checked by Western blotting (**Fig. 11D**). I noticed that the expression levels of the mutant versions of OsTIR1(F74G and F74A) were 5-fold higher than that of WT. When auxinole was added, protein level of the WT OsTIR1 increased to 3-fold. This suggests that the WT version of OsTIR1 is susceptible to proteasome-mediated degradation. Overall, the isogenic background of these cell lines allowed for a direct comparison between the OsTIR1(WT) – auxin pair and the OsTIR1(F74G/A) – 5-Ph-IAA pair. Therefore, the representative clones were selected for further analysis.

Next, I analyzed degradation of the EGFP reporter before and after addition of the auxin derivatives by monitoring the fluorescent intensity of EGFP using flow cytometry (**Fig. 12A, B**). The parental clone that did not contain any TIR1 showed high fluorescent signal and this was used as standard control. I initially compared the EGFP signals of OsTIR1-integrated clones in the absence of the auxin derivatives to test if the mutations in OsTIR1 improve basal degradation. In the cells expressing OsTIR1(WT), the EGFP signal intensity was significantly reduced compared to the parental clone expressing the EGFP reporter only (**Fig. 12B**, compare “reporter only” and “OsTIR1(WT) / ligand –”). This corresponds to basal degradation of the target protein. On the other hand, in cells expressing OsTIR1(F74G/A), the EGFP reporter intensities were virtually same as that in the parental cells without TIR1, suggesting that the modified either of OsTIR1(F74G/A) prevent basal degradation. In all cells expressing different forms of TIR1, the addition of the auxin ligands led to reductions of the EGFP signal intensities, indicating efficient degradation of the EGFP reporter proteins. Interestingly, the degradation was less efficient in the OsTIR1(WT) background compared to the OsTIR1(F74G/A) (**Fig. 12B**).

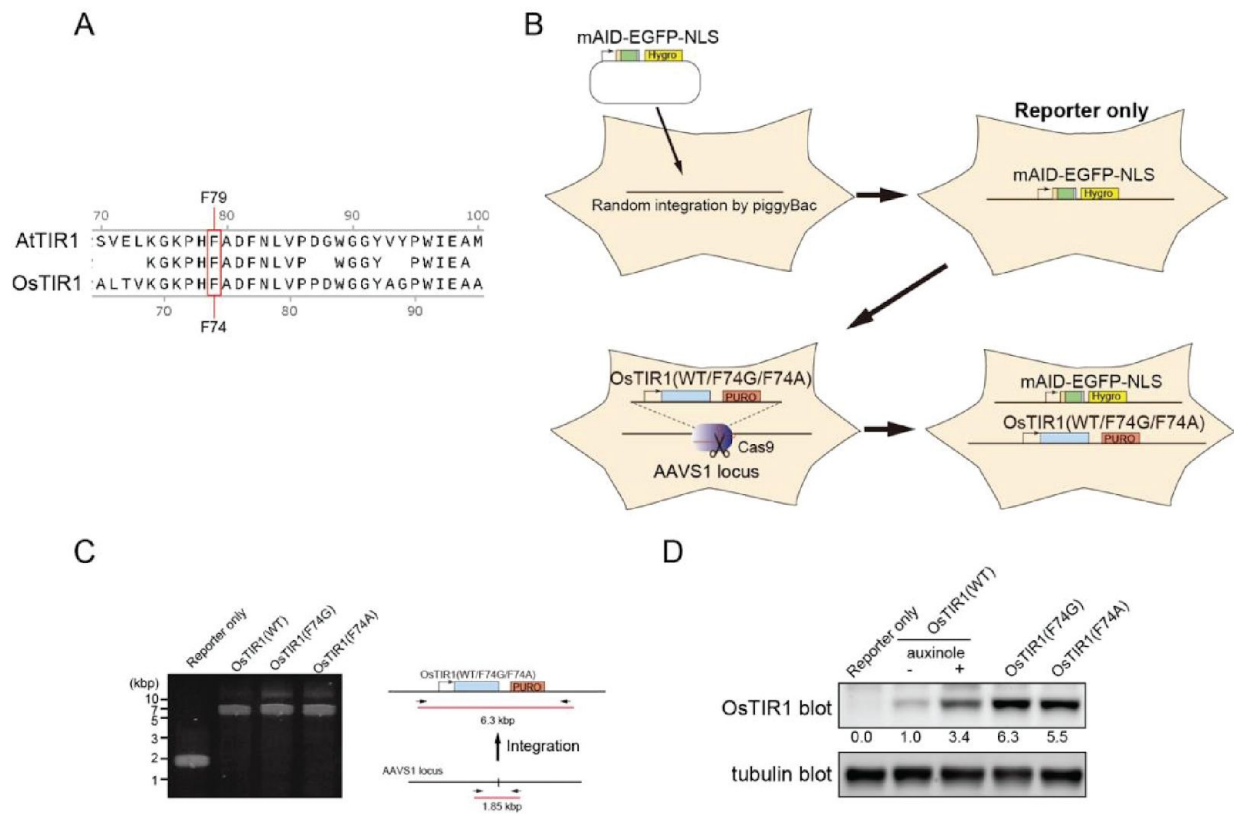


Figure 11. Overview of the reporter construction for direct comparison between the original and improved AID systems. (A) Sequence analysis between AtTIR1 and OsTIR1. The phenylalanine subjected to point mutation is highlighted by the red box. (B) Transfection strategy to generate isogenic reporters. (C) Bi-allelic integration of OsTIR1(WT) and OsTIR1(F74G/A) confirmed by the agarose gel electrophoresis of the PCR amplification product of the region shown on the right. (D) The expression level of OsTIR1(WT) and OsTIR1(F74G/A) analyzed by Western blot. Tubulin is a loading control.

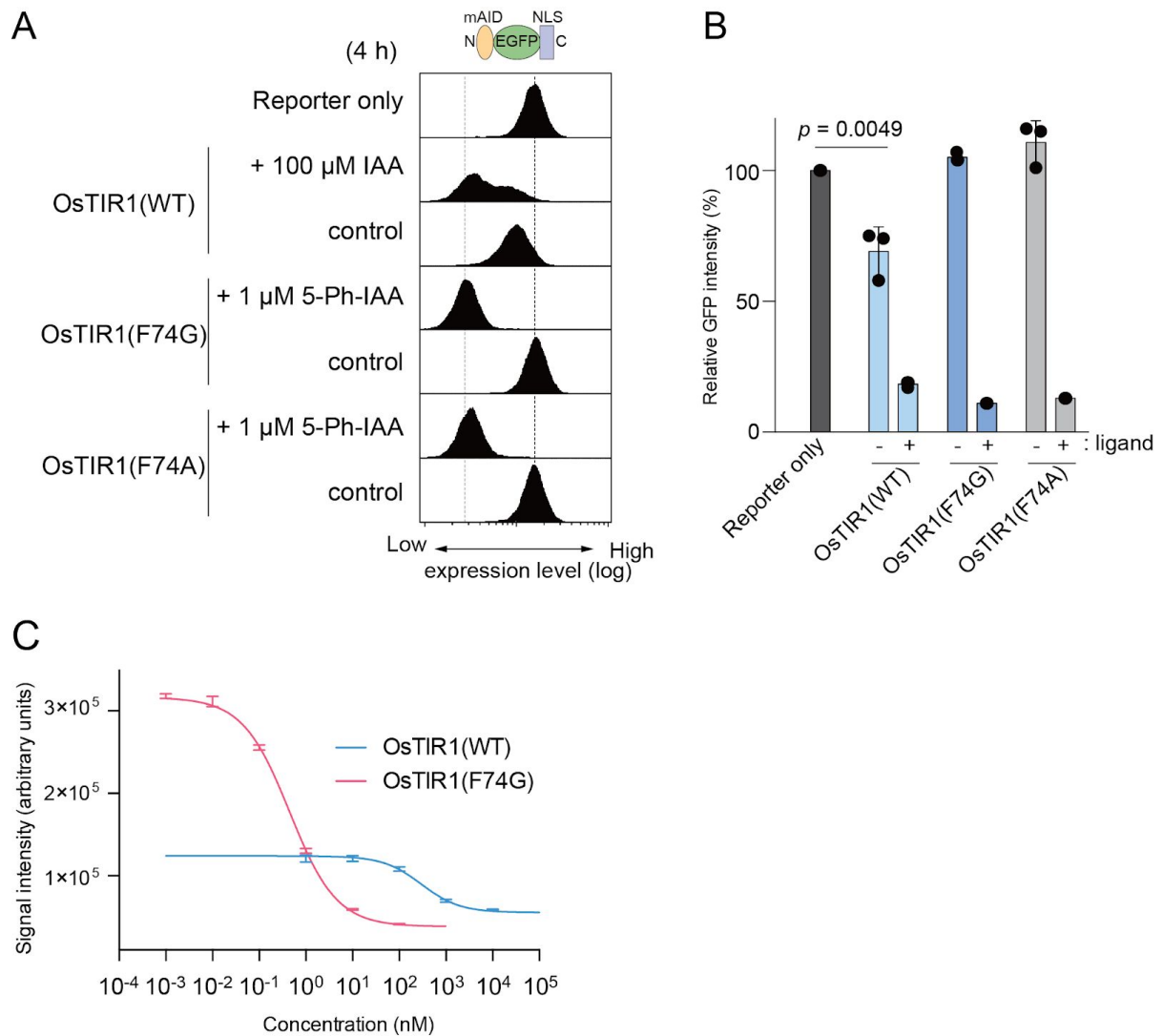


Figure 12. Comparison of the reporter degradation in the OsTIR1(WT) and OsTIR1(F74G/A) background. (A) The histograms of the fluorescent signal intensity before and after the inducer addition. (B) Quantification of the signal in A. Data are presented as mean values \pm SD ($n = 3$ independent experiments, two-tailed t-test). (C) The inducer concentration graph showing the quantification of the fluorescent signal intensity. IAA was used in cells expressing OsTIR1(WT) and 5-Ph-IAA was used in cells expressing OsTIR1(F74G/A). Data are presented as mean values \pm SD ($n = 3$ independent experiments). The data were fitted with non-linear regression using 4 parameters.

The concentration of IAA used in the experiment was higher than that of 5-Ph-IAA. To find the optimal concentration of auxin derivatives, I titrated the concentrations of either IAA (for OsTIR1(WT) or 5-Ph-IAA (for OsTIR1(F74G/A)) and analyzed the EGFP reporter signal by flow cytometry. As shown in **Fig. 12C**, the concentration as low as 10 μ M and 1 nM is sufficient for IAA and 5-Ph-IAA, respectively. Another observation is that the signal before the inducer addition was already drastically reduced due to basal degradation observed in **Fig. 12B**. Moreover, the degradation in the OsTIR1(WT) background did not reach the level seen in the OsTIR1(F74G) background.

To analyze the specificity of the OsTIR1 mutants for auxin derivatives, I tested their reactivity to increasing IAA concentrations. The reporter signal measured by flow cytometry is shown in **Fig. 13**. Overall, OsTIR1(F74G) exhibited less reactivity towards IAA in comparison with OsTIR1(F74A), thus I used the combination of OsTIR1(F74G) with 5-Ph-IAA for further analyses.

Having verified the improvement using the EGFP reporter experiments, I set out to generate the AID cells for DHC1 protein that could not be established using the original system due to the detrimental effect of basal degradation; shown in the part describing the use of auxinole. To generate the AID mutant for DHC1, I followed the strategy shown in **Fig. 14**. Using CRISPR–Cas9, I have knocked OsTIR1(F74G) in the AAVS1 locus in the HCT116 cell line and excised the selection marker using Cre–loxP recombinase. This new parental cell line now can be used for tagging any target protein. Next, using CRISPR–Cas9, I tagged the gene coding DHC1 with mAID–mClover (mAC) at the C-terminus. The indication of the successful tagging transfection came from the stained plates shown in **Fig. 15A**. While in the parental cell line with OsTIR1(WT), almost no clones were observed, there were many clones visible in the parental cell line with OsTIR1(F74G). After genotyping, a single clone was used for further analysis.

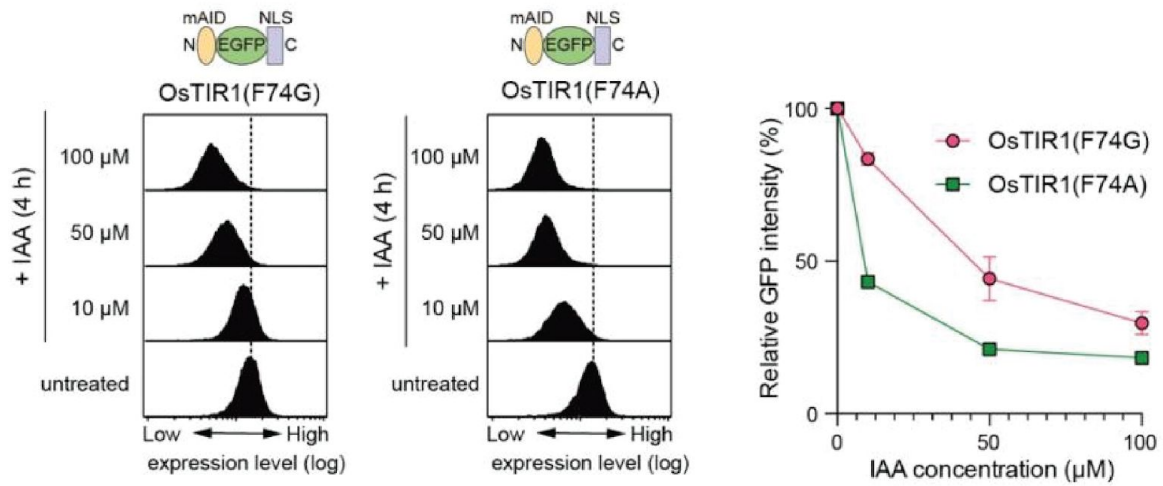


Figure 13. Reactivity of mutant receptors to IAA. The reporter cells were treated with the indicated concentrations of IAA for 4 h. The reporter expression was detected by flow cytometry (left) and quantified data are shown on the right. Data are presented as mean values \pm SD ($n= 3$ independent experiments).

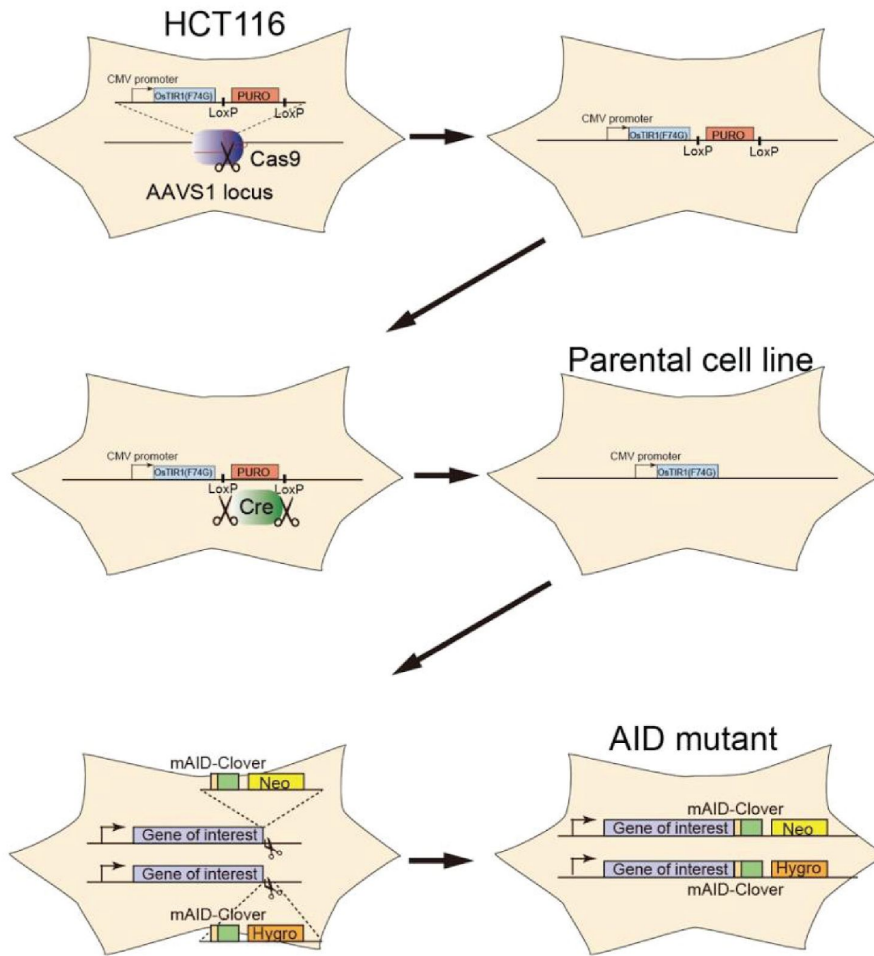


Figure 14. The schematic of the strategy for AID mutant generation in the improved system. After the initial CRISPR–Cas9-mediated knock-in of *OsTIR1(F74G)* and antibiotic-resistance selection of positive clones, the puromycin selection marker was removed using the Cre–loxP recombination system to generate a new parental cell line for AID2. The following tagging of the gene of interest is the same as in the original technology.

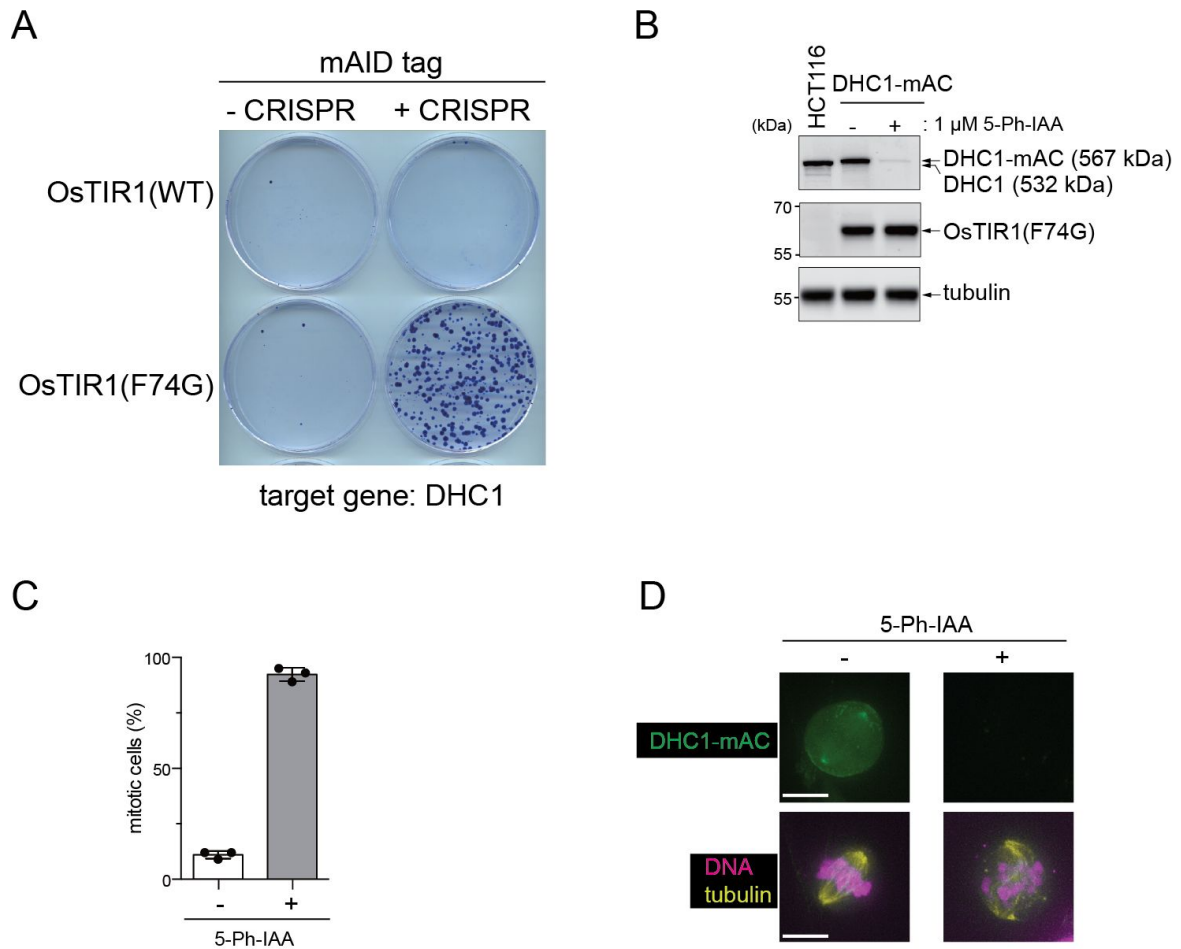


Figure 15. DHC1 degradation analysis. (A) Stained plates showing colonies formed after transfection tagging DHC1. Colonies were formed in the presence of 700 μ g/ml of neomycin and 100 μ g/ml of hygromycin for 11 days. (B) Western blotting showing the degradation of DHC1-mAC after 6-h treatment. Tubulin is a loading control. (C) Calculated mitotic index upon DHC1-mAC degradation. Data are presented as mean values \pm SD ($n=3$ independent experiments). (D) Microscopic images showing DHC1-mAC, DNA, and tubulin upon DHC1-mAC degradation. Scale bars show 11 μ m.

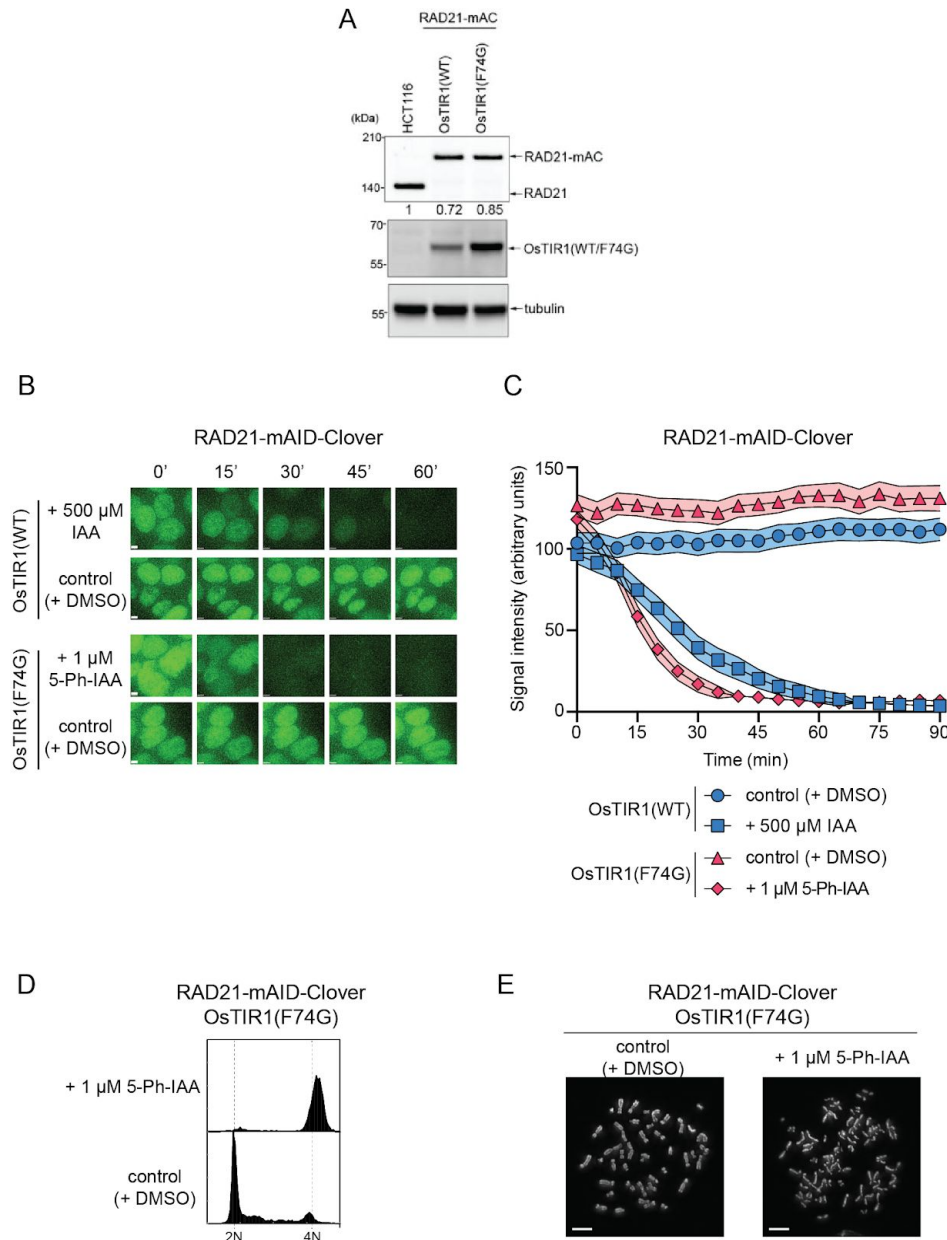


Figure 16. RAD21 degradation analysis. (A) The initial expression level of RAD21-mAC and OsTIR1. Tubulin is a loading control. RAD21 bands were quantified and these values are shown below the RAD21 blot. (B) Time-lapse microscopy images. Scale bars show 3.2 μm . (C) Quantification of the signal in the time-lapse microscopy experiment in B. Data are presented as mean values of 95% confidence interval ($n=60$ cells examined). (D) Cell cycle analysis upon RAD21-mAC degradation with 1 μM 5-Ph-IAA for 24 h. (E) Mitotic chromosome spread analysis upon RAD21-mAC degradation with 1 μM 5-Ph-IAA for 2 h. Scale bar shows 5.4 μm .

First, I confirmed the degradation of DHC1–mAC after a 6-hour treatment with 1 μ M 5-Ph-IAA by Western blot shown in **Fig. 15B**. The shifted tagged DHC1–mAC band completely disappeared after the inducer treatment. Next, using microscopy, I observed the mitotic arrest upon the treatment with 1 μ M 5-Ph-IAA for 24 hours (**Fig. 15C**), which is a phenotype of the DHC1 depletion. Finally, I have observed a strong defect in chromosome alignment and spindle formation in DHC1–mAC-depleted fixed cells in line with the function of the dynein complex (**Fig. 15D**).

Having confirmed that the improved AID can be established for proteins that were difficult to tag, I decided to test whether it can also improve the degradation speed at a low concentration for already successfully generated AID mutants. For this, I chose the RAD21 subunit of the human cohesin complex; shown in the part describing the use of auxinole.

Using the new parental cell line expressing OsTIR1(F74G) (**Fig. 14**), I have tagged the C-terminus of the gene coding for RAD21 with mAC. After genotyping, a single clone was used for further analysis. I confirmed the expression of RAD21–mAC and TIR1 by Western blot shown in **Fig. 16A**. From the band intensity quantification, RAD21–mAC signal is less in the OsTIR1(WT) background in comparison with the OsTIR1(F74G) background (0.72 vs 0.85, respectively) suggesting basal degradation happens with RAD21–mAC, although not easily visible. In addition, there is a noticeable difference in the expression of the TIR1.

Next, to track the degradation kinetics, I performed time-lapse imaging of RAD21–mAC in live HCT116 cells (**Fig. 16B**). For degrading RAD21–mAC, 500 μ M IAA was used in the case of OsTIR1(WT)-expressing cells and 1 μ M 5-Ph-IAA in the case of OsTIR1(F74G)-expressing cells. I initially compared the RAD21–mAC intensities of OsTIR1(WT) and OsTIR1(F74G) clones in the absence of auxin derivatives. At any time-point, the fluorescent intensities in the OsTIR1(F74G) clone were higher than those of the OsTIR1(WT) clone (**Fig. 16C**, compare “control (+ DMSO)”). Thus, the currently

established AID system appears to inhibit basal degradation of Rad21–mAC as compared to the original system. This means that although with the original AID system RAD21 tagging could be achieved, there was still basal degradation taking place. This is in agreement with the reporter basal degradation observed in the cells expressing OsTIR1(WT) shown in **Fig. 12**. To assess degradation kinetics, I have fitted the plot to the one-phase decay model and calculated the half-time $T_{1/2}$, which represents the time required to degrade half of the initial amount of the protein. The $T_{1/2}$ for OsTIR1(WT) and OsTIR1(F74G) was 26.5 min and 11.7 min, respectively, indicating that RAD21–mAC was degraded more quickly by the new system. These results indicate that the improved system allowed sharper and quicker control of RAD21–mAC than the original AID system.

To study the effect of RAD21 depletion on cells, I have analyzed the cell cycle using propidium iodide staining. After RAD21–mAC was depleted, most of the cells were arrested in the G2/M phase, as seen from **Fig. 16D**. In addition, I prepared the mitotic chromosome spread to inspect how sister chromatid cohesion is affected by RAD21 degradation. As expected, upon RAD21–mAC depletion, almost all sister chromatids were separated from each other, as shown in **Fig. 16E**, which is consistent with the essential function of this protein complex.

Discussion

AID is an excellent protein degradation technique for functional studies. However, the two main drawbacks that held it from being applied to mice is the leaky degradation of the target protein and toxicity of auxin at high concentration. In the first part of this chapter, I report the use of the degradation inhibitor auxinole for suppressing leaky degradation. In the second part, I showed a method to generate AID mutants in one step using all-in-one TOL2-transposon based vectors, which may be used for targeting proteins in polyploid cell lines

(such as HeLa) or serve as an efficient screening method. Finally, I show that both problems can be solved in the improved AID with the mutant OsTIR1(F74G) receptor and auxin analog 5-Ph-IAA.

First, to suppress basal degradation in cells expressing OsTIR1, I used the OsTIR1 antagonist auxinole. Even in the Tet-OsTIR1 background cells, it is now possible to induce rapid degradation of mAID-fused proteins by inducing OsTIR1 in the presence of auxinole. Moreover, auxinole is useful for the re-expression of mAID-fused POIs after depletion. The use of auxinole allows the quick degradation and robust control of the expression of mAID-fused POIs.

In the second part, I showed a series of all-in-one pAID5 plasmids that enable conditional degradation control of a mAID-fused POI. By using one of them, I demonstrated a method to generate an AID mutant of HeLa cells, in which MCM10 was conditionally degraded by adding IAA. It should be noted that the level of expression of mAID–MCM10 in clones 2 and 4 was more or less comparable to that in WT cells (**Fig. 9**). Because MCM10 is essential for viability, and multiple copies of the rescue plasmid can be integrated into the genome, clones having a sufficient level of mAID–MCM10 might have been positively selected during colony formation. In other words, it might be possible to select clones optimally expressing a mAID-fused POI by the strategy shown in **Fig. 8**. This strategy is less laborious than tagging an endogenous gene in all alleles, in particular when polyploid cell lines such as HeLa are used. It should be noted that the transcriptional regulation of a mAID-fused transgene is different from that of the endogenous gene. Therefore, the transgene cannot be controlled transcriptionally by endogenous biological processes, such as the cell-cycle control system.

Finally, in the AID2, the mutant for DHC1 can be constructed in cells constitutively expressing the receptor. Interestingly, even in the reporter cell lines and in the AID mutants

that could be generated with the original system, basal degradation still takes place, as can be seen from **Fig. 12** and **16B, C**. In addition, as evident from **Fig. 11D** and **16A**, in most cases, the expression level of OsTIR1(WT) decreases and results in subsequent inefficient degradation that requires high concentrations of IAA. This reduction in the expression level may be due to the basal degradation in which OsTIR1 is degraded together with the target reporter protein.

Subsequently, I applied the improved AID technology to confirm the loss of sister chromatid cohesion and G2/M arrest upon quicker degradation of the RAD21 subunit of cohesin in HCT116 cells. Although RAD21 could be targeted and degraded with the original system, in the new system the degradation kinetics is faster and basal degradation is reduced. Similarly, the improved AID may show enhanced efficiency for other target proteins. Another important aspect is the reduced concentration of the inducer used in the improved AID. As shown in **Fig. 12C**, a concentration as low as 1 nM is enough to efficiently degrade the reporter. Of course, this concentration of the new inducer may vary depending on the target protein, but so far, all functional proteins tested can be degraded with 1 μ M 5-Ph-IAA. This significant reduction in concentration paves the way to the use of the AID in mice.

Therefore, the main goal of this study to significantly improve the AID system, namely deal with the issues of basal degradation and high auxin concentration have been achieved. The updated AID2 is a robust technology that can be applied to many difficult targets. Moreover, AID2 can be used in mice and targeting functional proteins in murine models is awaited.

Materials and Methods

General AID cell line construction

HCT116 cells (ATCC, #CCL-247) were cultured in McCoy's 5A, supplemented with 10% FBS (Gibco, #26140-079), 2 mM L-glutamine, 100 U/ml penicillin, and 100 µg/ml streptomycin at 37°C in 5% CO₂. Cells were transfected with CRISPR–Cas9 and donor plasmids using FuGENE HD Transfection Reagent (Promega, #E2311) in a 12-well plate. One day after transfection, cells were plated in 10 cm dishes and selected with antibiotics. Selected clones were isolated and confirmed by following a published protocol⁶⁶. Confirmation of bi-allelic insertion of OsTIR1(WT, F74G, or F74A) at the AAVS1 locus was done using genomic PCR. The indicated primers shown in **Fig. 11C** as arrows (5'-CACTTTGAGCTCTACTGGCTTCTGC-3' and 5'-CCACCCAAAAGGCAGCCTGGTAGAC-3') were used for genomic PCR.

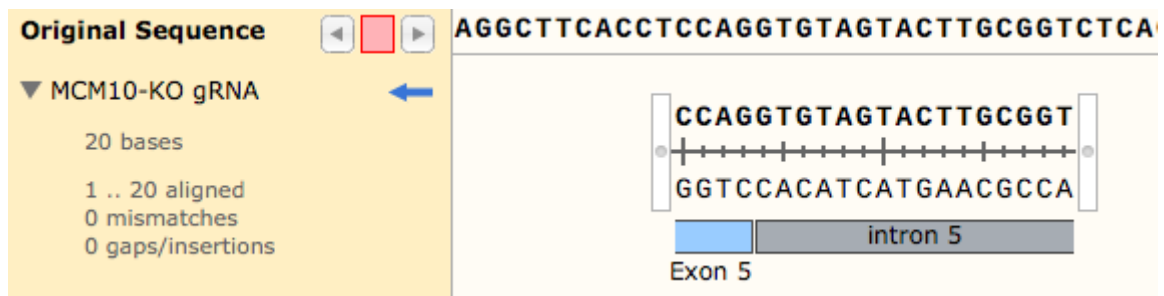
Plasmids for CRISPR-KO- and TOL2-transposon-combined one-step AID mutant generation

The pAID5 plasmids sequence information is available from the Addgene repository.

To construct a CRISPR-KO plasmid for targeting MCM10, two oligonucleotides (5'-CACCGACCGCAAGTACTACACCTGG-3' and 5'-

AAACCCAGGTGTAGTACTTGCGGTC-3') were hybridized. The hybridized DNA was cloned at the BbsI site of pX459 v2.0 (addgene, #62988).

The MCM10-KO gRNA sequence is highlighted in green and is complementary to the endogenous MCM10 splice site between the 3' end of exon 5 (ENSE00000999778) and intron 5 (ENSG00000065328:ENST00000378714.8 intron 5:protein_coding):



Thus, the MCM10-KO gRNA does not align with the transgene MCM10 cDNA at all, so the transgene MCM10 cDNA cannot be recognized and cleaved by Cas9.

An expression plasmid encoding TOL2 transposase, pCS-TP, was previously described⁸⁰.

HeLa cell culture, transfection, and isolation of clones

HeLa cells were cultured in DMEM, supplemented with 10% FBS, 100 U/mL penicillin, and 100 µg/mL streptomycin at 37°C under an atmosphere of 5% CO₂ in air. HeLa cells were seeded at 0.5×10^5 cells per well in a 6-well plate. A plasmid mixture was prepared by mixing 8 µg of CRISPR–Cas9-KO (CRISPR-KO) plasmid, 200 ng of pAID5-based plasmid, and 200 ng of pCS-TP. Opti-MEM (Thermo Fisher Scientific, #31985062) was added to bring the final volume to 50 µL. Subsequently, 4 µL of FuGENE HD Transfection Reagent (Promega, #E2311) was added. After incubating the transfection mixture for 15 min, the mixture was applied to the cells. One day after transfection, the cells were collected, resuspended in 2 mL of medium, and seeded in a 10-cm dish, which contained 10 mL of medium with 1 µg/mL puromycin. Two days later, the medium was exchanged with fresh medium containing 200 µg/mL hygromycin B without puromycin. The culture medium containing hygromycin B was exchanged every three to four days until colonies became visible. Colony formation took 19 to 22 days.

Addition of inducers

Indole-3-acetic acid (IAA) and 5-phenyl-indole-3-acetic acid (5-Ph-IAA) were dissolved in DMSO to make a 500 mM stock solution, and further diluted with DMSO to an appropriate concentration before the experiment. In experiments using cells expressing a reporter (mAID–EGFP–NLS), the culture medium was replaced with the medium containing an appropriate concentration of ligands. For inducing degradation of an endogenous protein fused with mAID, IAA or 5-Ph-IAA was added directly to the culture medium at an appropriate concentration. For control, the same volume of DMSO was added to the culture medium.

Flow cytometry

HCT116 cells were seeded at 1×10^5 cells/well in a six-well plate and grown for two days. For detecting EGFP and mClover signals after ligand treatment, cells were trypsinized and fixed in 4% methanol-free paraformaldehyde phosphate buffer (FUJIFILM Wako Pure Chemical Corporation) at 4°C overnight. Fixed cells were washed and resuspended in PBS containing 1% BSA. For measuring the DNA signal after ligand treatment, cells were trypsinized and fixed in 70% EtOH. Fixed cells were washed, resuspended in PBS containing 1% BSA, 50 µg/ml of RNase A, and 40 µg/ml of propidium iodide, and incubated at 37°C for 30 min. Flow cytometric analysis was performed on a BD Accuri C6 machine (BD Biosciences) using FCS4 Express Cytometry software (DeNovo Software). 10,000 cells were analyzed from each sample.

Western blot

HCT116 cells were seeded at 1×10^5 cells/well in a six-well plate and grown for two days. After 1 μ M 5-Ph-IAA treatment, cells were lysed in RIPA buffer (25 mM Tris-HCl pH7.6, 150 mM NaCl, 1% NP40, 1% sodium deoxycholate, 0.1% SDS). After centrifugation, the supernatant was mixed with 2xSDS sample buffer (Tris-HCl pH6.8, 4% SDS, 20% glycerol, 10% 2-mercaptoethanol, 0.004% bromophenol blue) before incubation at 95°C for 5 min. Equal amounts of protein (measured using Bradford (Bio-Rad Smart Spec 3000) assay) were loaded onto a TGX Stain-Free gel (Bio-Rad) and transferred onto a Hybond ECL membrane (GE Healthcare). The membrane was incubated with a primary antibody at 4°C overnight and subsequently incubated with a secondary antibody at room temperature for 3 h. Detection was performed using the Amersham ECL Prime reagents (GE Healthcare) in case of using an HRP-conjugated secondary antibody and images were acquired with a ChemiDoc Touch MP system (Bio-Rad). For protein detection, the following commercially available antibodies were used. Primary antibodies: anti-OsTIR1 (MBL, #PD048), anti-mAID (MBL, #M214-3), anti-DHC1 (SantaCruz, #sc-9115), anti-alpha-tubulin (MBL, #M175-3). All primary antibodies were used at a 1 in 1000 dilution with TBST containing 5% skim milk. Secondary antibodies: anti-rabbit IgG HRP (GE Healthcare, #NA934), anti-mouse IgG HRP (SantaCruz, #PI-2000), anti-rabbit IgG StarBright Blue 700 (Bio-Rad, #12004161). All secondary antibodies were used at a 1:5000 dilution with TBST containing 5% skim milk.

Live-cell imaging

HCT116 cells cultured in McCoy's 5A medium without phenol red, supplemented with 10% FBS (Gibco, #26140-079), 2 mM L-glutamine, 100 U/ml penicillin, and 100 μ g/ml streptomycin were imaged on a DeltaVision deconvolution microscope (GE Healthcare) equipped with an incubation chamber and a CO₂ supply system.

Microscopy

To visualize nuclei, 0.2 μ M SiR-DNA (Spirochrome) was added for 3 h (**Fig. 16E**) or 24 h (**Fig. 15D**) before observation. To visualize tubulin, cells were treated with CellLightTM Tubulin-RFP, BacMam 2.0 (Thermo Fisher Scientific) for 24 h before observation on a DeltaVision deconvolution microscope (GE Healthcare) (**Fig. 15D**). To calculate the mitotic index shown (**Fig. 15C**), brightfield images after 5-Ph-IAA treatment were acquired using an EVOS XL Core Configured Microscope (Thermo Fisher).

Chromosome spread

HCT116 cells were cultured to 70% confluency in a 60-mm dish. KaryoMAXTM ColcemidTM Solution in PBS (Gibco, #15212012) was added to a final concentration of 0.02 μ g/ml together with DMSO (control) or 1 μ M 5-Ph-IAA. Treated cells were incubated at 37°C 5% CO₂ for 2 h before trypsinization. Removed cells were treated with 75 mM KCl before fixation in MeOH/acetic acid (3:1) fixative solution. Fixed cells were adjusted to approximately 10⁷ cells/ml. Ten microliters of the cell suspension were applied onto a glass slide and dried at room temperature. Ten microliters of DAPI-containing Vectashield Mounting Medium (Vector Laboratories, #H-1200) was added before sealing with a coverslip. Chromosomes were observed under a DeltaVision deconvolution microscope (GE Healthcare).

Chapter 2

Biochemical Characterization of The Fission Yeast Cohesin Complexes

Introduction

During cell division, all sets of newly replicated chromosomes are successfully delivered to the daughter cells. In mitosis, spindle fibers emanating from both cell poles selectively capture sister chromatid pairs at kinetochore and convey them to the dividing cells. The fidelity of segregation is ensured by physical connection formed between replicated sister chromatids, called sister chromatid cohesion. “Cohesion” provides physical tension when spindle fibers from opposite poles attach to cohesive chromatids. This physical tension eventually dictates accurate establishment of bipolar spindle attachments among all sets of sister chromatid pairs, leading to error-free chromosome separation at anaphase.

Sister chromatid cohesion is formed by a cohesin complex, a ring-shaped ATPase assembly that holds two sister chromatids together^{87- 89}. Cohesin is composed of four subunits, Smc1, Smc3, Scc1 and Scc3 (Psm1, Psm3, Rad21 and Psc3 respectively, in the fission yeast *Schizosaccharomyces pombe*) (**Fig. 17**)⁹⁰. At the center of cohesin is a pair of structural maintenance of chromosomes (SMC) subunits, long flexible coiled coil proteins that form a heterodimer via hinge domain. At the opposite ends, the SMC ATPase heads dimerize upon ATP binding. Scc1 kleisin subunit further bridges both heads together to complete the proteinous ring. Scc1 also serves as a docking platform for the Scc3 HEAT-repeat subunit as well as other regulatory proteins⁹¹. Cohesin has been shown to have an ability to topologically embrace DNA, which is driven by SMC ATPase heads^{92, 93}.

Therefore, cohesin is thought to function as a topological device to hold a sister chromatid pair. In addition to sister chromatid cohesion, cohesin also contributes different chromosome

structures and activities including chromatin loop formation, gene regulation as well as DNA repair^{94, 95}.

Cohesin by itself is an inactive complex and requires a series of regulatory proteins to regulate sister chromatid cohesion. From telophase to G1, cohesin is loaded onto chromatin with an aid of the loader complex which is composed of Scc2 and Scc4 (Mis4 and Ssl3 respectively in the fission yeast)^{96, 97}. At the same time, cohesin also dissociates from chromatin in Pds5-Wapl dependent manner^{98 - 101}. Thus, cohesin displays dynamic chromatin association before creating sister chromatid cohesion¹⁰². During DNA replication, cohesin establishes “cohesion” between newly replicated sister DNAs¹⁰³. However, cohesin loading per se is not sufficient to create sister chromatid cohesion and requires additional establishment reactions, which occur at the replication fork. How cohesin creates “cohesion” is not fully understood. This process, at least, involves cohesin acetylation (Smc3’s ATPase heads) mediated by Eco1^{104 - 107}. This acetylation antagonizes Pds5-Wapl, thus stabilizes the cohesin molecules that mediate sister chromatid cohesion. In addition to Eco1, replisome-associated proteins including Csm3/Tof1, Mrc1, Ctf4, Chl1 also redundantly function in cohesion establishment^{108 - 111}. When a cell enters mitosis, cohesin dissociates from chromatin by two distinct pathways to achieve acute and faithful chromosome segregation. In mammalian cells, cohesin on chromosome arms are dissociated by Pds5-Wapl at prophase⁹⁸. Scc3 subunit is phosphorylated by Polo-like kinase 1, this appears to facilitate cohesin dissociation by Pds5-Wapl¹¹². At anaphase, residual cohesin on pericentromeric regions are cleaved by separase, allowing synchronous chromosomal separation (**Fig. 18**)¹¹³. Separase digests two specific sequences of Rad21 kleisin subunit, thus physically opens up the cohesin ring to facilitate its dissociation from chromatin. This cleavage is also facilitated by phosphorylation of Rad21, thus cohesin stability on chromatin is highly regulated by a series of protein modifications^{90, 114, 115}.

Biochemical studies using the purified fission yeast cohesin provides several molecular insights into how cohesin loads and dissociates from DNA¹¹⁶. Cohesin topologically embraces DNA in an ATP-dependent manner, which is stimulated by the loader complex. The loader initially forms a ternary complex with cohesin on DNA, then transports DNA into the proteinous ring¹¹⁷. In contrast, Pds5-Wapl promotes cohesin dissociation from DNA, by transiently opening Psm3^{Smc3}-Rad21 interface¹¹⁸. These studies have also demonstrated that acetyl-accepter lysins on Psm3^{Smc3} head function as a DNA sensor to facilitate both cohesin loading and dissociation. This implies that cohesin acetylation erases the DNA sensor to stop cohesin dynamics on DNA, leading to stable cohesin association that is required for establishment of sister chromatid cohesion. In addition to bulk biochemical analyses, single-molecule studies of human cohesin have demonstrated cohesin dynamics on DNA including, random diffusion, ATP-dependent directional movement as well as DNA loop formation¹¹⁹⁻¹²². Furthermore, recent structural studies using cryo-electron microscopy have revealed the loading intermediate state of cohesin/loader complex¹²³⁻¹²⁵. Together, biochemical studies start to reveal cohesin's mechanical properties that handles series of genome organization.

Like in somatic cells, cohesin is also vital for proper chromosome segregation during meiosis¹²⁶. In meiosis, the kleisin subunit (Rad21) is commonly replaced to Rec8 (hereafter, Rec8-cohesin)¹²⁷. Meiosis is a special type of cell division which generates haploid gametes in sexual reproduction. This process consists of a single round of DNA replication, followed by two consecutive rounds of chromosomal segregation. At the first division, homologous chromosomes are separated and delivered to dividing cells (Meiosis I). Sister chromatids are segregated during meiosis II, in a similar way to somatic cells. Therefore, meiosis I is qualitatively distinct from meiosis II and mitosis¹²⁶. Two factors drive homologous chromosome segregation; chiasmata formation between homologues and monopolar spindle attachment. Rec8-cohesin plays essential roles in both pathways. During meiotic prophase I,

homologous chromosomes are paired and aligned by forming a higher-order proteinaceous structure called synaptonemal complex^{128, 129}. At this stage, pairs of paternal/maternal chromosomes are reciprocally exchanged by crossover recombination to create physical links between homologues called chiasmata¹³⁰. Therefore, cohesin complexes at chromosome arms generate physical tension when spindle fibers capture each homologue (chromatid pair) to segregate them to opposite poles. In addition to sister chromatid cohesion, Rec8-cohesin creates chromosome axis structure, which is a foundation of synaptonemal complex^{131 - 134}. This axis consists of chromatin loops and Rec8-cohesin is thought to directly build them. A study from fission yeast has shown that Rec8-cohesin mediated axis/loop is vital for homologue pairing as well as chiasmata formation¹³⁵. In parallel to chiasmata formation, kinetochores on each pair of sister chromatids are merged¹³⁶. This facilitates spindle fiber emanating from one pole to capture and convey a chromatid pair. This monopolar spindle attachment relies on sister chromatid cohesion at centromere, which is regulated by meiosis-specific kinetochore Meikin family proteins (Moa1 in fission yeast)^{137 - 139}. Rec8-cohesins on chromosome arms are cleaved by separase, leading to homologue segregation during meiosis I. In contrast to mitosis, cohesion at pericentromere lasts until meiosis I. The protected cohesin provides cohesion to guide equal chromosome segregation in meiosis II. This Rec8-cohesin protection is mediated by Shugoshin^{140 - 142}. Shugoshin localizes to centromere and recruits protein phosphatase 2A (PP2A) complex¹⁴³. Thus, phosphorylation of Rec8-cohesin around centromere is continuously reversed by PP2A, protecting Rec8 from separase cleavage.

In fission yeast, there are two types of Rec8-cohesin; Rec11/Rec8-cohesin and Psc3/Rec8-cohesin. They share Psm1^{Smc1}, Psm3^{Smc3} and Rec8, but use different types of HEAT-repeat regulatory subunits (Psc3 and Rec11)¹⁴⁴. In yeast cells, each Rec8-cohesin shows different chromosome localization. Rec11/Rec8-cohesin are found on chromosome

arms whereas Psc3/Rec8-cohesin specifically localizes at centromere. Reflecting their localization, genetic studies have suggested that Rec11/Rec8-cohesin mediates cohesion on chromosome arms and axis/loop formation whereas Psc3/Rec8-cohesin function in regulation of sister chromatid cohesion at centromeric regions^{134, 135}. These findings raise a possibility that both Rec8-cohesin exert common and distinct biochemical properties to shape meiosis-specific chromosomal structures guided by other regulatory proteins mentioned above. However, in contrast to somatic versions of cohesin from yeast to human, biochemical properties of meiotic cohesin have been poorly understood. Thus, I have purified the fission yeast meiotic cohesin complexes to study their biochemical properties by comparing them with somatic Rad21-cohesin.

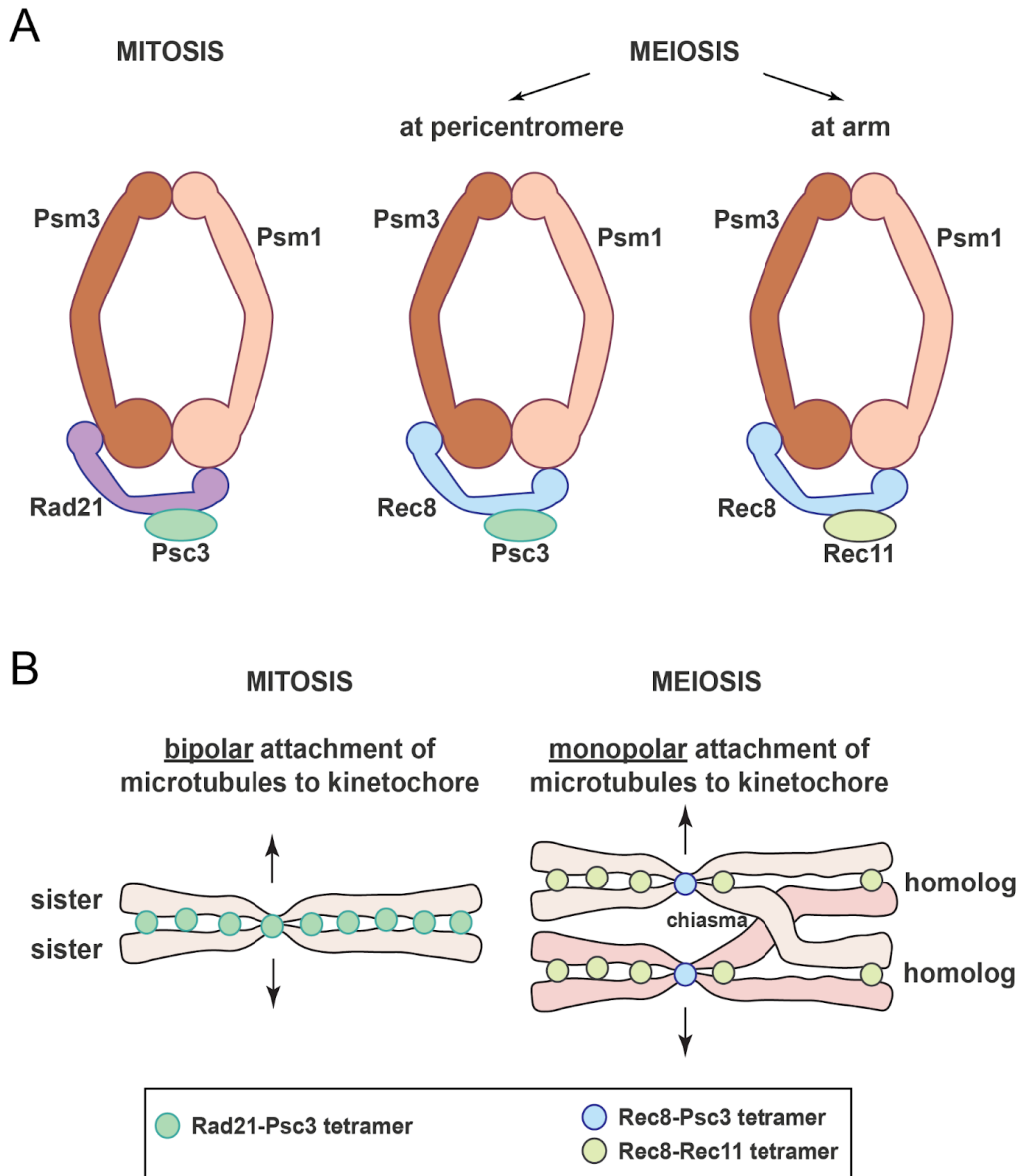


Figure 17. The fission yeast cohesin complexes and their chromosome localization. (A) Overall structures of the fission yeast cohesin complexes. All types of cohesin complexes share the same SMC subunits ($\text{Psm1}^{\text{Smc1}}$ and $\text{Psm3}^{\text{Smc3}}$). Somatic cells contain one type of cohesin (Rad21 and Psc3) whereas two cohesin variants (Psc3/Rec8- and Rec11/Rec8-cohesins) function in meiotic chromosome organization. **(B)** The localizations of the mitotic and meiotic cohesin complexes on chromosomes in fission yeast. Rad21-cohesin functions elsewhere in somatic chromosomes. In meiosis, Psc3/Rec8-cohesin specifically localizes at centromeric regions, whereas Rec11/Rec8-cohesin is loaded onto chromosome arms.

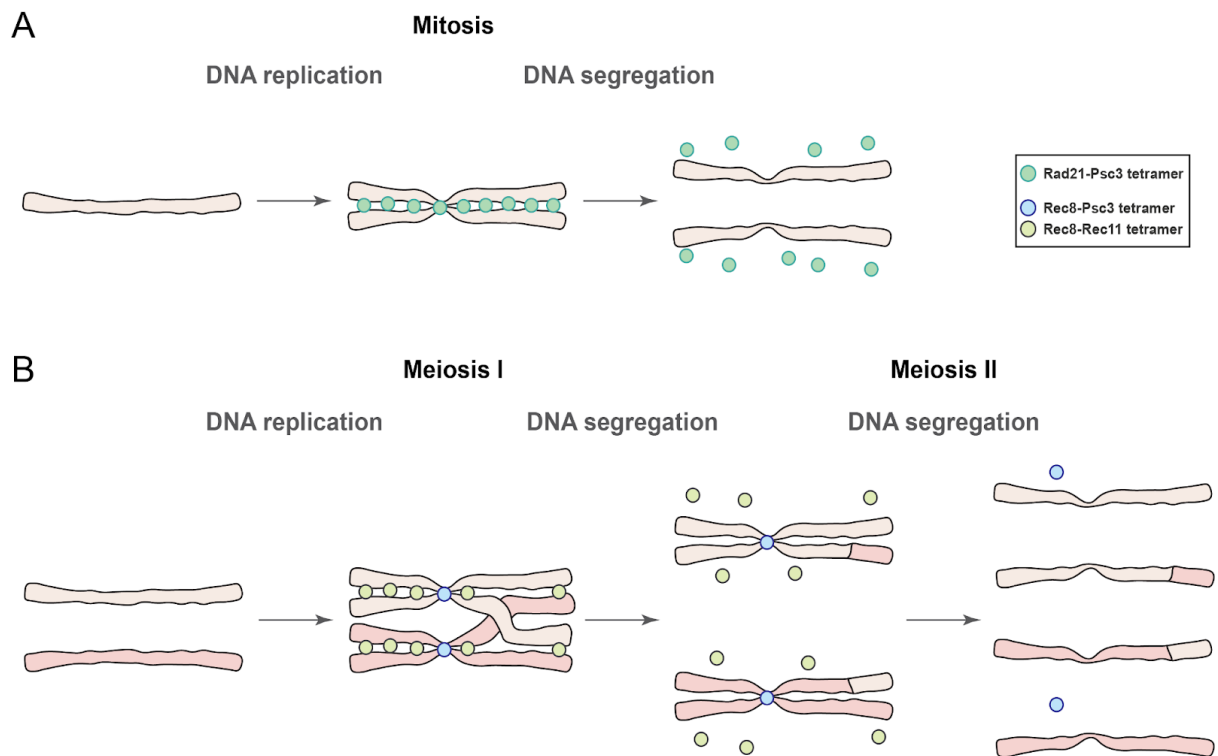


Figure 18. Overview of mitotic and meiotic chromosome segregation. (A) Chromosome segregation in mitosis. Rad21-cohesin creates sister chromatid cohesion during DNA replication. Spindle establishes bipolar attachment, resulting in separation of sister chromatids. Cohesin cleavage by separase initiates anaphase I. (B) In meiosis I, homologous chromosomes are initially segregated, followed by sister chromatid segregation during meiosis II. Rec11/Rec8-cohesin mediates both cohesion and axis/loop formation at chromosome arms. Psc3/Rec8-cohesin exclusively functions at centromere to sustain sister chromatid cohesion and meiosis-specific kinetochore structure that enable monopolar spindle attachment in meiosis I. Cohesion at chromosome arms are destroyed to execute homologue segregation whereas centromeric cohesion lasts to ensure proper sister chromatid separation in meiosis II.

Results

To study biochemical properties of the fission yeast meiotic cohesin complexes, I initially purified core trimer Rec8-cohesin complex by overexpressing Psm1^{Smc1}, Psm3^{Smc3} and Rec8 in budding yeast, followed by sequential column chromatography (The outline of the purification including the affinity tag pull-down and gel filtration is shown in **Sup. Fig. 7A**). Although the yield was low, I obtained a Rec8-cohesin trimer. To reconstitute Rec8-cohesin tetramer with Rec11 or Psc3, I also purified Rec11 by overexpressing it using fission yeast (**Sup. Fig. 8**). Psc3 was obtained using a previously established procedure.

Next, I tested the topological loading of Rec8-cohesin, by adapting an assay which was previously established for Rad21-cohesin¹¹⁶. As shown in **Fig. 19A**, Rec8-cohesin trimer was incubated with relaxed circular DNA in the presence of ATP at low-ionic concentration. Then, Rec8-cohesin was immunoprecipitated by utilizing the Pk affinity tag fused to the Psm3^{Smc3} subunit in a high-salt buffer to remove non-topologically bound DNA. After overnight incubation, the beads were extensively washed with the same high-salt buffer then DNA bound to Rec8-cohesin was eluted by treating with proteinase K (ProK) and SDS and was analyzed by agarose gel electrophoresis.

When incubated DNA with Rec8-cohesin alone, less than 1% of input DNA was recovered (**Fig. 19B**). Addition of Rec11 or Psc3 did not virtually change the DNA binding. About 7% of input DNA was bound to Rec8-cohesin when the loader complex (Mis4-Ssl3) was included in the reaction. The amounts of DNA recoveries were increased to ~2-fold when Psc3 (~14%) or Rec11 (~12%) was further included in addition to the loader complex. These results indicated that both Psc3 and Rec11 stimulated DNA loading of Rec8-trimer in the presence of the loader complex. Psc3 is expressed in both somatic and meiotic cells, whereas Rec11 is a meiosis-specific HEAT-repeat subunit. To confirm if Rec11 specifically functions with Rec8-cohesin, I carried out the same loading assay using Rad21-cohesin

trimer (**Fig. 19C**). As previously reported, Rad21-cohesin was efficiently loaded onto DNA when Psc3 and the loader complex were present. In contrast, no detectable loading was observed in the presence of Rec11. Thus, Rec11 specifically functions with Rec8-cohesin, being consistent with the meiosis specificity of Rec11.

The results mentioned above indicate that Rec11 and Psc3 promote salt-resistant DNA binding by Rec8-trimer. To confirm if this salt-resistant binding reflects topological DNA loading, like Rad21-cohesin, I performed a linearization of the circular DNA bound to Rec8-cohesin after carrying out the loading reaction. As illustrated in **Fig. 20A**, cleaved DNA by a restriction enzyme PstI is supposed to release from Rec8-cohesin into the supernatant whereas residual intact circular DNA remains on the beads. I tested 3 combinations where efficient DNA bindings were observed (Rec8-cohesin with the loader, Rec8-cohesin with the loader and Psc3 or Rec11). In all cases, DNAs kept bound with the beads fraction in the absence of PstI, whereas most of the linearized DNAs were found in supernatant fractions (**Fig. 20**, lanes 5-16). These results indicated that Rec8-cohesin topologically entraps the DNA strand inside of its ring cavity.

As mentioned above, the yield of Rec8-cohesin trimer was relatively low, which limited further biochemical analyses. Thus, I tried Rec8-cohesin as a tetramer complex. Psc3/Rec8-cohesin could be purified with higher yields by overexpression of the four subunits at the same time (**Sup. Fig. 7B**). However, this method could not be applicable to purify Rec11/Rec8-cohesin (After several attempts, I found that Rec11 appears to be not expressed efficiently in host budding yeast cells). Using the purified Psc3/Rec8-cohesin, I optimized the DNA loading reaction. This indicated that topological DNA loading of Rec8-cohesin occurred efficiently in lower salt concentration and lower temperature than Rad21-cohesin (summarized in **Sup. Fig. 9** and **Fig. 18B**, lanes 1-4).

Wapl, functioning together with Pds5, controls cohesin dissociation from chromatin⁹⁸.¹⁰⁰ Previous biochemical study has shown that Pds5-Wapl interacts with Rad21-cohesin and directly promotes its dissociation from DNA¹¹⁷. To test if Pds5-Wapl also regulates Rec8-cohesin, I set up the in vitro assay to monitor the DNA unloading activity as described previously. The outline of the experimental procedure is shown in **Fig. 21A**. First, cohesin was topologically loaded onto circular DNA in the presence of the loader complex in a low-ionic buffer. Then, the reaction was adjusted to higher salt concentration (150 mM) when incubated with Pds5 and Wapl. Cohesin was immunoprecipitated after first (loading reaction) and second (with Pds5-Wapl) incubation. After extensive high-salt wash, bound DNA was analyzed by agarose gel electrophoresis. If DNA was released from cohesin, DNA recovery after immunoprecipitation is supposed to be reduced.

When carrying out the unloading reaction using Rad21/Psc3-cohesin, DNA was efficiently released from Rad21-cohesin in the presence of Pds5-Wapl, consistent with a previous study (**Fig. 21B**) (note that small reduction of bound DNA without Pds5-Wapl was observed, which would reflect spontaneous DNA unloading). In contrast, similar amounts of DNAs were bound to Rec8/Psc3-cohesin both in the presence and absence of Pds5-Wapl (**Fig. 21C**). This result suggests that Rec8-cohesin is intrinsically resistant to the unloading activity mediated by Pds5-Wapl.

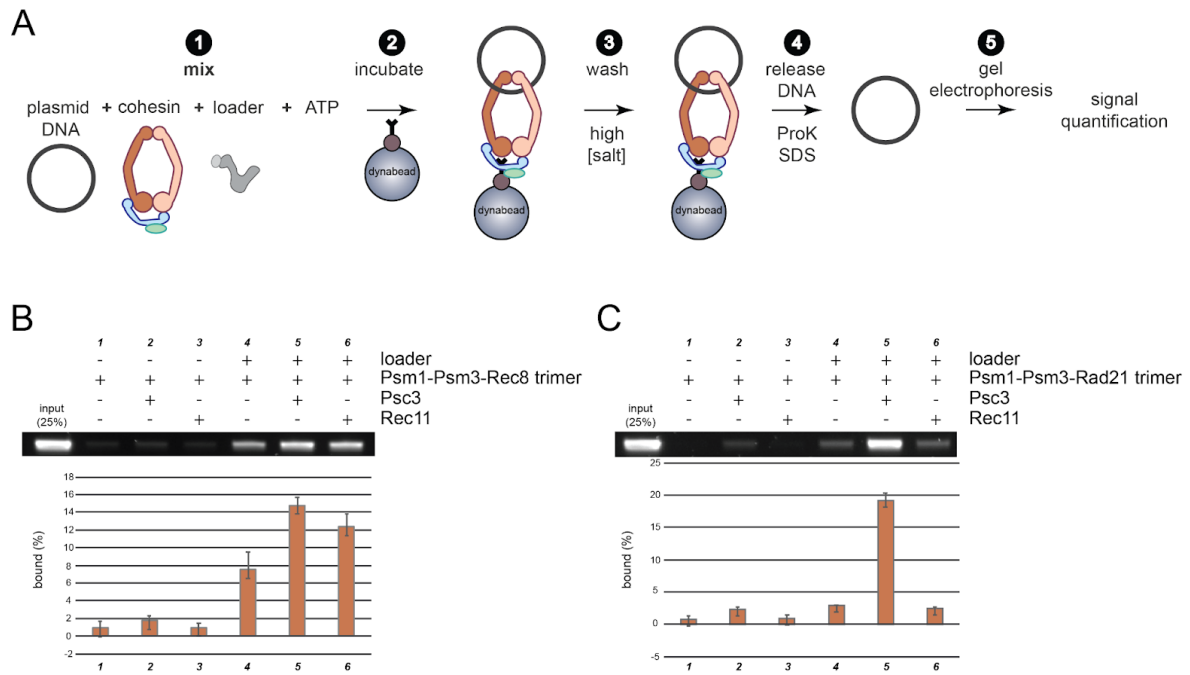


Figure 19. Biochemical reconstitutions of meiotic cohesin loading onto DNA. (A) Schematic of the cohesin loading assay. This assay monitors topological cohesin loading onto a circular DNA substrate. Rec8-cohesin trimer was reacted with relaxed circular DNA in the presence or absence of accessory proteins. Cohesin was purified by immunoprecipitation to monitor the bound DNA. Representative gel images of the cohesin loading assay using Rec8-cohesin trimer (B) and Rad21-cohesin trimer (C) are presented with the quantification of DNA band intensities. All graphs show means and standard deviations from at least three independent experiments.

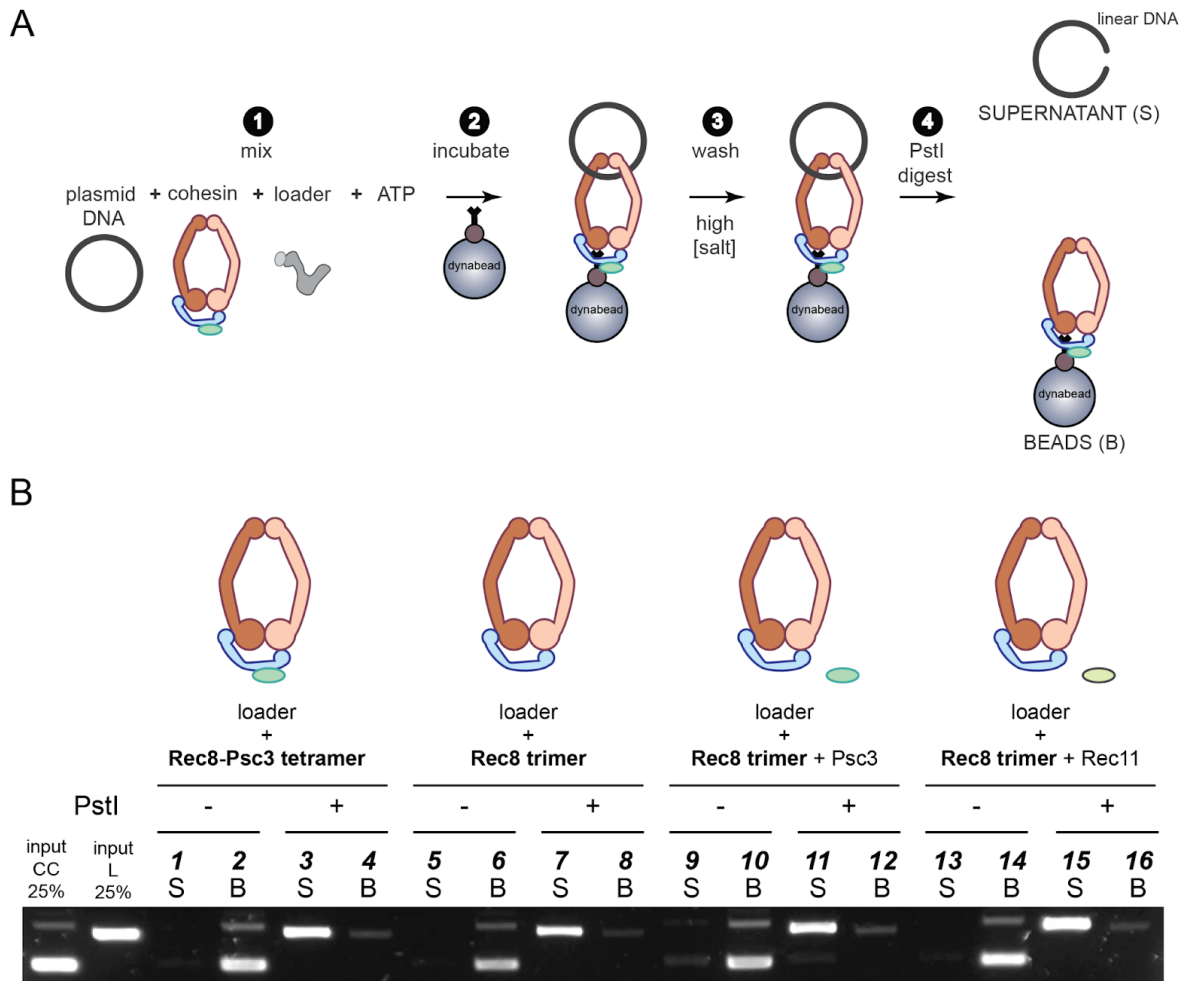


Figure 20. The meiotic cohesin complexes topologically embrace DNA. (A) Confirmation of topological cohesin loading onto DNA. DNA-bound cohesin was immobilized on magnetic beads, then linearized the DNA by restriction enzyme at one site. If the loading was an embrace, cohesin releases linear DNA to supernatant. (B) The agarose gel image represents the results of the DNA release assays performed with indicated cohesin and the HEAT-repeat subunits. S; supernatant fraction, B; beads fraction, CC; covalently closed circular DNA, L; linear DNA.

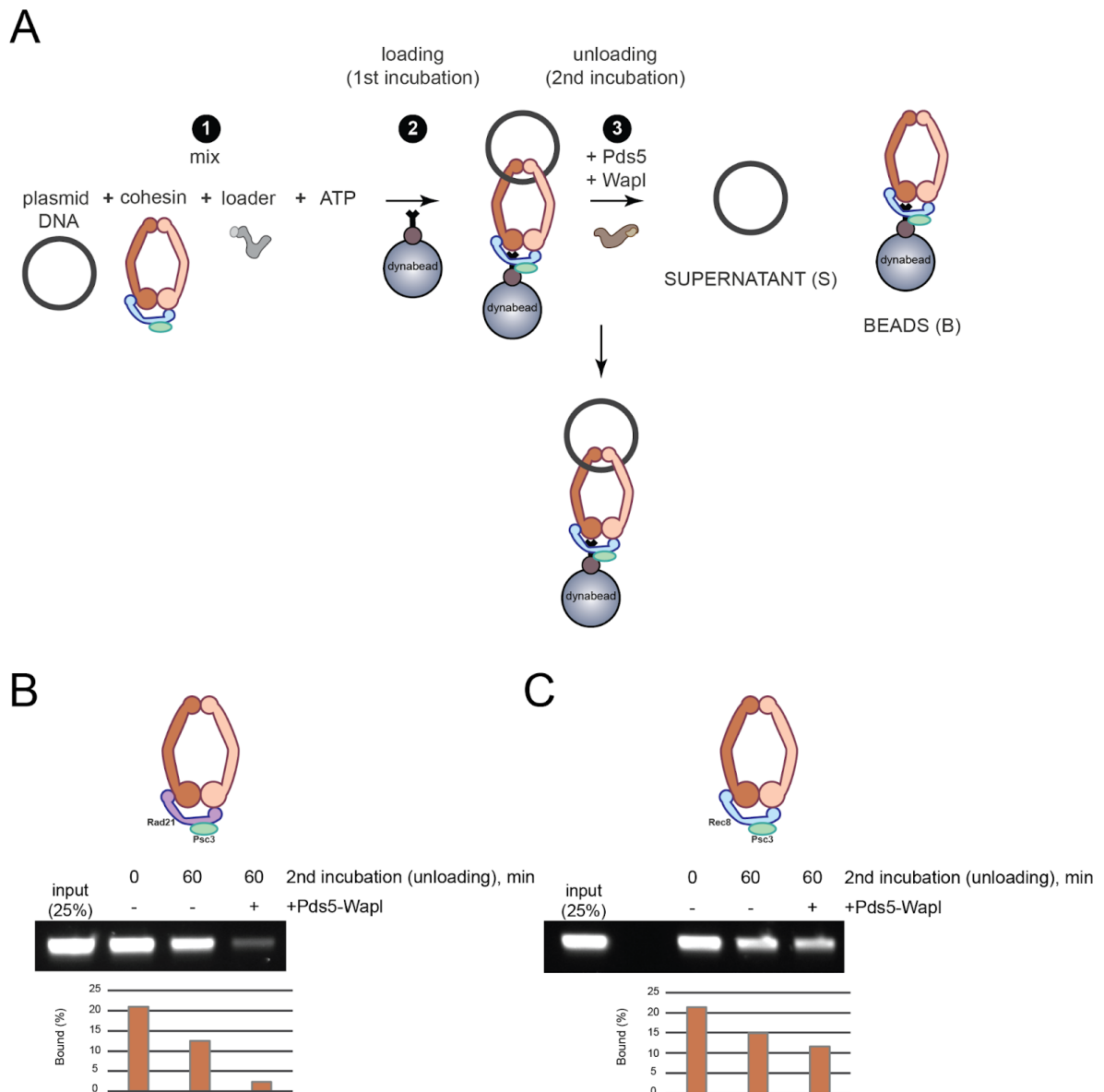


Figure 21. The effect of Pds5-Wapl unloader on Rec8-cohesin. (A) Schematic of the cohesin unloading assay. Psc3/Rec8-Cohesin was topologically loaded onto circular DNA, then Pds5-Wapl was added to initiate cohesin unloading. Cohesin was immunoprecipitated to monitor the bound DNA. This would be reduced as compared with the control experiment if Pds5-Wapl releases DNA from cohesin. (B) Gel images and quantifications of the unloading assay using (B) Psc3/Rec8-cohesin and (C) Psc3/Rad21-cohesin. Pds5-Wapl efficiently dissociated Rad21-cohesin from DNA whereas Rec8-cohesin is insensitive to the unloader.

Discussion

In this study, I have biochemically studied the fission yeast Rec8-cohesin using purified proteins. For DNA loading, the current study has shown that both types of Rec8-cohesins were loaded onto DNA in a similar way to Rad21-cohesin. An interesting difference is that DNA loading of Rec8-cohesin trimer is stimulated by the cohesin loader, but not Psc3 or Rec11 HEAT-repeat subunit. This feature was not observed in Rad21-cohesin, which requires both Psc3 and the loader complex for efficient DNA loading. This suggests that Rec8-cohesin intrinsically has a bias to entrap DNA rather than Rad21-cohesin and the loader is more critical to achieve topological loading rather than Psc3 or Rec11. In yeast, Rec11 and Psc3 is essential for cohesin loading on chromatin¹⁴⁴. In fission yeast, Psc3 has been reported to be recruited to centromere in Swi6 heterochromatin protein dependent manner¹⁴⁵. These HEAT-repeat proteins might have an additional role in cohesin recruitment in chromatin context.

For DNA unloading, Rec8-cohesin is less sensitive to Pds5-Wapl than Rad21-cohesin. Although this is a distinct property from Rad21-cohesin, it is still unclear the underlying molecular mechanism at the moment. Rec8 subunit has been reported to be phosphorylated by casein kinase 1 (CK1)¹⁴⁶. This phosphorylation is required for cohesin dissociation, at least by facilitating separase cleavage of Rec8. In mammalian cells, cohesin phosphorylation appears to be one of the prerequisites for cohesin dissociation by Pds5-Wapl^{112, 142}. I purified one of CK1 homologue Hhp2 to test the effect of cohesin phosphorylation on Pds5-Wapl dependent cohesin unloading (**Sup. Fig. 10**). Although Hhp2 phosphorylate Rec8 subunit of the purified Rec8-cohesin, this did not affect both cohesin loading onto and dissociation from DNA in my reconstitution assays (**Fig. 22**). Further studies should be required to clarify if Rec8-cohesin is intrinsically resistant to the Pds5-Wapl unloader or additional factors

including protein modification renders Rec8-cohesin being susceptible to the dissociation activity.

Fission yeast is widely used for studying many aspects of meiosis that are related to cohesin function. Rec8-cohesin is a central player for meiotic chromosome segregation, functions of which have been mainly analyzed by cytological and genetic analyses. Despite many layers of efforts, it remains a big mystery how Rec8-cohesin mediates meiotic chromosome structures including chromosome axis/loop as well as monopolar kinetochore. I expect that the currently established biochemical assays provide novel opportunities to study molecular function of Rec8-cohesin in the wider context of meiotic chromosome architectures.

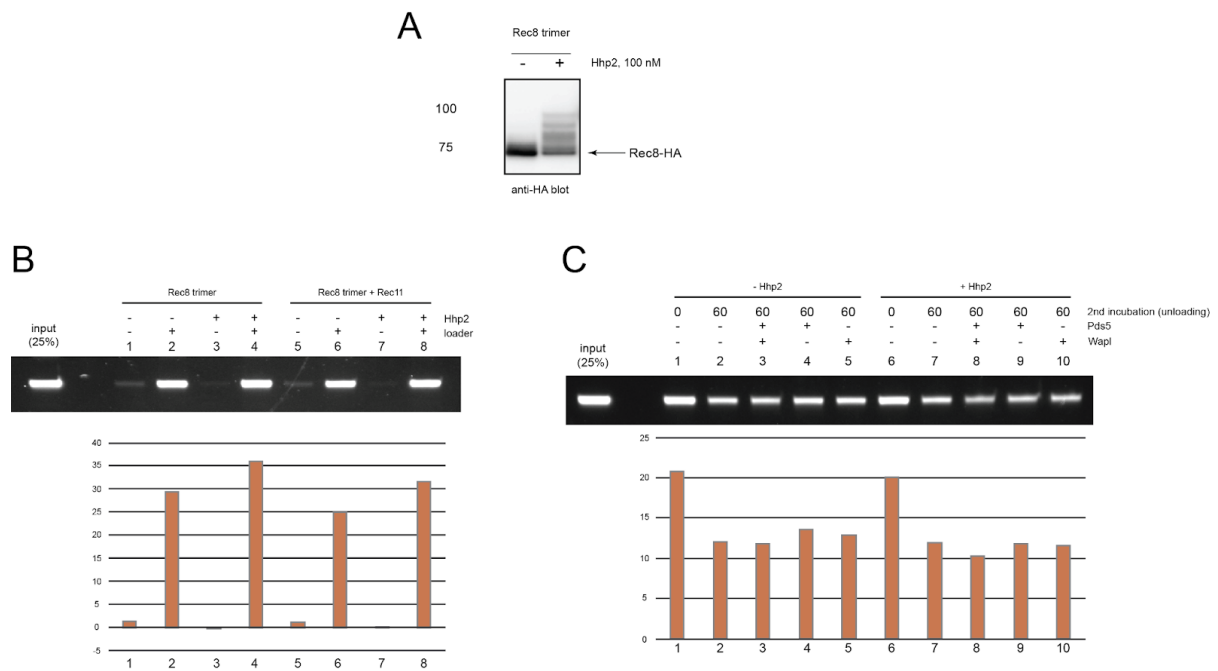


Figure 22. Examination of Rec8-cohesin phosphorylation by casein kinase I and its effects on the DNA associations. (A) Hhp2 casein kinase I phosphorylates Rec8-cohesin in vitro. Rec8-cohesin trimer was incubated with purified Hhp2 in the presence of ATP. The products were separated by SDS-PAGE, and Rec8 protein was detected by Western blot using the HA epitope tag on the C terminus of Rec8. This confirmed Hhp2 phosphorylated Rec8 subunit. (B) Rec8 cohesin was initially reacted with Hhp2, then DNA loading assay was performed in the presence of indicated proteins. (C) as (B) but continued the DNA unloading assay in the presence of indicated proteins. These results suggest that Rec8-cohesin phosphorylation by Hhp2 did not alter its DNA loading and unloading activities. Hhp2 was purified as GST fusion protein from *E. coli*.

Materials and Methods

Purification of Rec8-cohesin complex

For expression of Rec8-cohesin trimer, the Psm3 cDNA fused to 3x Pk epitope and 7 histidine tag at the C terminus and the Psm1 cDNA were cloned into the budding yeast *Saccharomyces cerevisiae* shuttle vector YIplac211 under control of GAL1/10 bidirectional promoter. The Rec8 cDNA fused to 1x HA epitope tag and 2x protein A tag, which are separate by a PreScission Protease sequence at the C terminus, was cloned into YIplac128 under control of GAL1 promoter. The linearized plasmids were sequentially integrated into the budding yeast (MATa, ade2-1, trp1-1, can1-100, leu2,3,112, his3-11,15, ura3-52, pep4Δ::HIS3MX). For Psc3/Rec8-cohesin tetramer, the Psc3 cDNA fused to 7 histidine tag at

N terminus is cloned into the YIplac128 plasmid carrying the Rec8 cDNA. The Psm1/Psm3 and the Rec8/Psc3 plasmids are linearized and integrated into the budding yeast. The budding yeast cells expressing Psm1-Psm3-Rec8, or Psm1-Psm3-Rec8-Psc3 were grown in a YP medium containing 1.5% raffinose to an OD600 = 2.0 at 30°C. Galactose was added to the culture at a final concentration of 2% and the cells were grown for further 4 h at 30°C. Cells were harvested by centrifugation and pellets were resuspended in an equal volume of CLH buffer (50 mM HEPES/KOH, pH 7.5, 1 mM DTT, 300 mM NaCl, 20% (v/v) glycerol, 0.5 mM phenylmethylsulfonyl fluoride (PMSF) and protease inhibitor cocktail (Roche)), frozen in liquid nitrogen and broken in a freezer mill (SPEX CertiPrep 6850). The cell powder was thawed at 4°C, then twice the volume of the CLH buffer was added. The lysate was clarified at 4°C by centrifugation at 45,000g for 30 min, and then at 200,000g for 1 h. The clarified lysate was mixed with IgG agarose (Sigma, 1 ml resin slurry per 50 ml of lysate) and RNase A (10 µg/ml final) at 4°C for 3 h. The resin was washed with 15 bed volumes of R buffer (20 mM Tris/HCl, pH 7.5, 0.5 mM tris(2-carboxyethyl)phosphine (TCEP), 10% (v/v) glycerol) containing 250 mM NaCl and 0.5 mM PMSF, and then with 15 bed volumes of the same buffer lacking PMSF. The resin was then suspended in two bed volumes of R buffer containing, 10 µg/ml RNase A and 5 U/ml 3C protease and incubated overnight at 4°C. Two volumes of R buffer were added to the eluate to bring the salt concentration to 100 mM before loading onto a HiTrap Heparin HP column (1 ml, Cytiva). Bound proteins were eluted with steps of 100 mM, 250 mM, 600 mM and 1 M NaCl in R buffer. Cohesin was retrieved in the 600 mM NaCl fraction. This fraction was applied to a Superose 6 10/300 GL gel filtration column (GE Healthcare) that was developed in R buffer containing 200 mM NaCl. The peak fractions were concentrated to approximately 450 µl by ultrafiltration.

Purification of Rec11

The Rec11 encoding cDNA fused with 1xHA epitope tag and 2x protein A tag, which are separate by a PreScission Protease sequence, at the C terminus was cloned into the fission yeast shuttle vector pREP1 under control of the *nmt1* + promoter. The episomal plasmid was introduced into fission yeast (h-, *ura4-D18*, *leu1-32*). The cells were grown in Edinburgh minimal medium (EMM2) lacking thiamine at 30 °C for 15 h to induce protein expression. Cell lysate preparation and purification using IgG agarose followed the same procedure for Rec8-cohesin purification. The eluate from the IgG resin was diluted with twice-amount of R buffer (100 mM NaCl final), then applied to a HiTrap Heparin HP column (1 ml, Cytiva) which was pre-equilibrated with R buffer containing 100 mM NaCl. The column was developed with a linear gradient of 100 mM to 1 M NaCl in the R buffer. The peak fractions (~500 mM NaCl) were pooled and loaded onto the Superdex 200 10/300 GL gel filtration column (Cytiva) that was developed with the R buffer containing 200 mM NaCl. The peak fractions were pooled and concentrated by ultrafiltration.

Preparation of other proteins

The fission yeast Rad21-cohesins (trimer and tetramer), Mis4-Ssl3 (the loader complex), Psc3, Pds5 and Wapl were prepared as described previously^{116, 118}.

DNA and antibody

The circular DNA used for in vitro assays was pBluescript KSII (+). The covalently closed circular DNA was purified by equilibrium ultracentrifugation in a CsCl-ethidium bromide gradient as described elsewhere. The relaxed circular DNA (rcDNA) was prepared by treating the covalently closed circular DNA with *E. coli* topoisomerase I (New England Biolabs). Anti-Pk antibody was purchased from Bio-Rad.

In vitro cohesin loading assay

The standard reaction volume was 15 μ l final volume. Mis4-Ssl3 (100 nM), Rec8-cohesin trimer (100 nM) and Psc3 or Rec11 (100 nM) were mixed on ice in the CL1 buffer (25 mM Tris-HCl (pH 7.5), 1 mM TCEP, 50 mM NaCl, 0.5 mM MgCl₂, 15% (v/v) glycerol, 0.003% Tween 20 and 0.5 mM ATP). Psc3 or Rec11 was omitted if Psc3/Rec8-cohesin tetramer was used. The reaction was initiated by addition of relaxed circular DNA (3.3 nM) and incubated at 25°C for 90 min. For Rad21-cohesin, the reaction was carried out at 32°C for 30 min in the CL2 buffer (as CL1 but 1 mM MgCl₂) with the same protein and DNA concentrations.

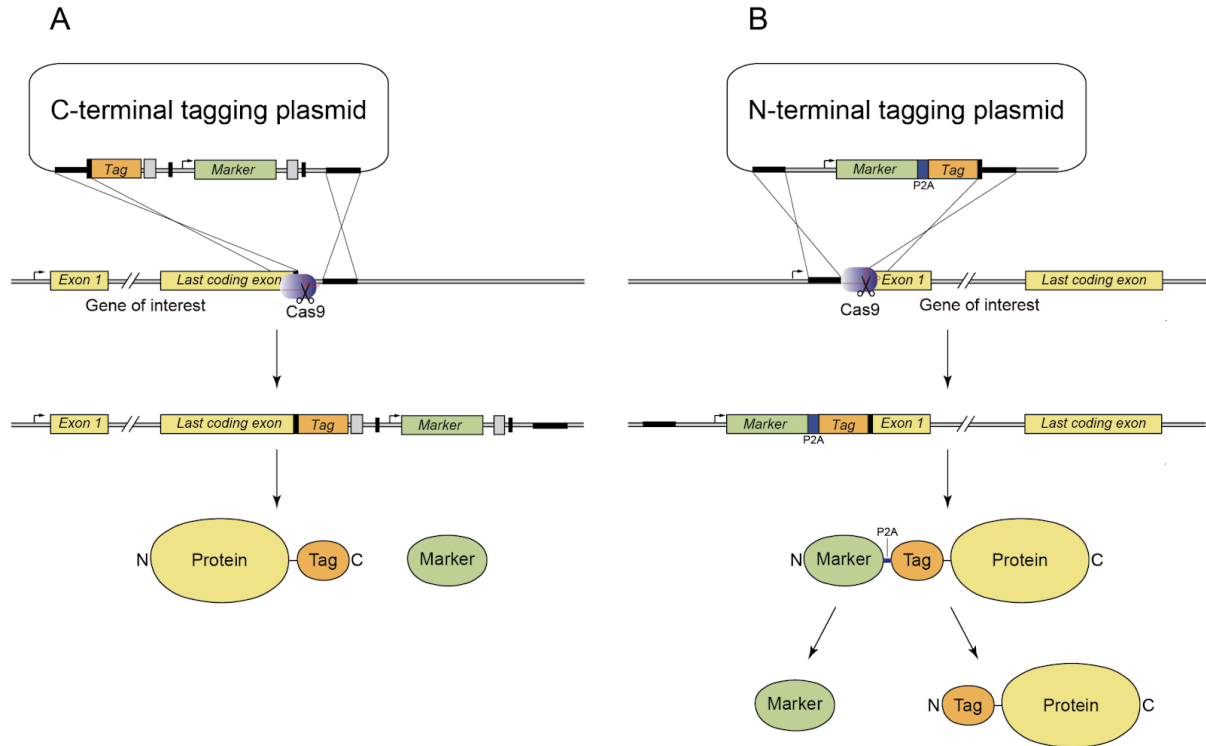
Reactions were terminated by addition of 500 μ l of CW1 buffer (35 mM Tris-HCl (pH 7.5), 0.5 mM TCEP, 800 mM NaCl, 10 mM EDTA, 0.35% (w/v) Triton X-100). Anti-Pk-antibody-coated, protein-A-conjugated magnetic beads were added and rocked at 4°C for 15 h. The magnetic beads were washed three times with CW1 buffer and then once with CW2 buffer (35 mM Tris-HCl (pH 7.5), 0.5 mM TCEP, 100 mM NaCl, 0.1% (w/v) Triton X-100). The beads were then suspended in 15 μ l elution buffer (10 mM Tris-HCl (pH 7.5), 1 mM EDTA, 50 mM NaCl, 0.75% SDS, 1 mg/ml proteinase K (ProK)) and incubated at 37°C for 15 min. The recovered DNA was analyzed by 1% agarose gel electrophoresis in 1 \times TAE and the gel was stained with SYBRGold. Gel images were captured using a LAS Imager and band intensities quantified using ImageQuant. Confirmation of topological DNA entrapment by cohesin Cohesin-bound DNA obtained in the *in vitro* loading reaction was retrieved by anti-Pk immunoprecipitation as described above. The magnetic beads were further washed twice with RE buffer (35 mM Tris-HCl (pH 7.5), 1 mM TCEP, 100 mM NaCl, 10 mM MgCl₂, 0.1% (w/v) Triton X-100). The beads were incubated with PstI (20 U, New England BioLabs) in 10 μ l of RE buffer at 20 °C for 45 min. NaCl concentration was adjusted to 500 mM in 15 μ l and further incubated on ice for 15 min. DNA in the supernatant and the beads fractions were analyzed as described above.

In vitro cohesin unloading assay

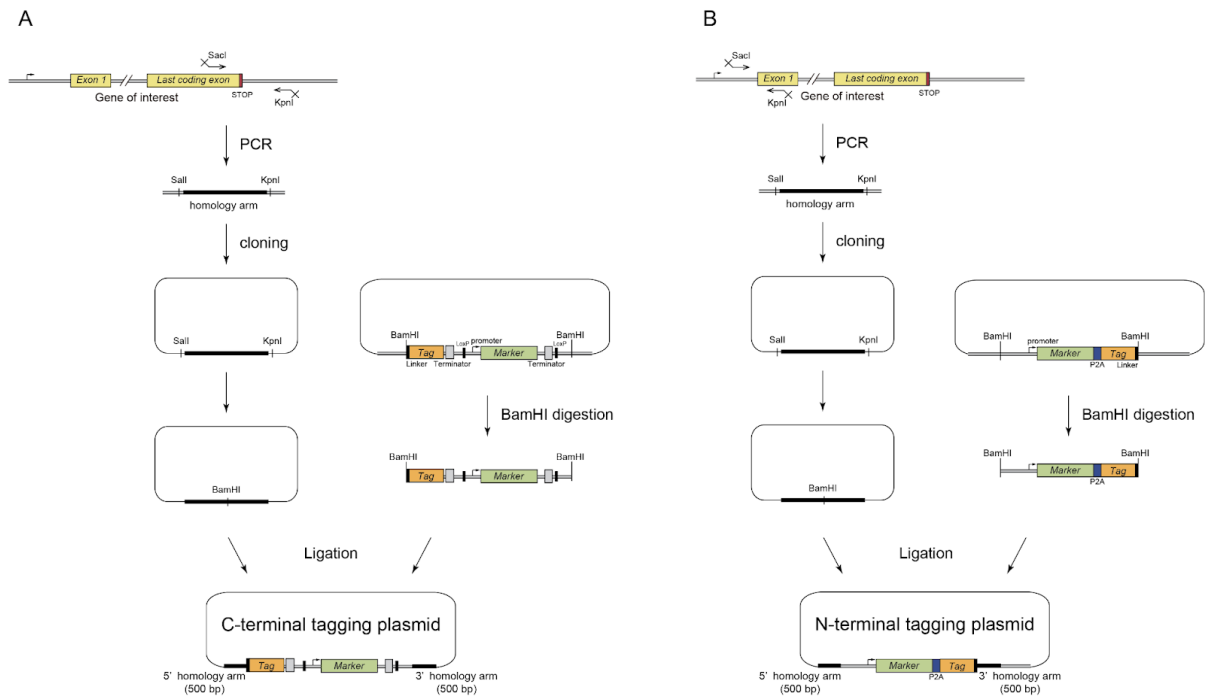
Cohesin loading reactions were carried out as described above. Meanwhile, Pds5 (200 nM) and Wapl (200 nM) were incubated in 15 μ l of CL buffer containing 270 mM NaCl and 0.5 mM ATP at 32°C for 5 min. The unloading reactions were initiated in the tubes containing Pds5 and Wapl (15 μ l) by adding the 15 μ l of the cohesin loading reaction and subsequent incubation at 32°C for the indicated time. Note that the final concentrations were now 50 nM Mis4-Ssl3, 50 nM cohesin (Psc3/Rec8-cohesin or Psc3/Rad21-cohesin), 100 nM Pds5, 100 nM Wapl and 150 mM NaCl. The reactions were terminated and cohesin-bound DNA was analyzed as described above.

Supplementary Materials

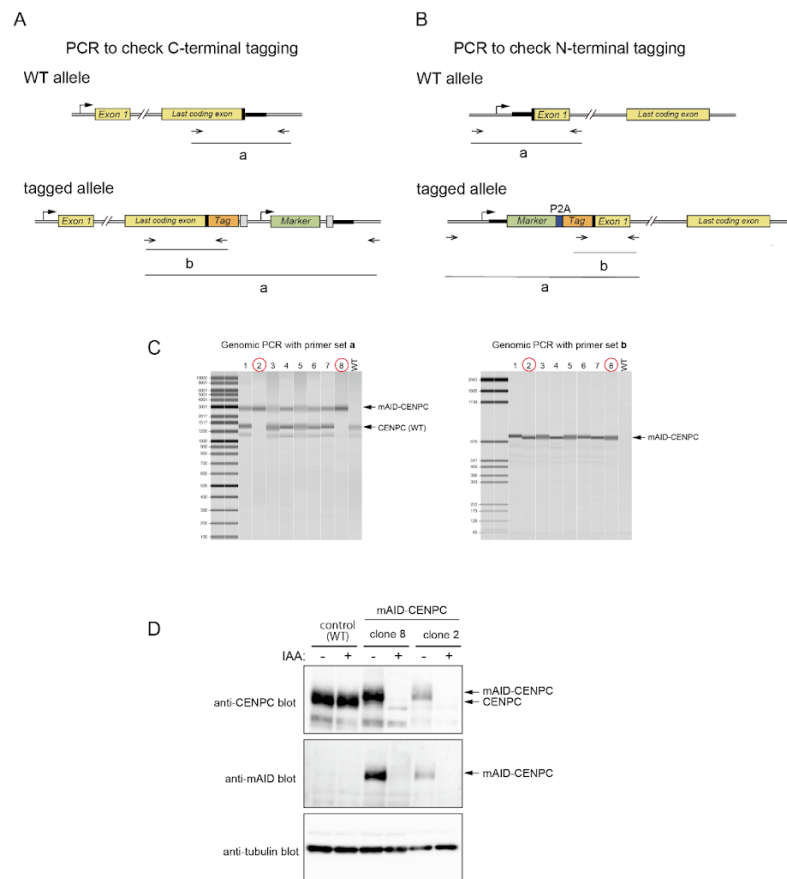
Chapter 1



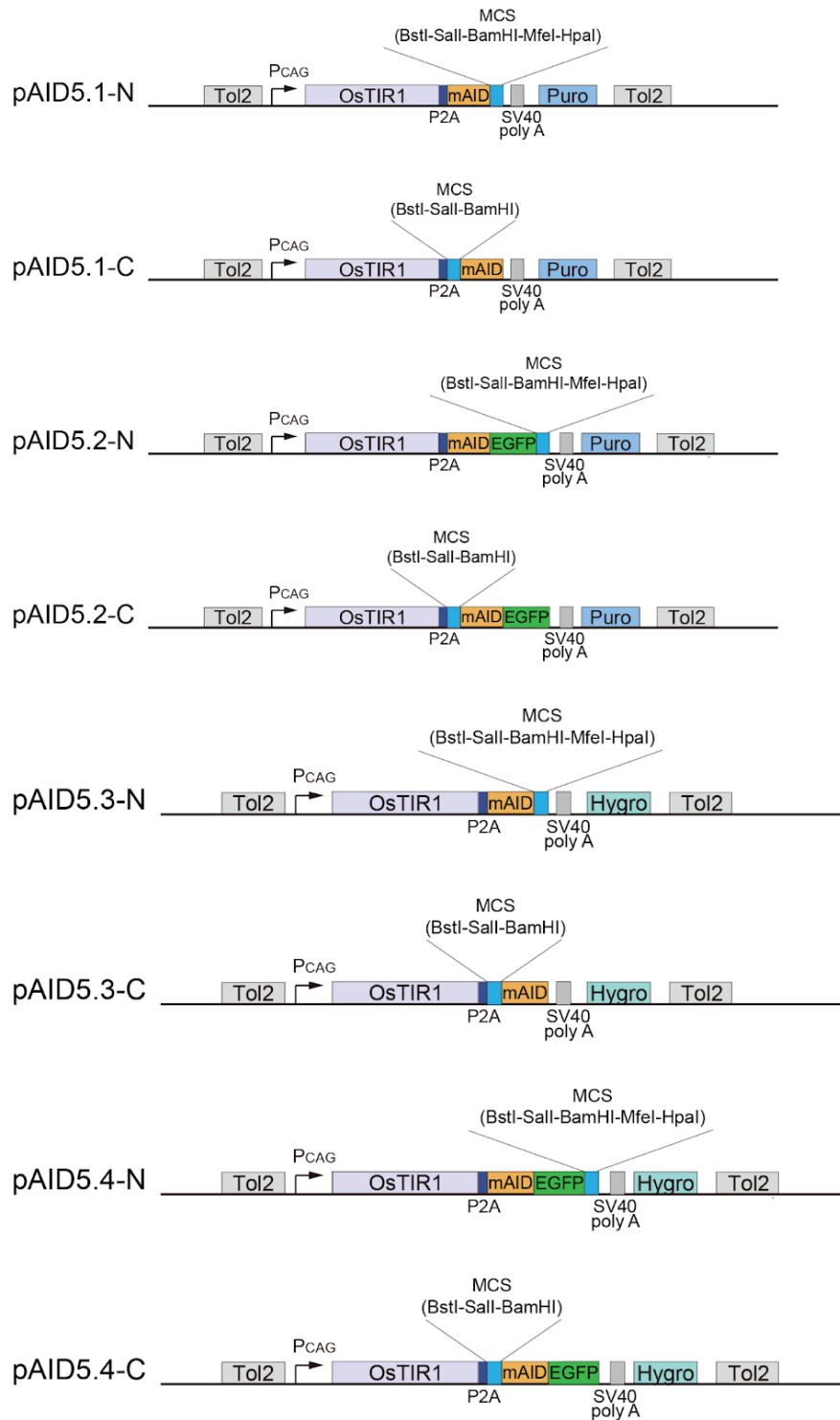
Supplementary Figure 1. Tagging of an endogenous POI using CRISPR–Cas9-based genome editing at the C- and N-terminus. (A) CRISPR–Cas9 generates a double-strand break (DSB) near the stop site for insertion of a donor harboring a tag and a marker. The fusion protein and the marker are expressed independently. (B) CRISPR–Cas9 generates a DSB near the first ATG site for insertion of a donor harboring a marker-P2A-tag cassette. The fusion protein is processed at P2A to express the marker and the tag-fused POI separately.



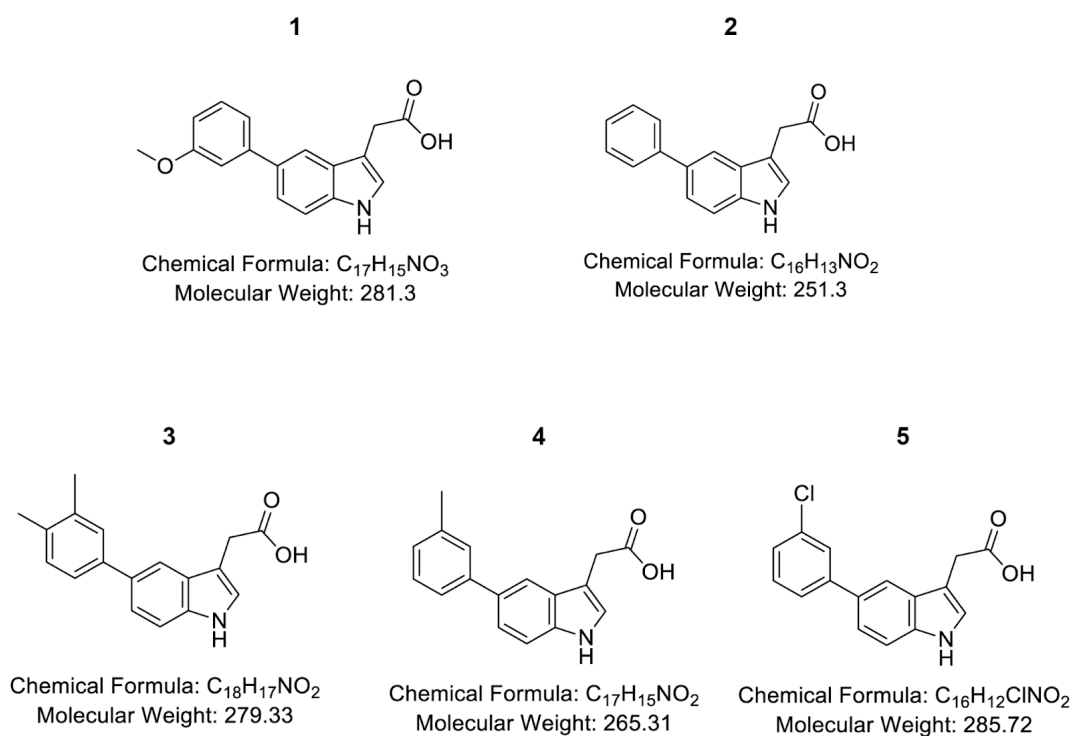
Supplementary Figure 2. Outline of donor plasmid construction for C-terminal and N-terminal tagging. (A) A DNA fragment containing the stop site (about 1 kb) is cloned into a cloning plasmid (such as pBluescript II). Using inverse PCR, a restriction enzyme site (such as BamHI) is created, and a DNA fragment containing a tag and a marker is inserted into the plasmid, to generate a donor vector. (B) A DNA fragment containing the first ATG site (about 1 kb) is cloned into a cloning plasmid (such as pBluescript II). Using inverse PCR, a restriction enzyme site (such as Sall and BamHI) is created, and a DNA fragment containing marker-P2A-tag is inserted into the plasmid, to generate a donor vector.



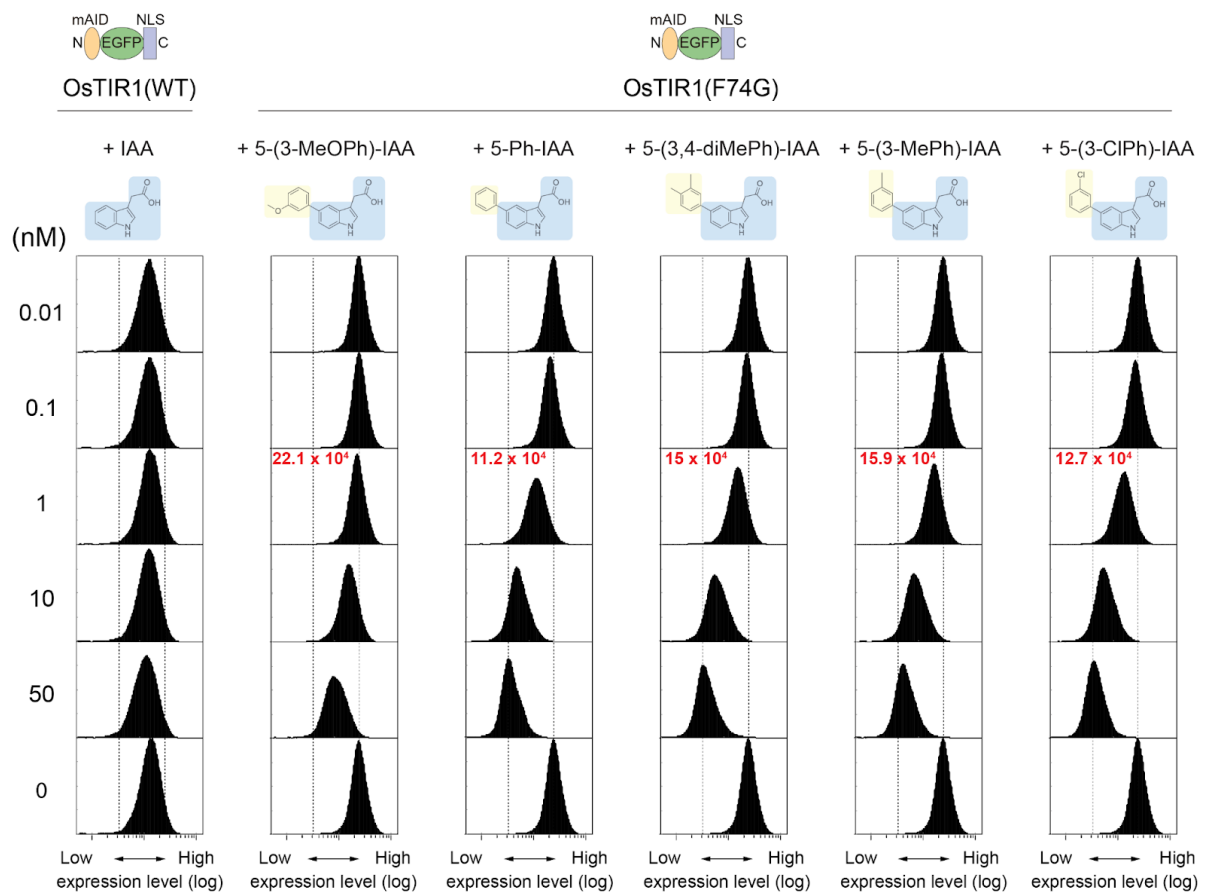
Supplementary Figure 3. Confirmation of isolated clones. (A) PCR-genotype check of the C-terminally tagged alleles. The primer set (a) amplifies a shorter PCR product (1–1.5 kb) from the wild-type (WT) allele, while it amplifies a longer product (1–1.5 kb plus the size of the insertion) from the tagged allele. The primer set (b) generates a PCR product from the tagged allele exclusively (and not from the WT allele). The primer set (a) must be designed outside of the homology arms. (B) PCR-genotype check of the N-terminally tagged alleles. The PCR strategy is analogous to that used to analyze C-terminal tagging. (C) PCR genotyping of the CENPC allele, in which a Hygro–P2A–mAID–mClover cassette was inserted at the N-terminal coding region. HCT116 CMV-OsTIR1 parental cells were used. (D) Confirmation of the fusion protein by immunoblotting. WT or mAID–CENPC clones in the HCT116 CMV-OsTIR1 background were treated with DMSO or 500 μ M IAA for 24 h. Anti-CENPC, anti-mAID and anti-tubulin antibodies (MBL, PD030, M214-3 and M175-3, respectively) were used for detection.



Supplementary Figure 4. Schematic illustration of all-in-one bicistronic plasmids for controlling a mAID-fused protein. The plasmids include pAID5.1-N, pAID5.1-C, pAID5.2-N, pAID5.2-C, pAID5.3-N, pAID5.3-C, pAID5.4-N, pAID5.4-C. A multiple cloning site (MCS) for transgene cDNA cloning is shown in blue. Tol2 are inverted terminal repeats (ITRs) for the TOL2 transposase recognition.

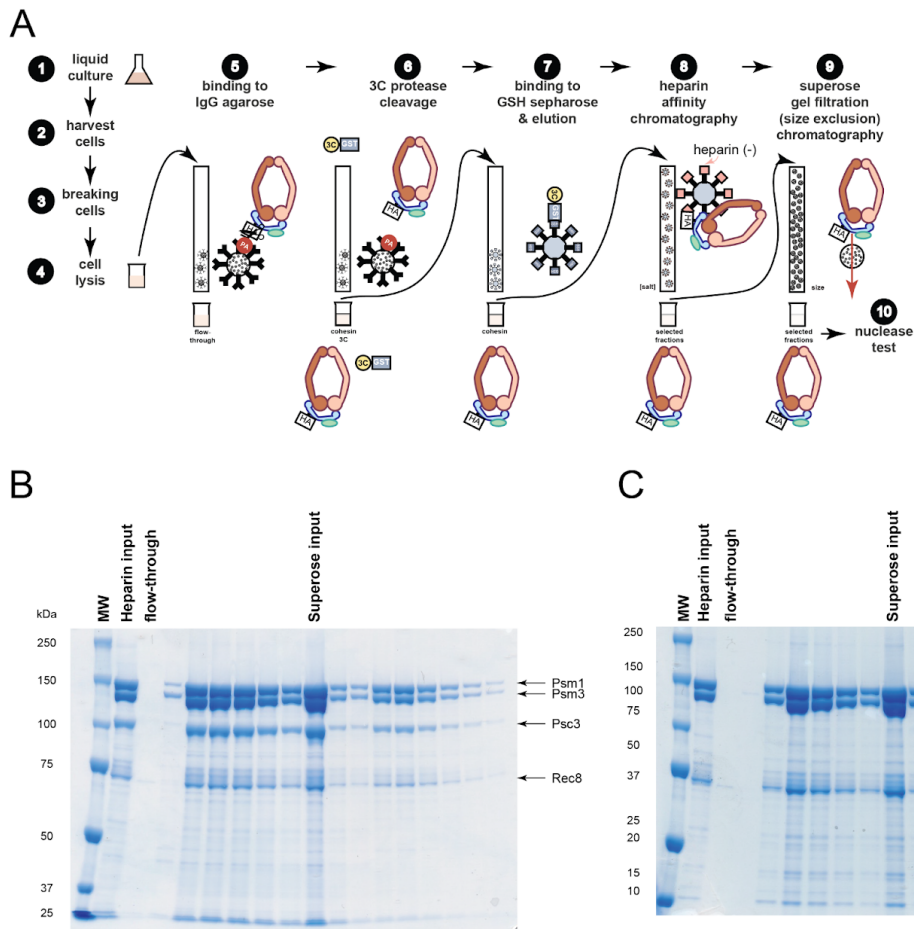


Supplementary Figure 5. The structures of ‘bump’ moiety IAA analog inducer candidates. The "bumped" IAA analogs are as follows: 5-(3-methoxyphenyl)-indole-3-acetic acid (5-(3-MeOPh)-IAA, **1**), 5-phenyl-indole-3-acetic acid (5-Ph-IAA, **2**), 5-(3,4-dimethylphenyl)-indole-3-acetic acid (5-(3,4-diMePh)-IAA, **3**), 5-(3-methylphenyl)-indole-3-acetic acid (5-(3-MePh)-IAA, **4**), 5-(3-chlorophenyl)-indole-3-acetic acid (5-(3-ClPh)-IAA, **5**).

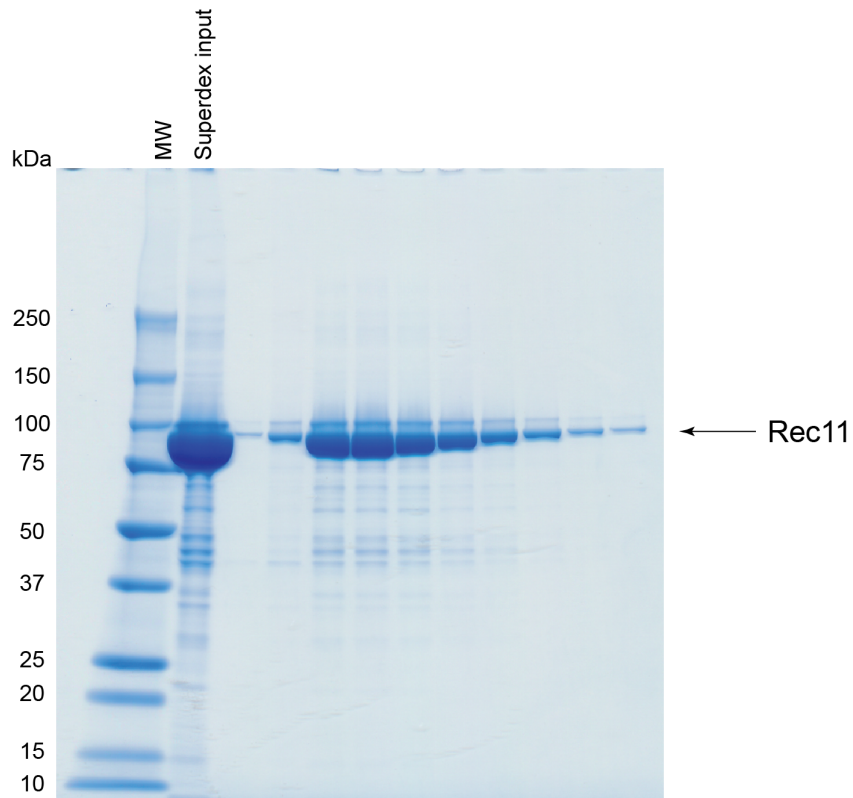


Supplementary Figure 6. Screening to identify an effective bumped-IAA analog.
 Indicated ligands were added to cells expressing a mAID–EGFP–NLS reporter with OsTIR1(WT or F74G) for 4 h. The median values at 1 nM are also indicated (arbitrary units).

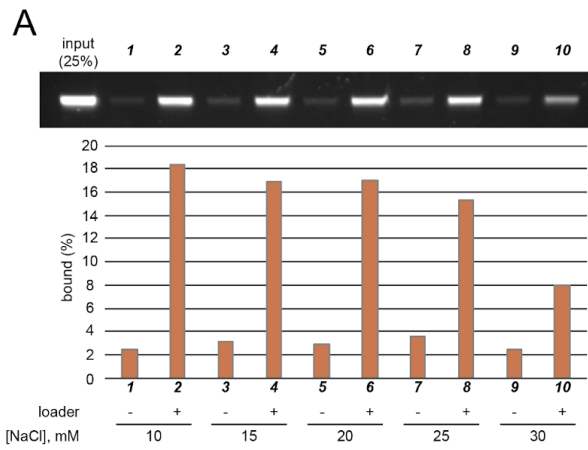
Chapter 2



Supplementary Figure 7. Outline of the purification. (A) The schematic of the procedure starts from the culturing cells that express the protein (step 1) up to the nuclease test (step 10) to check the presence of nucleases in the final sample before proceeding to in vitro assays. (B) Coomassie brilliant blue (CBB)-stained SDS-PAGE of selected fractions collected during the affinity (heparin) and gel filtration (superose) chromatography of the Psm1-Psm3-Psc3-Rec8 meiotic cohesin tetramer. (C) Coomassie brilliant blue (CBB)-stained SDS-PAGE of selected fractions collected during the affinity (heparin) and gel filtration (superose) chromatography of the Psm1-Psm3-Rec8 meiotic cohesin trimer. The subunits are indicated with arrows according to the molecular weight.



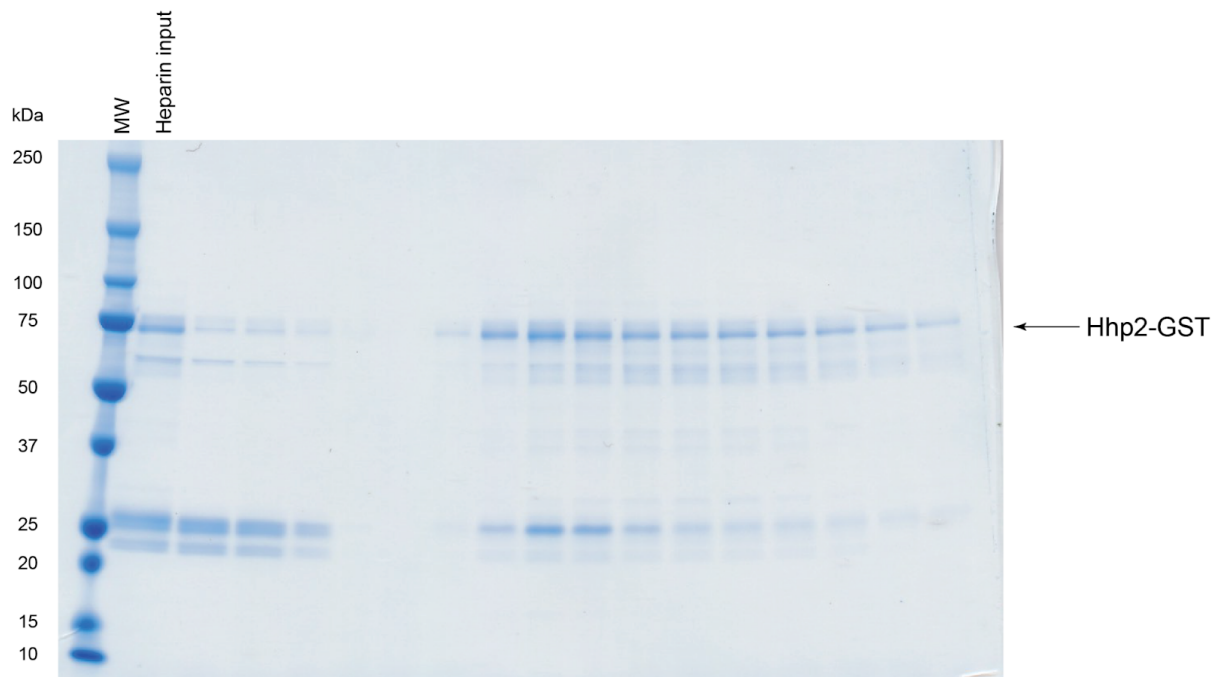
Supplementary Figure 8. SDS-PAGE of selected fractions collected during the gel filtration (superdex) chromatography of the Rec11 meiotic cohesin subunit. The band corresponding to Rec11 is indicated with an arrow according to the molecular weight. SDS-PAGE was stained with Coomassie brilliant blue (CBB).



B

	Difference in optimal conditions	
	meiotic cohesin	mitotic cohesin
[NaCl], mM	20	50
t _{incubation} , °C	25	32
time _{incubation} , min	90	30
[cohesin], nM	100	100
[loader], nM	150	100
[ATP], mM	0.5	0.5
[Mg ²⁺], mM	0.5	1

Supplementary Figure 9. Optimization of the cohesin loading assay conditions. (A) Titration to identify the optimum salt concentration for the meiotic Rec8-Psc3 cohesin loading assay. (B) Comparison of the optimal conditions for the meiotic Rec8-Psc3 and mitotic Rad21-Psc3 cohesin.



Supplementary Figure 10. SDS-PAGE of selected fractions collected during the affinity (heparin) chromatography of the Hhp2-GST meiosis-specific kinase. The band corresponding to Hhp2-GST is indicated with an arrow according to the molecular weight. SDS-PAGE was stained with Coomassie brilliant blue (CBB).

References

Chapter 1

1. Hinnen, A., Hicks, J. B., & Fink, G. R. (1978). Transformation of yeast. *Proceedings of the National Academy of Sciences*, 75(4), 1929-1933.
2. Capecchi, M. R. (1980). High efficiency transformation by direct microinjection of DNA into cultured mammalian cells. *Cell*, 22(2), 479-488.
3. Gordon, J. W., Scangos, G. A., Plotkin, D. J., Barbosa, J. A., & Ruddle, F. H. (1980). Genetic transformation of mouse embryos by microinjection of purified DNA. *Proceedings of the National Academy of Sciences*, 77(12), 7380-7384.
4. Brinster, R. L., Chen, H. Y., Trumbauer, M., Senear, A. W., Warren, R., & Palmiter, R. D. (1981). Somatic expression of herpes thymidine kinase in mice following injection of a fusion gene into eggs. *Cell*, 27(1), 223-231.
5. Rothstein, R. J. (1983). [12] One-step gene disruption in yeast. In *Methods in enzymology* (Vol. 101, pp. 202-211). Academic Press.
6. Costantini, F., & Lacy, E. (1981). Introduction of a rabbit β -globin gene into the mouse germ line. *Nature*, 294(5836), 92-94.
7. Orr-Weaver, T. L., Szostak, J. W., & Rothstein, R. J. (1981). Yeast transformation: a model system for the study of recombination. *Proceedings of the National Academy of Sciences*, 78(10), 6354-6358.
8. Gordon, K., & Ruddle, F. H. (1986). Gene transfer into mouse embryos. *Manipulation of Mammalian Development*, 1-36.
9. Folger, K. R., Wong, E. A., Wahl, G., & Capecchi, M. R. (1982). Patterns of integration of DNA microinjected into cultured mammalian cells: evidence for homologous recombination

- between injected plasmid DNA molecules. *Molecular and cellular biology*, 2(11), 1372-1387.
10. Thomas, K. R., Folger, K. R., & Capecchi, M. R. (1986). High frequency targeting of genes to specific sites in the mammalian genome. *Cell*, 44(3), 419-428.
 11. Thomas, K. R., & Capecchi, M. R. (1987). Site-directed mutagenesis by gene targeting in mouse embryo-derived stem cells. *Cell*, 51(3), 503-512.
 12. Capecchi, M. R. (1989). Altering the genome by homologous recombination. *Science*, 244(4910), 1288-1292.
 13. Gaj, T., Gersbach, C. A., & Barbas III, C. F. (2013). ZFN, TALEN, and CRISPR/Cas-based methods for genome engineering. *Trends in biotechnology*, 31(7), 397-405.
 14. Fire, A., Xu, S., Montgomery, M. K., Kostas, S. A., Driver, S. E., & Mello, C. C. (1998). Potent and specific genetic interference by double-stranded RNA in *Caenorhabditis elegans*. *Nature*, 391(6669), 806-811.
 15. Fire, A., Xu, S., Montgomery, M. K., Kostas, S. A., Driver, S. E., & Mello, C. C. (1998). Potent and specific genetic interference by double-stranded RNA in *Caenorhabditis elegans*. *Nature*, 391(6669), 806-811.
 16. Zhu, L., Somlo, G., Zhou, B., Shao, J., Bedell, V., Slovak, M. L., ... & Yen, Y. (2005). Fibroblast growth factor receptor 3 inhibition by short hairpin RNAs leads to apoptosis in multiple myeloma. *Molecular cancer therapeutics*, 4(5), 787-798.
 17. Sui, G., Soohoo, C., Affar, E. B., Gay, F., Shi, Y., Forrester, W. C., & Shi, Y. (2002). A DNA vector-based RNAi technology to suppress gene expression in mammalian cells. *Proceedings of the National Academy of Sciences*, 99(8), 5515-5520.
 18. Cartegni, L., & Krainer, A. R. (2003). Correction of disease-associated exon skipping by synthetic exon-specific activators. *Nature structural biology*, 10(2), 120-125.

19. Qi, L. S., Larson, M. H., Gilbert, L. A., Doudna, J. A., Weissman, J. S., Arkin, A. P., & Lim, W. A. (2013). Repurposing CRISPR as an RNA-guided platform for sequence-specific control of gene expression. *Cell*, 152(5), 1173-1183.
20. Gilbert, L. A., Larson, M. H., Morsut, L., Liu, Z., Brar, G. A., Torres, S. E., ... & Qi, L. S. (2013). CRISPR-mediated modular RNA-guided regulation of transcription in eukaryotes. *Cell*, 154(2), 442-451.
21. Abudayyeh, O. O., Gootenberg, J. S., Essletzbichler, P., Han, S., Joung, J., Belanto, J. J., ... & Zhang, F. (2017). RNA targeting with CRISPR–Cas13. *Nature*, 550(7675), 280-284.
22. Cox, D. B., Gootenberg, J. S., Abudayyeh, O. O., Franklin, B., Kellner, M. J., Joung, J., & Zhang, F. (2017). RNA editing with CRISPR-Cas13. *Science*, 358(6366), 1019-1027.
23. Konermann, S., Lotfy, P., Brideau, N. J., Oki, J., Shokhirev, M. N., & Hsu, P. D. (2018). Transcriptome engineering with RNA-targeting type VI-D CRISPR effectors. *Cell*, 173(3), 665-676.
24. Nabet, B., Roberts, J. M., Buckley, D. L., Paulk, J., Dastjerdi, S., Yang, A., ... & Bradner, J. E. (2018). The dTAG system for immediate and target-specific protein degradation. *Nature chemical biology*, 14(5), 431-441.
25. England, C. G., Luo, H., & Cai, W. (2015). HaloTag technology: a versatile platform for biomedical applications. *Bioconjugate chemistry*, 26(6), 975-986.
26. Buckley, D. L., Raina, K., Darricarrere, N., Hines, J., Gustafson, J. L., Smith, I. E., ... & Crews, C. M. (2015). HaloPROTACS: use of small molecule PROTACs to induce degradation of HaloTag fusion proteins. *ACS chemical biology*, 10(8), 1831-1837.
27. Banaszynski, L. A., Chen, L. C., Maynard-Smith, L. A., Ooi, A. L., & Wandless, T. J. (2006). A rapid, reversible, and tunable method to regulate protein function in living cells using synthetic small molecules. *Cell*, 126(5), 995-1004.

28. Natsume, T., Kiyomitsu, T., Saga, Y., & Kanemaki, M. T. (2016). Rapid protein depletion in human cells by auxin-inducible degron tagging with short homology donors. *Cell reports*, 15(1), 210-218.
29. Yesbolatova, A., Tominari, Y., & Kanemaki, M. T. (2019). Ligand-induced genetic degradation as a tool for target validation. *Drug Discovery Today: Technologies*, 31, 91-98.
30. Schapira, M., Calabrese, M. F., Bullock, A. N., & Crews, C. M. (2019). Targeted protein degradation: expanding the toolbox. *Nature reviews Drug discovery*, 18(12), 949-963.
31. Prozzillo, Y., Fattorini, G., Santopietro, M. V., Suglia, L., Ruggiero, A., Ferreri, D., & Messina, G. (2020). Targeted protein degradation tools: overview and future perspectives. *Biology*, 9(12), 421.
32. Metzger, M. B., Pruneda, J. N., Klevit, R. E., & Weissman, A. M. (2014). RING-type E3 ligases: master manipulators of E2 ubiquitin-conjugating enzymes and ubiquitination. *Biochimica et Biophysica Acta (BBA)-Molecular Cell Research*, 1843(1), 47-60.
33. Wenzel, D. M., Stoll, K. E., & Klevit, R. E. (2011). E2s: structurally economical and functionally replete. *Biochemical Journal*, 433(1), 31-42.
34. Komander, D., & Rape, M. (2012). The ubiquitin code. *Annual review of biochemistry*, 81, 203-229.
35. Ye, Y., & Rape, M. (2009). Building ubiquitin chains: E2 enzymes at work. *Nature reviews Molecular cell biology*, 10(11), 755-764.
36. Schulman, B. A., & Wade Harper, J. (2009). Ubiquitin-like protein activation by E1 enzymes: the apex for downstream signalling pathways. *Nature reviews Molecular cell biology*, 10(5), 319-331.
37. Lydeard, J. R., Schulman, B. A., & Harper, J. W. (2013). Building and remodelling Cullin–RING E3 ubiquitin ligases. *EMBO reports*, 14(12), 1050-1061.

38. Petroski, M. D., & Deshaies, R. J. (2005). Function and regulation of cullin–RING ubiquitin ligases. *Nature reviews Molecular cell biology*, 6(1), 9-20.
39. Li, W., Bengtson, M. H., Ulbrich, A., Matsuda, A., Reddy, V. A., Orth, A., ... & Joazeiro, C. A. (2008). Genome-wide and functional annotation of human E3 ubiquitin ligases identifies MULAN, a mitochondrial E3 that regulates the organelle's dynamics and signaling. *PloS one*, 3(1), e1487.
40. Clackson, T., Yang, W., Rozamus, L. W., Hatada, M., Amara, J. F., Rollins, C. T., ... & Holt, D. A. (1998). Redesigning an FKBP–ligand interface to generate chemical dimerizers with novel specificity. *Proceedings of the National Academy of Sciences*, 95(18), 10437-10442.
41. Brand, M., & Winter, G. E. (2019). Locus-specific knock-in of a degradable tag for target validation studies. In *Target Identification and Validation in Drug Discovery* (pp. 105-119). Humana Press, New York, NY.
42. Neklesa, T. K., Tae, H. S., Schneekloth, A. R., Stulberg, M. J., Corson, T. W., Sundberg, T. B., ... & Crews, C. M. (2011). Small-molecule hydrophobic tagging–induced degradation of HaloTag fusion proteins. *Nature chemical biology*, 7(8), 538-543.
43. Tae, H. S., Sundberg, T. B., Neklesa, T. K., Noblin, D. J., Gustafson, J. L., Roth, A. G., ... & Crews, C. M. (2012). Identification of hydrophobic tags for the degradation of stabilized proteins. *ChemBioChem*, 13(4), 538-541.
44. Ohana, R. F., Encell, L. P., Zhao, K., Simpson, D., Slater, M. R., Urh, M., & Wood, K. V. (2009). HaloTag7: a genetically engineered tag that enhances bacterial expression of soluble proteins and improves protein purification. *Protein expression and purification*, 68(1), 110-120.

45. Los, G. V., Encell, L. P., McDougall, M. G., Hartzell, D. D., Karassina, N., Zimprich, C., ... & Wood, K. V. (2008). HaloTag: a novel protein labeling technology for cell imaging and protein analysis. *ACS chemical biology*, 3(6), 373-382.
46. Banaszynski, L. A., Sellmyer, M. A., Contag, C. H., Wandless, T. J., & Thorne, S. H. (2008). Chemical control of protein stability and function in living mice. *Nature medicine*, 14(10), 1123-1127.
47. Park, A., Won, S. T., Pentecost, M., Bartkowski, W., & Lee, B. (2014). CRISPR/Cas9 allows efficient and complete knock-in of a destabilization domain-tagged essential protein in a human cell line, allowing rapid knockdown of protein function. *PloS one*, 9(4), e95101.
48. Gong, Y., & de Lange, T. (2010). A Shld1-controlled POT1a provides support for repression of ATR signaling at telomeres through RPA exclusion. *Molecular cell*, 40(3), 377-387.
49. Bongers, K. M., Chen, L. C., Liu, C. W., & Wandless, T. J. (2011). Small-molecule displacement of a cryptic degron causes conditional protein degradation. *Nature chemical biology*, 7(8), 531-537.
50. Leyser, O. (2002). Molecular genetics of auxin signaling. *Annual review of plant biology*, 53(1), 377-398.
51. Guilfoyle, T. J., & Hagen, G. (2007). Auxin response factors. *Current opinion in plant biology*, 10(5), 453-460.
52. Ulmasov, T., Hagen, G., & Guilfoyle, T. J. (1999). Dimerization and DNA binding of auxin response factors. *The plant journal*, 19(3), 309-319.
53. Tiwari, S. B., Hagen, G., & Guilfoyle, T. (2003). The roles of auxin response factor domains in auxin-responsive transcription. *The Plant Cell*, 15(2), 533-543.

54. Ruegger, M., Dewey, E., Gray, W. M., Hobbie, L., Turner, J., & Estelle, M. (1998). The TIR1 protein of *Arabidopsis* functions in auxin response and is related to human SKP2 and yeast grr1p. *Genes & development*, 12(2), 198-207.
55. Leyser, O. (2006). Dynamic integration of auxin transport and signalling. *Current Biology*, 16(11), R424-R433.
56. Mockaitis, K., & Estelle, M. (2008). Auxin receptors and plant development: a new signaling paradigm. *Annual review of cell and developmental biology*, 24.
57. Zenser, N., Ellsmore, A., Leasure, C., & Callis, J. (2001). Auxin modulates the degradation rate of Aux/IAA proteins. *Proceedings of the National Academy of Sciences*, 98(20), 11795-11800.
58. Calderon-Villalobos, L. I., Tan, X., Zheng, N., & Estelle, M. (2010). Auxin perception—structural insights. *Cold Spring Harbor perspectives in biology*, 2(7), a005546.
59. Nishimura, K., Fukagawa, T., Takisawa, H., Kakimoto, T., & Kanemaki, M. (2009). An auxin-based degron system for the rapid depletion of proteins in nonplant cells. *Nature methods*, 6(12), 917-922.
60. Nishimura, K., & Kanemaki, M. T. (2014). Rapid depletion of budding yeast proteins via the fusion of an auxin-inducible degron (AID). *Current protocols in cell biology*, 64(1), 20-9.
61. Tan, X., Calderon-Villalobos, L. I. A., Sharon, M., Zheng, C., Robinson, C. V., Estelle, M., & Zheng, N. (2007). Mechanism of auxin perception by the TIR1 ubiquitin ligase. *Nature*, 446(7136), 640-645.
62. Tomasello, G., Armenia, I., & Molla, G. (2020). The Protein Imager: a full-featured online molecular viewer interface with server-side HQ-rendering capabilities. *Bioinformatics*, 36(9), 2909-2911.

63. Zheng, N., Schulman, B. A., Song, L., Miller, J. J., Jeffrey, P. D., Wang, P., ... & Pavletich, N. P. (2002). Structure of the Cul1–Rbx1–Skp1–F boxSkp2 SCF ubiquitin ligase complex. *Nature*, 416(6882), 703-709.
64. Özkan, E., Yu, H., & Deisenhofer, J. (2005). Mechanistic insight into the allosteric activation of a ubiquitin-conjugating enzyme by RING-type ubiquitin ligases. *Proceedings of the National Academy of Sciences*, 102(52), 18890-18895.
65. Komander, D., Reyes-Turcu, F., Licchesi, J. D., Odenwaelder, P., Wilkinson, K. D., & Barford, D. (2009). Molecular discrimination of structurally equivalent Lys 63-linked and linear polyubiquitin chains. *EMBO reports*, 10(5), 466-473.
66. Yesbolatova, A., Natsume, T., Hayashi, K. I., & Kanemaki, M. T. (2019). Generation of conditional auxin-inducible degron (AID) cells and tight control of degron-fused proteins using the degradation inhibitor auxinole. *Methods*, 164, 73-80.
67. Hayashi, K. I., Tan, X., Zheng, N., Hatate, T., Kimura, Y., Kepinski, S., & Nozaki, H. (2008). Small-molecule agonists and antagonists of F-box protein–substrate interactions in auxin perception and signaling. *Proceedings of the national academy of sciences*, 105(14), 5632-5637.
68. Hayashi, K. I., Neve, J., Hirose, M., Kuboki, A., Shimada, Y., Kepinski, S., & Nozaki, H. (2012). Rational design of an auxin antagonist of the SCFTIR1 auxin receptor complex. *ACS chemical biology*, 7(3), 590-598.
69. Hayashi, K. I. (2012). The interaction and integration of auxin signaling components. *Plant and Cell Physiology*, 53(6), 965-975.
70. Ma, Q., Grones, P., & Robert, S. (2018). Auxin signaling: a big question to be addressed by small molecules. *Journal of Experimental Botany*, 69(2), 313-328.

71. Vain, T., Raggi, S., Ferro, N., Barange, D. K., Kieffer, M., Ma, Q., ... & Robert, S. (2019). Selective auxin agonists induce specific AUX/IAA protein degradation to modulate plant development. *Proceedings of the National Academy of Sciences*, 116(13), 6463-6472.
72. Sharp, D. J., Rogers, G. C., & Scholey, J. M. (2000). Cytoplasmic dynein is required for poleward chromosome movement during mitosis in *Drosophila* embryos. *Nature cell biology*, 2(12), 922-930.
73. Howell, B. J., McEwen, B. F., Canman, J. C., Hoffman, D. B., Farrar, E. M., Rieder, C. L., & Salmon, E. D. (2001). Cytoplasmic dynein/dynactin drives kinetochore protein transport to the spindle poles and has a role in mitotic spindle checkpoint inactivation. *The Journal of cell biology*, 155(7), 1159-1172.
74. Varma, D., Monzo, P., Stehman, S. A., & Vallee, R. B. (2008). Direct role of dynein motor in stable kinetochore-microtubule attachment, orientation, and alignment. *The Journal of cell biology*, 182(6), 1045-1054.
75. Firestone, A. J., Weinger, J. S., Maldonado, M., Barlan, K., Langston, L. D., O'donnell, M., ... & Chen, J. K. (2012). Small-molecule inhibitors of the AAA+ ATPase motor cytoplasmic dynein. *Nature*, 484(7392), 125-129.
76. Raaijmakers, J. A., Tanenbaum, M. E., & Medema, R. H. (2013). Systematic dissection of dynein regulators in mitosis. *Journal of Cell Biology*, 201(2), 201-215.
77. Yesbolatova, A., Saito, Y., & Kanemaki, M. T. (2020). Constructing auxin-inducible degron mutants using an all-in-one vector. *Pharmaceuticals*, 13(5), 103.
78. Kim, J. H., Lee, S. R., Li, L. H., Park, H. J., Park, J. H., Lee, K. Y., ... & Choi, S. Y. (2011). High cleavage efficiency of a 2A peptide derived from porcine teschovirus-1 in human cell lines, zebrafish and mice. *PloS one*, 6(4), e18556.

79. Kawakami, K., Takeda, H., Kawakami, N., Kobayashi, M., Matsuda, N., & Mishina, M. (2004). A transposon-mediated gene trap approach identifies developmentally regulated genes in zebrafish. *Developmental cell*, 7(1), 133-144.
80. Ran, F. A. F. A., Hsu, P. D., Wright, J., Agarwala, V., Scott, D. A., & Zhang, F. (2013). Genome engineering using the CRISPR-Cas9 system. *Nature protocols*, 8(11), 2281-2308.
81. Van Deursen, F., Sengupta, S., De Piccoli, G., Sanchez-Diaz, A., & Labib, K. (2012). Mcm10 associates with the loaded DNA helicase at replication origins and defines a novel step in its activation. *The EMBO journal*, 31(9), 2195-2206.
82. Kanke, M., Kodama, Y., Takahashi, T. S., Nakagawa, T., & Masukata, H. (2012). Mcm10 plays an essential role in origin DNA unwinding after loading of the CMG components. *The EMBO journal*, 31(9), 2182-2194.
83. Watase, G., Takisawa, H., & Kanemaki, M. T. (2012). Mcm10 plays a role in functioning of the eukaryotic replicative DNA helicase, Cdc45-Mcm-GINS. *Current Biology*, 22(4), 343-349.
84. Izumi, M., Mizuno, T., Yanagi, K. I., Sugimura, K., Okumura, K., Imamoto, N., ... & Hanaoka, F. (2017). The Mcm2–7-interacting domain of human mini-chromosome maintenance 10 (Mcm10) protein is important for stable chromatin association and origin firing. *Journal of Biological Chemistry*, 292(31), 13008-13021.
85. Yesbolatova, A., Saito, Y., Kitamoto, N., Makino-Itou, H., Ajima, R., Nakano, R., ... & Kanemaki, M. T. (2020). The auxin-inducible degron 2 technology provides sharp degradation control in yeast, mammalian cells, and mice. *Nature communications*, 11(1), 1-13.
86. Uchida, N., Takahashi, K., Iwasaki, R., Yamada, R., Yoshimura, M., Endo, T. A., ... & Torii, K. U. (2018). Chemical hijacking of auxin signaling with an engineered auxin–TIR1 pair. *Nature Chemical Biology*, 14(3), 299-305.

Chapter 2

87. Peters, J. M., & Nishiyama, T. (2012). Sister chromatid cohesion. *Cold Spring Harbor Perspectives in Biology*, 4(11), a011130.
88. Uhlmann, F. (2016). SMC complexes: from DNA to chromosomes. *Nature reviews Molecular cell biology*, 17(7), 399-412.
89. Yatskevich, S., Rhodes, J., & Nasmyth, K. (2019). Organization of chromosomal DNA by SMC complexes. *Annual review of genetics*, 53, 445-482.
90. Tomonaga, T., Nagao, K., Kawasaki, Y., Furuya, K., Murakami, A., Morishita, J., ... & Yanagida, M. (2000). Characterization of fission yeast cohesin: essential anaphase proteolysis of Rad21 phosphorylated in the S phase. *Genes & Development*, 14(21), 2757-2770.
91. Gligoris, T., & Löwe, J. (2016). Structural insights into ring formation of cohesin and related Smc complexes. *Trends in cell biology*, 26(9), 680-693.
92. Haering, C. H., Farcas, A. M., Arumugam, P., Metson, J., & Nasmyth, K. (2008). The cohesin ring concatenates sister DNA molecules. *Nature*, 454(7202), 297-301.
93. Srinivasan, M., Scheinost, J. C., Petela, N. J., Gligoris, T. G., Wissler, M., Ogushi, S., ... & Nasmyth, K. A. (2018). The cohesin ring uses its hinge to organize DNA using non-topological as well as topological mechanisms. *Cell*, 173(6), 1508-1519.
94. Rao, S. S., Huang, S. C., St Hilaire, B. G., Engreitz, J. M., Perez, E. M., Kieffer-Kwon, K. R., ... & Aiden, E. L. (2017). Cohesin loss eliminates all loop domains. *Cell*, 171(2), 305-320.
95. Piazza, A., Bordelet, H., Dumont, A., Thierry, A., Savocco, J., Girard, F., & Koszul, R. (2021). Cohesin regulates homology search during recombinational DNA repair. *Nature Cell Biology*, 23(11), 1176-1186.

96. Ciosk, R., Shirayama, M., Shevchenko, A., Tanaka, T., Toth, A., Shevchenko, A., & Nasmyth, K. (2000). Cohesin's binding to chromosomes depends on a separate complex consisting of Scc2 and Scc4 proteins. *Molecular cell*, 5(2), 243-254.
97. Furuya, K., Takahashi, K., & Yanagida, M. (1998). Faithful anaphase is ensured by Mis4, a sister chromatid cohesion molecule required in S phase and not destroyed in G1 phase. *Genes & Development*, 12(21), 3408-3418.
98. Kueng, S., Hegemann, B., Peters, B. H., Lipp, J. J., Schleiffer, A., Mechtler, K., & Peters, J. M. (2006). Wapl controls the dynamic association of cohesin with chromatin. *Cell*, 127(5), 955-967.
99. Bernard, P., Schmidt, C. K., Vaur, S., Dheur, S., Drogat, J., Genier, S., ... & Javerzat, J. P. (2008). Cell-cycle regulation of cohesin stability along fission yeast chromosomes. *The EMBO journal*, 27(1), 111-121.
100. Chan, K. L., Roig, M. B., Hu, B., Beckouët, F., Metson, J., & Nasmyth, K. (2012). Cohesin's DNA exit gate is distinct from its entrance gate and is regulated by acetylation. *Cell*, 150(5), 961-974.
101. Lopez-Serra, L., Lengronne, A., Borges, V., Kelly, G., & Uhlmann, F. (2013). Budding yeast Wapl controls sister chromatid cohesion maintenance and chromosome condensation. *Current Biology*, 23(1), 64-69.
102. Gerlich, D., Koch, B., Dupeux, F., Peters, J. M., & Ellenberg, J. (2006). Live-cell imaging reveals a stable cohesin-chromatin interaction after but not before DNA replication. *Current Biology*, 16(15), 1571-1578.
103. Uhlmann, F., Lottspeich, F., & Nasmyth, K. (1999). Sister-chromatid separation at anaphase onset is promoted by cleavage of the cohesin subunit Scc1. *Nature*, 400(6739), 37-42.

104. Ben-Shahar, T. R., Heeger, S., Lehane, C., East, P., Flynn, H., Skehel, M., & Uhlmann, F. (2008). Eco1-dependent cohesin acetylation during establishment of sister chromatid cohesion. *Science*, 321(5888), 563-566.
105. Ünal, E., Heidinger-Pauli, J. M., Kim, W., Guacci, V., Onn, I., Gygi, S. P., & Koshland, D. E. (2008). A molecular determinant for the establishment of sister chromatid cohesion. *Science*, 321(5888), 566-569.
106. Rowland, B. D., Roig, M. B., Nishino, T., Kurze, A., Uluocak, P., Mishra, A., ... & Nasmyth, K. (2009). Building sister chromatid cohesion: smc3 acetylation counteracts an antiestablishment activity. *Molecular cell*, 33(6), 763-774.
107. Feytout, A., Vaur, S., Genier, S., Vazquez, S., & Javerzat, J. P. (2011). Psm3 acetylation on conserved lysine residues is dispensable for viability in fission yeast but contributes to Eso1-mediated sister chromatid cohesion by antagonizing Wpl1. *Molecular and Cellular Biology*, 31(8), 1771-1786.
108. Xu, H., Boone, C., & Brown, G. W. (2007). Genetic dissection of parallel sister-chromatid cohesion pathways. *Genetics*, 176(3), 1417-1429.
109. Ansbach, A. B., Noguchi, C., Klansek, I. W., Heidlebaugh, M., Nakamura, T. M., & Noguchi, E. (2008). RFCCtf18 and the Swi1-Swi3 complex function in separate and redundant pathways required for the stabilization of replication forks to facilitate sister chromatid cohesion in *Schizosaccharomyces pombe*. *Molecular biology of the cell*, 19(2), 595-607.
110. Borges, V., Smith, D. J., Whitehouse, I., & Uhlmann, F. (2013). An Eco1-independent sister chromatid cohesion establishment pathway in *S. cerevisiae*. *Chromosoma*, 122(1), 121-134.

111. Srinivasan, M., Fumasoni, M., Petela, N. J., Murray, A., & Nasmyth, K. A. (2020). Cohesion is established during DNA replication utilising chromosome associated cohesin rings as well as those loaded de novo onto nascent DNAs. *Elife*, 9, e56611.
112. Hauf, S., Roitinger, E., Koch, B., Dittrich, C. M., Mechtler, K., & Peters, J. M. (2005). Dissociation of cohesin from chromosome arms and loss of arm cohesion during early mitosis depends on phosphorylation of SA2. *PLoS biology*, 3(3), e69.
113. Uhlmann, F., Lottspeich, F., & Nasmyth, K. (1999). Sister-chromatid separation at anaphase onset is promoted by cleavage of the cohesin subunit Scc1. *Nature*, 400(6739), 37-42.
114. Uhlmann, F., Wernic, D., Poupart, M. A., Koonin, E. V., & Nasmyth, K. (2000). Cleavage of cohesin by the CD clan protease separin triggers anaphase in yeast. *Cell*, 103(3), 375-386.
115. Alexandru, G., Uhlmann, F., Mechtler, K., Poupart, M. A., & Nasmyth, K. (2001). Phosphorylation of the cohesin subunit Scc1 by Polo/Cdc5 kinase regulates sister chromatid separation in yeast. *Cell*, 105(4), 459-472.
116. Murayama, Y., & Uhlmann, F. (2014). Biochemical reconstitution of topological DNA binding by the cohesin ring. *Nature*, 505(7483), 367-371.
117. Kurokawa, Y., & Murayama, Y. (2020). DNA binding by the Mis4^{Scc2} loader promotes topological DNA entrapment by the cohesin ring. *Cell Reports*, 33(6), 108357.
118. Murayama, Y., & Uhlmann, F. (2015). DNA entry into and exit out of the cohesin ring by an interlocking gate mechanism. *Cell*, 163(7), 1628-1640.
119. Stigler, J., Çamdere, G. Ö., Koshland, D. E., & Greene, E. C. (2016). Single-molecule imaging reveals a collapsed conformational state for DNA-bound cohesin. *Cell reports*, 15(5), 988-998.

120. Kanke, M., Tahara, E., Huis in't Veld, P. J., & Nishiyama, T. (2016). Cohesin acetylation and Wapl-Pds5 oppositely regulate translocation of cohesin along DNA. *The EMBO journal*, 35(24), 2686-2698.
121. Davidson, I. F., Bauer, B., Goetz, D., Tang, W., Wutz, G., & Peters, J. M. (2019). DNA loop extrusion by human cohesin. *Science*, 366(6471), 1338-1345.
122. Kim, Y., Shi, Z., Zhang, H., Finkelstein, I. J., & Yu, H. (2019). Human cohesin compacts DNA by loop extrusion. *Science*, 366(6471), 1345-1349.
123. Shi, Z., Gao, H., Bai, X. C., & Yu, H. (2020). Cryo-EM structure of the human cohesin-NIPBL-DNA complex. *Science*, 368(6498), 1454-1459.
124. Higashi, T. L., Eickhoff, P., Sousa, J. S., Locke, J., Nans, A., Flynn, H. R., ... & Uhlmann, F. (2020). A structure-based mechanism for DNA entry into the cohesin ring. *Molecular cell*, 79(6), 917-933.
125. Collier, J. E., Lee, B. G., Roig, M. B., Yatskevich, S., Petela, N. J., Metson, J., ... & Nasmyth, K. A. (2020). Transport of DNA within cohesin involves clamping on top of engaged heads by Scc2 and entrapment within the ring by Scc3. *Elife*, 9, e59560.
126. Petronczki, M., Siomos, M. F., & Nasmyth, K. (2003). Un ménage à quatre: the molecular biology of chromosome segregation in meiosis. *Cell*, 112(4), 423-440.
[https://doi.org/10.1016/s0092-8674\(03\)00083-7](https://doi.org/10.1016/s0092-8674(03)00083-7)
127. Watanabe, Y., & Nurse, P. (1999). Cohesin Rec8 is required for reductional chromosome segregation at meiosis. *Nature*, 400(6743), 461-464.
128. Loidl J. (2006). *S. pombe* linear elements: the modest cousins of synaptonemal complexes. *Chromosoma*, 115(3), 260-271. <https://doi.org/10.1007/s00412-006-0047-7>
129. Gao, J., & Colaiácovo, M. P. (2018). Zipping and Unzipping: Protein Modifications Regulating Synaptonemal Complex Dynamics. *Trends in genetics : TIG*, 34(3), 232-245.
<https://doi.org/10.1016/j.tig.2017.12.001>

130. Kleckner, N. (2006). Chiasma formation: chromatin/axis interplay and the role (s) of the synaptonemal complex. *Chromosoma*, 115(3), 175-194.
131. Klein, F., Mahr, P., Galova, M., Buonomo, S. B., Michaelis, C., Nairz, K., & Nasmyth, K. (1999). A central role for cohesins in sister chromatid cohesion, formation of axial elements, and recombination during yeast meiosis. *Cell*, 98(1), 91-103.
132. Winters, T., McNicoll, F., & Jessberger, R. (2014). Meiotic cohesin STAG 3 is required for chromosome axis formation and sister chromatid cohesion. *The EMBO journal*, 33(11), 1256-1270.
133. Fukuda, T., Fukuda, N., Agostinho, A., Hernández-Hernández, A., Kouznetsova, A., & Höög, C. (2014). STAG 3-mediated stabilization of REC 8 cohesin complexes promotes chromosome synapsis during meiosis. *The EMBO journal*, 33(11), 1243-1255.
134. Sakuno, T., & Watanabe, Y. (2015). Phosphorylation of cohesin Rec11/SA3 by casein kinase 1 promotes homologous recombination by assembling the meiotic chromosome axis. *Developmental cell*, 32(2), 220-230.
135. Sakuno, T., Tashiro, S., Tanizawa, H., Iwasaki, O., Ding, D. Q., Haraguchi, T., ... & Hiraoka, Y. (2022). Rec8 Cohesin-mediated Axis-loop chromatin architecture is required for meiotic recombination. *Nucleic acids research*, 50(7), 3799-3816.
136. Duro, E., & Marston, A. L. (2015). From equator to pole: splitting chromosomes in mitosis and meiosis. *Genes & development*, 29(2), 109-122.
137. Shonn, M. A., McCarroll, R., & Murray, A. W. (2002). Spo13 protects meiotic cohesin at centromeres in meiosis I. *Genes & development*, 16(13), 1659-1671.
138. Yokobayashi, S., & Watanabe, Y. (2005). The kinetochore protein Moa1 enables cohesion-mediated monopolar attachment at meiosis I. *Cell*, 123(5), 803-817.

139. Kim, J., Ishiguro, K. I., Nambu, A., Akiyoshi, B., Yokobayashi, S., Kagami, A., ... & Watanabe, Y. (2015). Meikin is a conserved regulator of meiosis-I-specific kinetochore function. *Nature*, 517(7535), 466-471.
140. Kitajima, T. S., Kawashima, S. A., & Watanabe, Y. (2004). The conserved kinetochore protein shugoshin protects centromeric cohesion during meiosis. *Nature*, 427(6974), 510-517.
141. Rabitsch, K. P., Gregan, J., Schleiffer, A., Javerzat, J. P., Eisenhaber, F., & Nasmyth, K. (2004). Two fission yeast homologs of *Drosophila* Mei-S332 are required for chromosome segregation during meiosis I and II. *Current Biology*, 14(4), 287-301.
142. Marston, A. L., Tham, W. H., Shah, H., & Amon, A. (2004). A genome-wide screen identifies genes required for centromeric cohesion. *Science*, 303(5662), 1367-1370.
143. Kitajima, T. S., Sakuno, T., Ishiguro, K. I., Iemura, S. I., Natsume, T., Kawashima, S. A., & Watanabe, Y. (2006). Shugoshin collaborates with protein phosphatase 2A to protect cohesin. *Nature*, 441(7089), 46-52.
144. Kitajima, T. S., Yokobayashi, S., Yamamoto, M., & Watanabe, Y. (2003). Distinct cohesin complexes organize meiotic chromosome domains. *Science*, 300(5622), 1152-1155.
145. Nonaka, N., Kitajima, T., Yokobayashi, S., Xiao, G., Yamamoto, M., Grewal, S. I., & Watanabe, Y. (2002). Recruitment of cohesin to heterochromatic regions by Swi6/HP1 in fission yeast. *Nature cell biology*, 4(1), 89-93.
146. Ishiguro, T., Tanaka, K., Sakuno, T., & Watanabe, Y. (2010). Shugoshin-PP2A counteracts casein-kinase-1-dependent cleavage of Rec8 by separase. *Nature cell biology*, 12(5), 500-506.

Acknowledgments

First, I would like to extend my deepest gratitude to my supervisor Prof. Yasuto Murayama for guiding me throughout the research work over the last two years. Prof. Murayama's immense knowledge, motivation, and patience have given me the power to start a new project well into my graduate studies. Prof. Murayama introduced me to the field of biochemistry. As a mentor, Prof. Murayama always challenged my thinking and knowledge and taught me to think and read critically and refine scientific questions. I am grateful to Dr. Yumiko Kurokawa for encouraging me and sharing insightful suggestions. Thank you also to all members of the Murayama group for their support and friendship.

Apart from my supervisor, I would like to pay special regards to my previous host laboratory: Prof. Masato Kanemaki, Dr. Toyooki Natsume, and Dr. Yuichiro Saito, and all members of the Kanemaki group for my first three years at the National Institute of Genetics (NIG). They all have played a major role in setting my beginnings in research. Prof. Kanemaki introduced me to the field of protein degradation and taught me how to be a productive worker. Dr. Natsume guided me from day one when I first came to NIG as an intern and continued to teach me as I joined as a graduate student. I learned a great amount from Dr. Natsume's expertise in live cell imaging, human cell-based analyses, and flow cytometry. Dr. Saito supported me during the article writing and helped with immunoblotting experiments. I am very grateful to all collaborators, especially Prof. Ken-ichiro Hayashi, an outstanding chemist, who synthesized all of the molecules for my projects.

I would like to express my gratitude to my progress committee members throughout the years, Prof. Hiroyuki Araki, Prof. Kazuhiro Maeshima, Prof. Kuniaki Saito, Prof. Hironori Niki, Prof. Yumiko Saga, Prof. Hitoshi Sawa, Prof. Yuta Shimamoto, and Prof. Kenichi Nonomura. They have been an invaluable resource for me scientifically and personally.

I would like to express my gratitude to the student office for their continuous support and kind encouragement. Special thanks to the head of the NIG internationalization promotion committee, Prof. Akatsuki Kimura. Thank you to all members of NIG and The Graduate University for Advanced Studies, SOKENDAI.

This dissertation would not have been possible without the financial support from The Ministry of Education, Culture, Sports, Science and Technology of Japan (MEXT). I am grateful to SOKENDAI for awarding me with a Publication Grant for Research Papers.

Lastly, I am grateful to my parents, sister, friends, and acquaintances who gave me moral support, encouragement, and motivation to accomplish my goals.